DISSERTATION

submitted to the
Combined Faculties for the Natural Sciences and for Mathematics
of the Ruperto-Carola University of Heidelberg, Germany
for the degree of
Doctor of Natural Sciences

presented by
MSc. Ebru Ercan
born in Izmir, Turkey
Oral-examination: .....

The formation of endoplasmic reticulum-plasma membrane contact sites in mammalian cells

Presented by

Ebru Ercan

2011

Referees:

PD Dr. Matthias Seedorf

Prof. Dr. Walter Nickel

Declarations

I hereby declare that I have written the submitted dissertation myself and in this process have used no other sources or materials than those expressly indicated.

I hereby declare that I have not applied to be examined at any other institution, nor have I used the dissertation in this or any other form at any other institution as an examination paper, nor submitted it to any other faculty as a dissertation.

Heidelberg, May 17, 2011

Ebru Ercan

Acknowledgements

Foremost, I would like to express my deepest gratitude to my advisor, Matthias Seedorf, for his continuous support during my PhD study. I am really grateful for his attitude during this challenging time period. I learned a lot from him. He showed me not only how to do science but also how to give a proper education. I am sure, in the future his way of doing science and teaching will be really helpful to develop my skills in my academic career.

Secondly, I would like to thank to Walter Nickel, for his advices throughout my studies. This thesis work would not have been possible without his generous support and collaboration.

I feel lucky to have the chance to be taught by Bernhard Dobberstein. I am really grateful to him, since he made me think big and always see the big picture in the small figure.

During my Germany adventure, starting from Dresden, I had many adoring friends. They all made my life joyful and I guess without them my last seven years would not be so pleasant. Chronologically, I would like to thank Fuat Yigit Aksoy, Emral Cakmak Devany, Günes Bozkurt, Balca Mardin, Ilker Satiroglu, Oya Kuseyri, Dönem Avci, Pinar Kunt, Anton Khmelinskii, Fitnat Topbas, Baybars Külebi and many many more…

I especially want to thank Günes and Pinar, for always being there for me even from far away and for their endless friendship. I would like to thank Ilker, filled my days in Heidelberg with his great music, Balca, for making my life more than exciting and being always supportive for evetything, Anton for challenging pool games. And special thanks go to Dönem, for her support during writing and printing my thesis. Fuat and Baybars for reading my thesis and correcting my “the”s. Generally, I thank to my “Turkish Community” for making me feel comfortable as if I am at home. I am also grateful to Andrew Isaak not only for his native English but also for his sudden appearance in my life and making it spicy.

I of course thank my great lab members. It was always fun to work in the same environment with you. I am grateful not only for your scientific support but also for your warm friendship.

Last but not least, I owe my deepest gratitude to my family. My lovely parents and my adoring sister, I am grateful for your endless support and understanding. It was and it will be always hard to be physically away from you.

Summary

The endoplasmic reticulum (ER) has a distinct morphology, which is formed of sheets and tubules. These different domains are devoted to diverse functions such as co-translational protein translocation, lipid synthesis, protein folding, quality control and transport of proteins and lipids to different organelles. Close contacts of the ER with other organelles promote survival and growth of cells. The contacts with the plasma membrane (PM) are essential for lipid transport and Ca^{2+} signalling.

A component of the cortical ER in yeast is the polytopic membrane protein Ist2. Sorting of Ist2 into the cortical ER depends on its cortical sorting signal (CSS), which directly binds PM-lipids. Since it was unknown whether Ist2 remains in the cortical ER or travels to the PM by an unconventional pathway, I investigated the localization of Ist2 in mammalian cells. I found that Ist2 resides in the ER, where it forms peripheral domains that are in close proximity of the PM. In order to further investigate the features of the peripheral ER structures, I tagged mammalian type 1 membrane proteins with the CSS^{Ist2} and analyzed their localization. As a consequence of the interaction of CSS^{Ist2} with the PM-lipids, all tested chimeras were recruited to peripheral ER structures. Moreover, I demonstrated that these peripheral ER domains are static and in continuity with the rest of the ER.

Besides yeast Ist2, mammalian STIM1 and STIM2 proteins, are capable of forming ER-PM contact sites. STIM proteins function in signal amplification during store-operated Ca^{2+} entry. They sense the ER Ca^{2+} levels by their N-terminal EF-hand domains and upon depletion of ER Ca^{2+}, they multimerize and form ER-PM contact sites. At these sites they interact with and activate the PM Ca^{2+} channel, Orai1. I investigated the molecular mechanism behind this ER-PM contact site formation. By *in vitro* liposome binding experiments, I showed that both STIM1 and STIM2 cytosolic C-termini bind to PM-lipids via their lysine (K)-rich domains. Taken together, I found that the formation of ER-PM contact sites is dependent on expression of a transmembrane protein with a PM-lipid binding signal.

Finally, since STIM1 was previously shown to localize to the cell surface, I focused on its ER-retention mechanisms. I identified two types of mechanisms. In the first mechanism, the ER-retention is achieved by multiple di-arginine signals. The second mechanism is dependent on cytosolic Ca^{2+} levels. I found that depletion of cytosolic Ca^{2+} promoted trafficking of STIM1 to the cell surface, where it may activate Orai1. I propose that STIM1 indirectly senses the cytosolic Ca^{2+} via its K-rich domain, which binds to Ca^{2+}/calmodulin. Thus, STIM1 integrates the Ca^{2+} signals in the ER and the cytosol.

Zusammenfassung

Das endoplasmatische Retikulum (ER) ist in seiner Morphologie verschiedenartig. Es setzt sich aus plattenförmigen und tubulären Strukturen zusammen. Die verschiedenen Domänen des ERs erfüllen vielfache Funktionen u.a. in der kotranslationalen Proteintranslokation, der Lipidsynthese, der Qualtitätskontrolle und dem Protein- und Lipidtransport zu unterschiedlichen Organellen. Das ER steht in engem Kontakt mit anderen Organellen, um Überleben und Wachstum einer Zelle zu gewährleisten. Zusätzlich bildet das ER Kontakte mit der Plasmamembran (PM) aus. An diesen Kontakten finden Lipidtransfer und Kopplung von Ca^{2+}-Signalen statt.

Eine Komponente des kortikalen ERs in der Bäcker-Hefe ist das integrale Membranprotein Ist2. Die Sortierung von Ist2 in das kortikale ER erfolgt mit Hilfe seines kortikalen Sortierungssignals (CSS), das an Lipide der PM bindet. Da bisher nicht bekannt war, ob Ist2 im kortikalen ER verbleibt oder durch einen unkonventionellen Weg zur Plasmamembran gelangt, habe ich die Lokalisation von Ist2 in mammalischen Zellen untersucht. Meine Ergebnisse demonstrieren, dass Ist2 das ER nicht verläßt und dort periphere Domänen ausbildet, die in enger Nachbarschaft zur PM liegen. Um die Merkmale dieser peripheren ER-Strukturen weiter zu analysieren, habe ich mammalische Typ1-Membranproteine mit dem CSS^{Ist2} markiert und deren Lokalisation untersucht. Durch die Interaktion des CSS^{Ist2} mit Lipiden der PM wurden alle getesteten Chimären zu den peripheren ER-Strukturen rekrutiert. Weiterhin konnte ich zeigen, daß diese peripheren ER-Strukturen statisch und mit dem restlichen ER verbunden sind.

Neben dem Hefeprotein Ist2 sind die mammalischen Proteine STIM1 und STIM2 ebenfalls in der Lage, ER-PM-Kontaktstellen zu bilden. STIM-Proteine haben ihre Funktion in der Signalverstärkung während des Speicher-abhängigen Ca^{2+}-Eintritts. Sie erkennen Ca^{2+}-Konzentrationen durch ihre N-terminalen EF-Hand-Domänen. Nach Ca^{2+}-Depletion des ERs multimerisieren sie und formen ER-PM-Kontaktstellen, an denen sie mit dem Ca^{2+}-Kanal der PM, Orai1, interagieren und diesen aktivieren. Darüber hinaus habe ich den molekularen Mechanismus der Ausbildung von ER-PM-Kontaktstellen aufgedeckt. Durch *in vitro* Liposomen-Bindungsstudien habe ich gezeigt, dass die C-Termini von STIM1 und STIM2 mittels ihrer Lysin (K)-reichen Domänen an Lipide der PM binden. Diese Ergebnisse verdeutlichen, daß die Ausbildung der ER-PM-Kontaktstellen von der Expression einen integralen membranenprotein mit einem PM-Lipid-Bindungssignal abhängig ist.

Da für das STIM1-Protein bereits eine Lokalisation an der Zelloberfläche demonstriert worden war, habe ich seine Retention im ER untersucht. Dabei konnte ich zwei Mechanismen identifizieren. Der erste Mechanismus beruht auf dem Zurückhalten des STIM1-Proteins im ER über mehrere Di-Arginin ER-Retentionssignale. Der zweite Mechanismus ist abhängig von der cytosolischen Ca^{2+}-Konzentrationen. Meine Ergebnisse zeigen, dass die Depletion von

cytosolischem Ca^{2+} den Transport von STIM1 an die Zelloberfläche fördert, wo STIM1 Orai1 aktiviert. Ausgehend von meinen Daten erkennt STIM1 indirekt das cytosolische Ca^{2+} durch seine K-reiche Domäne, die Ca^{2+} im Komplex mit Calmodulin bindet. Somit integriert STIM1 Ca^{2+}-Signale im ER und im Cytosol.

Abbreviation List

Amp	Ampicillin
2-APB	2-Aminoethyldiphenyl borate
ARC	Arachidonate-regulated Ca^{2+}-selective
BFA	Brefeldin A
BSA	Bovine Serum Albumin
CAD	CRAC activation domain
CaM	Calmodulin
CC	Coiled-coil
CERT	Ceramide-transfer protein
cFI	Corrected Fluorescence Intensity
cFU	Corrected Fluorescence Units
COP	Coat protein complex
CSS^{Ist2}	Cortical sorting signal of Ist2
CRAC	Ca^{2+} release-activated Ca^{2+}
DMEM	Dulbecco's modified Eagle's medium
DMSO	Dimethyl sulfoxide
DNA	Deoxyribonucleic acid
dNTP	Deoxynecleotide triphosphate
ER	Endoplasmic reticulum
ERMES	ER-Mitochondria encounter structure
ER/SR	Endo/sarcoplasmic reticulum
FACS	Fluorescence-activated cell sorting
FBS	Fetal Bovine Serum
FLIP	Fluorescence loss in photobleaching
FRAP	Fluorescent recovery after photobleaching
FRB	FKBP-rapamycin binding
GFP	Green fluorescent protein
HA	Hemagglutinin
HEK293	Human embryonic kidney cells
HeLa	Human cervix cancer cells
IP_3	Inositol 1,4,5 triphosphate
IP_3R	IP_3 receptors
IPTG	Isopropyl-β-D-thiogalactopyranosid
JPHs	Junctophilins
Kan	Kanamycin
kb	kilobase
kDa	kilodalton
LB	Luria-Bertani

LTPs	Lipid transfer proteins
min	Minute
MORN	Membrane occupation and recognition nexus
NA	Numerical aperture
NCX	Na^{+}-Ca^{2+} exchangers
NEB	New England Biolabs
NFAT	Nuclear factor of activated T cells
ng	nanogram
Ni-NTA	Nickel Nitrilotriacetic acid
ORD	OSBP-related domain
ORPs	OSBP-related proteins
OSBP	Oxysterol-binding protein
PAGE	Polyacrylamide Gel Electrophoresis
PBS	Phosphate buffered saline
PCR	Polymerase Chain Reaction
PDI	Protein disulfide isomerase
PH	Pleckstrin homology
PI	Propidium Iodide
PI3P	Phosphoinositide 3 phosphate
PI4P	Phosphoinositide 4 phosphate
$PI(4,5)P_2$	Phosphoinositide 4,5 bisphosphate
$PI(3,4,5)P_3$	Phosphoinositide 3,4,5 trisphosphate
PK	Proteinase K
PLC-δ1	PhospholipaseC-δ1
PM	Plasma membrane
PMCA	PM Ca^{2+} ATPase
RER	Rough ER
RFP	Red fluorescent protein
RPE-1	Retinal pigment epithelium cells
RT	Room Temperature
RXR	Di-arginine ER retention signals
RyR	Ryanodine Receptors
s	Second
SAM	Sterile α motif domain
SDS	Sodium Dodecyl Sulfate
s.e.m.	Standard Error of the Mean
SER	Smooth ER
SERCA	Sarco/endoplasmic Reticulum Ca^{2+} ATPase
SOAR	STIM1 Orai-activating domain
SOCE	Store-operated Ca^{2+} entry

STIM	Stromal interaction molecule
TAE	Tris base, Acetic acid, EDTA
TCR	T cell receptors
Tg	Thapsigargin
TIRFM	Total internal reflection fluorescence microscopy
TMDs	Transmembrane domains
TRPC	Transient receptor potential channel
U2OS	Human bone osteosarcoma cells
UV	Ultraviolet
VGCC	Voltage-gated Ca^{2+} channels
YFP	Yellow fluorescent protein

Table of contents

1 Introduction 1

1.1 The morphology of the ER 1
1.1.1 Factors that determine the structure of ER 2
1.1.2 Interaction of ER with the cytoskeleton 3

1.2 Interaction of ER with other organelles 4
1.2.1 Interaction of ER with mitochondria 4
1.2.2 Interaction of ER with Golgi 6

1.3 Interaction of ER with the plasma membrane 9
1.3.1 OSBP proteins 10
1.3.2 Junctophilin proteins 11
1.3.3 Ist2 protein 12
1.3.4 STIM proteins 15

1.4 Aim of the thesis 20

2 Materials and methods 21

2.1 Molecular Biology Methods 21
2.1.1 Polymerase Chain Reaction (PCR) 21
2.1.2 Cloning 23
2.1.3 Transformation 24
2.1.4 Plasmid DNA Isolation 24

2.2 Mammalian Cell Culture Methods 26
2.2.1 Cell lines 27
2.2.2 Maintaining cells in culture 27
2.2.3 Transfection of cells 28

2.3 Microscopy Techniques 29
2.3.1 Immunofluorescence 30
2.3.2 Epi-fluorescence microscopy of fixed cells 31
2.3.3 Epi-fluorescence microscopy of live cells 31
2.3.4 Total Internal Reflection Fluorescence Microscopy (TIRFM) 31
2.3.5 Confocal Microscopy 32
2.3.6 Intracellular Ca^{2+} Imaging 33

2.4 Biochemistry Techniques 34
2.4.1 Expression and purification of 6xHis-GFP-fusion proteins 34
2.4.2 Calmodulin binding assay 35
2.4.3 Liposome binding assay 36
2.4.4 Preparation of yeast membranes and proteinase K treatment 38
2.4.5 SDS-PAGE and Immunoblotting 39

2.5 Flow cytometry 40
2.5.1 Flow cytometry of cells 41
2.5.2 Flow cytometry of liposomes 42

3 Results 43

3.1 Yeast Ist2 forms ER-PM contact sites in mammalian cells 43
3.1.1 Yeast Ist2 localizes at intracellular patch-like structures 45
3.1.2 Yeast Ist2 localizes at peripheral ER structures 46
3.1.3 The CSS^{Ist2} targets integral membrane proteins to PM-associated domains of the ER 47
3.1.4 Mutations in CSS^{Ist2} changes the morphology of the ER 49
3.1.5 The peripheral ER structures are in close proximity to PM 50
3.1.6 The CSS^{Ist2} functions as dominant sorting signal in mammalian cells 52

3.1.7 The CSS^{Ist2}-dependent peripheral ER formation does not alter the function of the ER……55
3.1.8 CSS^{Ist2}-induced PM-associated ER domains are stable structures....56
3.1.9 The CSS^{Ist2} binds $PI(4,5)P_2$ at the PM....58

3.2 Mammalian STIM proteins form Ist2-like ER-PM contact sites....60
3.2.1 Comparison of features of CSS^{Ist2} with STIM1 and STIM2 C-termini....60
3.2.2 The C-termini of STIM1 and STIM2 interact with PM lipids....63
3.2.3 Basic and hydrophobic residues are required for the function of the STIM2 lipid binding signal....67

3.3 Trafficking of STIM1 to the cell surface is regulated by multiple signals 70
3.3.1 Di-arginine signals retain STIM1 in the ER....70
3.3.2 The flexible extreme N-terminus of STIM1 interferes with its localization to the cell surface....74
3.3.3 The K-rich domain of STIM1 functions as an additional ER-retention signal, which is regulated by Ca^{2+}/calmodulin....75
3.3.4 Store-operated Ca^{2+}-entry interferes with STIM1 trafficking to the cell surface…..78
3.3.5 Multiple Ca^{2+}/CaM binding sites regulate the function of STIM1....80
3.3.6 The cell surface pool of STIM1 activates Orai1....83

4 Discussion....86

4.1 Features required for ER-PM contact site formation....86

4.2 Regulation of ER-PM contact site formation....89

4.3 Importance of ER-retention signals in STIM proteins....92

4.4 Regulated trafficking of STIM1 to the cell surface.... Error! Bookmark not defined.

4.5 Possible function of STIM1 at the cell surface....94

5 Appendix....97

6 List of figures and tables....98

6.1 List of figures....98

6.2 List of Tables....99

7 References....100

1 Introduction

The eukaryotic endoplasmic reticulum (ER) is an organelle that is devoted to diverse functions. These functions include the co-translational translocations of proteins across or into the ER membrane, proper folding and modification of proteins, and synthesis of phospholipids and sterols. In addition to its functions in synthesis of proteins and lipids, the ER is the major store of calcium ions (Ca^{2+}). The ER regulates the release of the Ca^{2+} into the cytosol and the uptake of cytosolic Ca^{2+}.

1.1 The morphology of the ER

Among all eukaryotic organelles, the ER has a striking architecture, which is made up of distinct domains that are devoted to different functions and structures (1). This complex structure can be divided into morphologically different regions, which can easily be visualized by fluorescence microscopy. The nuclear envelope that separates the nuclear material from cytosol is formed of sheet-like structures (2). In continuity with the nuclear envelope, the ER extends throughout the cytosol by forming tubular and sheet-like structures (3) (Figure 1.1).

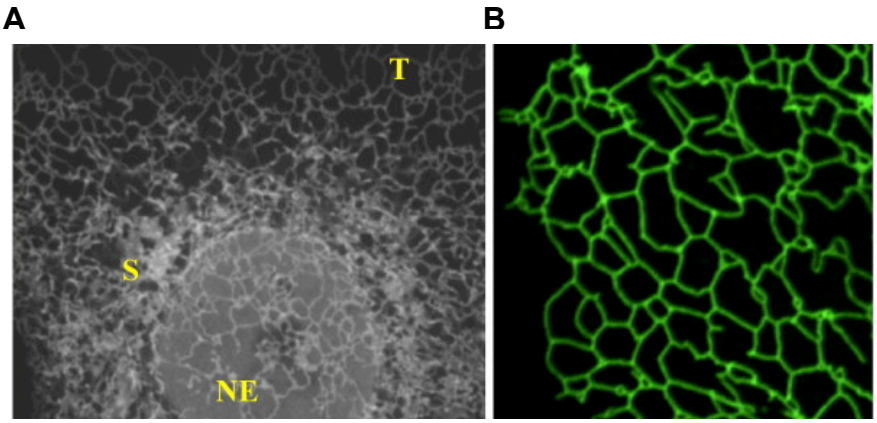

Figure 1.1 Morphology of the ER.
(A) COS cells expressing GFP-Sec61β at morphologically distinct ER regions, nuclear envelope (NE), peripheral sheets (S) and tubules (T). **(B)** Magnification of tubular ER structures. Taken from and modified after (1).

Initially, the ER was classified as rough ER (RER) and smooth ER (SER) (4). The RER is the domain where the ribosomes are attached and the translation of most membrane or luminal proteins takes place (5, 6). On the other hand the SER does not contain ribosomes and it functions as a transitional domain where the budding of the vesicles and transport of proteins to the other organelles occur. Moreover, the SER makes contacts with the other organelles (1, 7, 8).

Since the co-translational translocation of proteins into the ER is essential, RER is the universal domain of ER in all eukaryotic cells. SER also has some common roles in all cell types, such as the trafficking of proteins. However, the amount of the SER membrane changes according to cell type and the activities of SER can vary for different cell types. For instance in muscle cells the SER has a role in Ca^{2+} release and uptake for contraction (Sarcoplasmic Reticulum) and in liver cells it is important for detoxification of hydrophobic substances (9).

1.1.1 Factors that determine the structure of ER

Membranes, which are formed of phospholipid bilayers, are spherical or laminar structures in aqueous environment. However, some organelles such as Golgi and ER have distinct and complex structures compared to spherical lysosomes and peroxisomes (10). In order to create these distinct membrane structures, such as ER tubules and sheets, functions of specific proteins are required. These proteins maintain the morphology of the ER by either giving a shape by stabilizing the membrane curvature or tethering two membranes to each other or to the cytoskeleton (10).

1.1.1.1 Formation of ER-tubules

Two leaflets of a lipid bilayer have the tendency to remain together. Insertion of a protein only into one leaflet can facilitate membrane bending. Membrane-shaping proteins often have a common mechanism to induce membrane curvature. This mechanism is the insertion of an amphipathic α-helix into the cytosolic leaflet of the membrane (e.g. epsin and dynamin) (11, 12). The reticulons and DP1/Yop1 proteins are highly abundant integral membrane proteins that are required for the generation of the tubular ER (10, 13). These two classes of proteins are highly conserved and are able to homo-oligomerize. They are not only capable of forming networks of ER tubules *in vivo* but also *in vitro* (13, 14, 15).

Apart from other membrane-shaping proteins, reticulons and DP1/Yop1 have distinct structures. They do not have amphipathic helices; instead they contain two approximately 33-amino acid-long hairpin transmembrane domains (TMDs). These TMDs are too long to span the membrane bilayer once, and too short to span the membrane bilayer twice. They indeed are only inserted into the cytosolic leaflet of the ER membrane. This insertion of reticulons and DP1/Yop1 results in bending of the membrane and consequently generates tubules, which are around 50 nm in diameter (13, 16). Moreover, their depletion in yeast and as well in mammalian cells converts the ER tubules into sheets and their overexpression results in increased ER tubulation (13, 17).

1.1.1.2 Formation of ER-sheets

Peripheral ER sheets are enriched in polyribosomes and complexes for translocation of proteins. This enrichment of polyribosomes and large protein complexes, promote the generation of a flat ER structure. The studies proved that stripping of the ribosomes from the ER membrane by puromycin creates more tubular structures compared to untreated cells (18). In contrast, overexpression of p180, a ribosome binding integral ER membrane protein, increases the amount of stacked ER sheets (19). Moreover, compared to the ER tubules, the planes of the ER sheets contain only little or no reticulon or DP1/Yop1 proteins (1).

A recent study showed that a coiled-coil protein Climp63 serves as a luminal ER spacer and thereby helps forming sheets. However, the Climp63 and/or polyribosomes are not sufficient to form the ER sheets on their own. Interestingly, reticulons and DP1/Yop1, which are localized to the edges of the sheets, play a crucial role in generation of the sheets. It is suggested that Climp63 has a role in spacing the luminal space of the ER sheets to accommodate necessary chaperone proteins, whereas reticulons and the DP1/Yop1 localize to the edges of the sheets and stabilize the high curvature of the edges. Indeed the abundance of reticulon and DP1/Yop1 is important for determining the whole ER morphology (20). Moreover, the function of reticulons and DP1/Yop1 in forming both tubules and sheets is evolutionarily conserved. These proteins are present in lower eukaryotes, whereas the Climp63 is not. Again this defines reticulons and DP1/Yop1 as the main factors for determining the morphology of the ER (20).

1.1.2 Interaction of ER with the cytoskeleton

The interaction of organelles with the cytoskeleton can facilitate the movement and positioning of the organelles in cells and might affect their morphologies. The interaction of microtubules with ER can easily be visualized in mammalian cells (21, 22, 23). The ER tubules, which are more dynamic than the ER sheets, can co-align with the growing microtubules. *In vitro* studies showed that the distribution and movement of ER but not the tubule formation are achieved by the help of microtubules (24).

The ER tubules travel along the microtubules by two different mechanisms (1). The first mechanism is the movement of ER by attachment to microtubule tips. In mammalian cells the interaction of two proteins, STIM1, which is an integral ER-membrane protein and EB1, a microtubule (+)-end binding protein, supports the movement of the ER together with the growing tip of microtubule towards the PM (25). The second mechanism is the sliding of the ER along the microtubule (1). During sliding, the ER tubules jump onto the shaft of the microtubule instead of binding to the growing tip. Kinectin, which is an integral ER membrane protein, is one of the proteins that function in the movement of the ER (26, 27). Kinectin interacts with the

motor protein kinesin and this allows the movement of the ER along the microtubules (27, 28). Moreover, the rate of sliding is found to be faster then tip movement (1, 23).

1.2 Interaction of ER with other organelles

The eukaryotic organelles are separate but interdependent units of the cells. In order to communicate and exchange metabolites, they form physical contacts. For instance, the ER forms different kind of contacts with the membranes of mitochondria, Golgi, and the PM. These interactions have crucial roles in mechanisms such as non-vesicular transport of lipids and Ca^{2+} signalling. Here some of these interactions are briefly described.

1.2.1 Interaction of ER with mitochondria

The interaction between the ER and the mitochondria is required for cell function and survival. These close contacts between these two organelles modulate Ca^{2+} signalling and provide lipid and protein transport (29, 30). The Ca^{2+} ions that are stored in the ER can be taken up by the mitochondria after their release during cell signalling. And the efficiency of this process requires a proper spacing between these two organelles. Moreover, during phospholipid synthesis, this linkage should be created precisely to provide the lipid transfer between two membranes. The proteins, which function in lipid transfer mechanism, remain unknown (31).

Studies on the ER-mitochondria contact sites showed that mitofusin protein, MFN2, which is a dynamin-like GTPase functions in formation of ER-mitochondria junctions. Either homo- or hetero-complexes of MFN2 at the ER membrane and MFN2 or MFN1 at the mitochondria are capable of forming these bridges (32). These contacts have crucial functions in Ca^{2+} signalling. The Ca^{2+} concentration of the ER is increased around 2-fold in mouse embryonic fibroblasts lacking MFN2 (29). Moreover, after release of Ca^{2+} from the ER resident inositol 3-phosphate (IP_3) receptors, the uptake of Ca^{2+} into MFN2-deficient mitochondria was found to be markedly reduced. These findings demonstrate the correlation between the ER-mitochondria contact sites and Ca^{2+} uptake into mitochondria. Therefore this juxtaposition of both organelles is crucial during Ca^{2+} signalling (29, 33).

A more recent study revealed that the ER-mitochondria contact sites are formed by a protein complex, called ERMES (ER-Mitochondria encounter structure). This complex is formed by at least four proteins: Mmm1 (integral ER membrane protein), Mdm12 (cytosolic protein), Mdm10 and Mdm34 (integral mitochondria outer membrane proteins) (30). The interactions of these proteins create ER-mitochondria junctions. Researches until now proposed that ERMES function is required for Ca^{2+} exchange from the ER to mitochondria and mitochondrial protein import (30, 34). In addition, this complex also has a role in regulation of lipid transfer from ER to the mitochondria (35).

In order to regulate mitochondrial morphology and motility, a tailed-anchored mitochondrial protein, Gem1 (Miro in metazoans), binds to kinesin motor protein. Gem1 needs to be bound to Ca^{2+} in order to bind kinesin, and release it from the microtubules, (36). This binding to Ca^{2+} occurs at the ERMES-mediated ER-mitochondria contact sites, where the local Ca^{2+} concentration reaches high levels (30) (Figure 1.2).

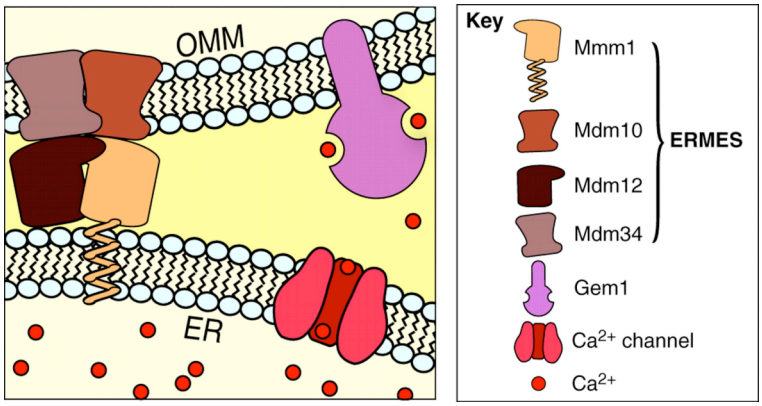

Figure 1.2 Proposed role of ERMES in Ca^{2+} exchange.

ER-mitochondria contact sites may create higher Ca^{2+} concentration compared to other sites of cytosol. In turn, Gem1 (Miro in metazoans) binds the Ca^{2+} ions and regulate mitochondrial morphology and motility. Taken from (30).

ERMES complex has also been shown to have a role in mitochondrial protein import. Mdm10 in addition to its function in ERMES regulates the assembly of β-barrel proteins (such as Tom40) by interaction with the SAM (sorting and assembly machinery) complex. Thus suggests a crosstalk between the ER-mitochondria junctions and mitochondrial protein import (34) (Figure 1.3).

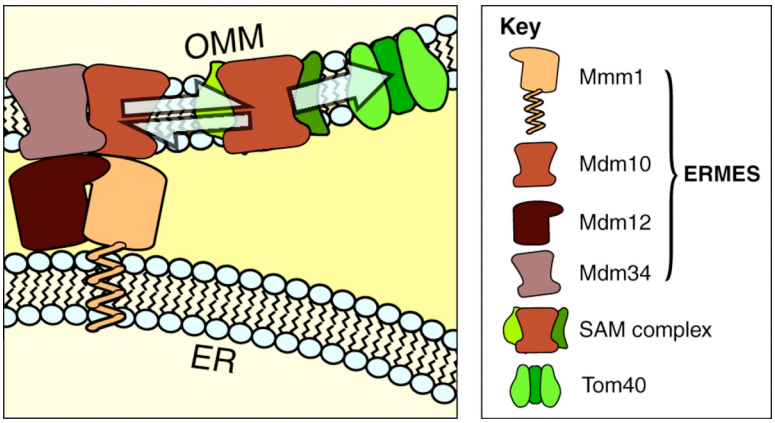

Figure 1.3 Proposed role of ERMES in mitochondrial protein import.

Mdm10, which has role in both ERMES complex and SAM complex may regulate the assembly of outer mitochondrial membrane β-barrel proteins such as Tom40. Taken from (30).

Furthermore, ERMES complex mediates a shorter distance between ER and mitochondria, and thereby allows non-vesicular transfer of lipids between ER and mitochondria. This distance facilitates the targeting of soluble lipid carrier proteins such as oxysterol-binding protein (OSBP) and ceramide-transfer protein (CERT) (30, 37) (Figure 1.4).

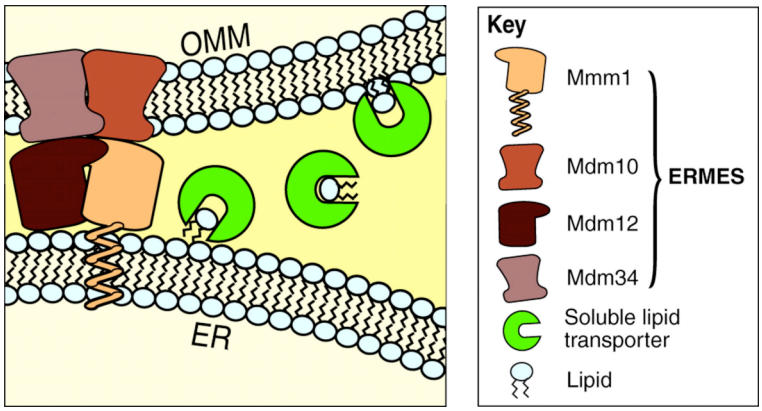

Figure 1.4 Proposed role of ERMES in phospholipids exchange.

ER-mitochondria contact sites may facilitate the targeting and shuttling of soluble lipid-carrier proteins between two organelles. Taken from (30).

1.2.2 Interaction of ER with Golgi

The ER makes physical and functional contacts with the Golgi. One of these contacts is created by apposing of ER and Golgi membrane in order to transport lipids. Another contact is formed during vesicular protein transport from ER to Golgi. These two mechanisms will be briefly described in the following sections.

1.2.2.1 Non-vesicular lipid transport

The studies, which investigate the interaction between the ER and the Golgi revealed that integral ER membrane proteins VAP-A and VAP-B interact with oxysterol-binding protein (OSBP) and ceramide-transfer protein (CERT), which are crucial for phosphoinositide and sphingolipid biosynthesis (38, 39). The interaction between VAPs and OSBP and CERT promotes non-vesicular lipid transport between two membranes. CERT is a soluble protein, comprised of three functionally important domains, which bind to VAP, ceramide and phosphoinositide of Golgi (phosphoinositide 4 phosphate, PI4P). The binding to the ER located VAPs and Golgi resident PI4P brings two organelles in a close proximity, where the ceramide can easily be transported. The transport of ceramide is crucial for the synthesis of sphingolipids, which occur in the Golgi (1). The high levels of sphingolipids and glycosphingolipids promote the phosphorylation of CERT, which inactivates it and results in the reduction in ceramide transport (40) (Figure 1.5).

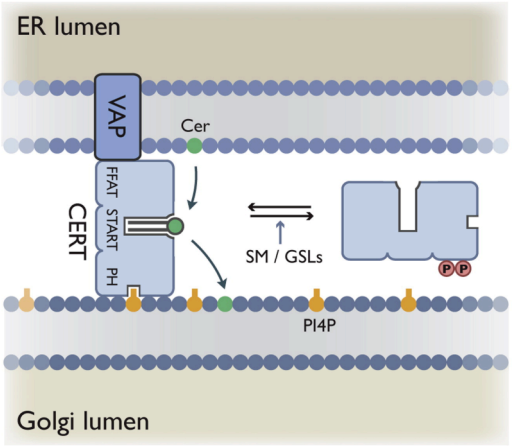

Figure 1.5 Lipid transport at ER-Golgi contact sites.

CERT functions in ceramide transport from ER to Golgi. CERT binds to ER-localized VAPby its FFAT domain and interacts with the Golgi membrane by its PH domain. The START domain binds and transfers the ceramide. CERT is inhibited by phosphorylation, which is regulated by the levels of sphingolipids such as sphingomyelin (SM) and glycosphingolipids (GSL). Taken from (40).

1.2.2.2 Vesicular protein transport

Proteins transported across the eukaryotic ER, include soluble proteins that are secreted from the cell and membrane proteins that either stay in the ER or reach other organelle membranes of the secretory pathway (41, 42). Most membrane proteins are co-translationally translocated into the ER through the translocon complex. The translocon, which is a protein conducting channel, is formed of the Sec61 complex, which is comprised of the channel forming α and γ subunits and the interacting β subunit (41). Translocated proteins start to fold co-translationally in the ER lumen. The ER lumen is similar to the extracellular space as it has a high Ca^{2+} concentration of around 500 μM and provides a more oxidizing environment than the cytosol (43). Specific set of enzymes and chaperone proteins, which are ubiquitously expressed, assist folding of proteins in the ER. In most cases, individual subunits of proteins are folded before the assembly into higher oligomeric structures takes place (44).

Protein folding and quality control in the ER

The ER not only provides a suitable environment for folding of proteins but also governs a crucial role in quality control. The quality control mechanism primarily depends on ER chaperones, which recognize the misfolded intermediates through exposed hydrophobic surfaces, immature gylcans or unpaired cysteines (43). As a consequence these misfolded proteins are retained in the ER or retrieved back from the Golgi complex. Moreover, immature proteins, which form aggregates, are also excluded from vesicles exiting from the ER (43, 45).

During the formation of multimolecular protein complexes, ER retention mechanisms indirectly control the correct folding and assembly (46, 47). For instance, ion channel subunits contain ER retention signals, which are masked by correct assembly of these subunits into a channel and this masking promotes exit from the ER. One of these retention signals is the cytosolic di-lysine (KKXX) ER retention signal, which is present in several immune receptor subunits (47, 48). The proteins with type I topology (the C terminus is in the cytosol), the di-lysine signal is found at -3 and -4/-5 positions from the C terminus (K(X)KXX) (49). The other retention signal is di-arginine ER-retention signal (RXR), which can be positioned nonspecifically at any place of cytosolic domains of both type I and type II membrane proteins (50). For example, the quality control during assembly of the inward rectifying potassium channel (Kir6.2/Sur1 complex) is achieved by these di-arginine ER retention signals (RXR). Both proteins contain RXR motifs and are localized to the ER if the channel is not correctly assembled. During the assembly of the channel, the RXR signals are shielded and after that the channel can travel through the Golgi to the cell surface (51) (Figure 1.6).

Protein transport between ER and Golgi

In order to move further along the secretory pathway, proteins exit the ER either by unspecific bulk flow or by selective recruitment into vesicles (52, 53). The proteins that are destined to be transported from ER to the other compartments through the Golgi are initially localized to specific sites of ER, which are called ER exit sites (54). At the ER exit sites, the cargo proteins are loaded into vesicles, which are formed by coatomer coat complex II (COPII). COPII vesicle formation at the ER is conserved in eukaryotic cells and requires the small GTPase Sar1, Sec23 and the cargo recruiter Sec24 (55). Moreover the Sec13/31 complex is required for the stabilization and the polymerization of coat subcomplexes, which provides a membrane bending force to allow the formation of COPII vesicle (54). In order to recruit proteins into the COPII vesicles, specific amino acid motifs, the so called ER export signals, are required. These signals are identified to be acidic in nature and usually have a DXE or EXD motif. This motif is recognized by the COPII component, Sec24 (53).

The ER-resident proteins that escape from ER or misassembled proteins are retrieved back to the ER from the Golgi via COPI vesicles. COPI vesicles recognize specific signals of soluble or membrane proteins. ER-resident soluble proteins that are retrieved back to the ER carry a retention signal, which is the KDEL sequence (56). This KDEL signal is recognized by a KDEL receptor in the Golgi membrane and retrieved back to the ER (57).

The signals that play a role in retention or retrieval of membrane proteins can be classified in two groups: di-lysine and di-arginine signals. The proteins that carry the di-lysine motif are recognized by α and β subunits of the COPI coat and thus retrieved back to the ER (58). On the

other hand, di-arginine ER retention signal has a more complex feature than the di-lysine signal. A combinatorial screening approach by using Kir6.2 C-terminal domain showed that Arg-based signals conform to the consensus Φ/Ψ/R-R-X-R, in which Φ/Ψ denotes an aromatic or bulky hydrophobic residue and X is any amino acid. The identity of X can modulate the signal, where negatively charged residues or small, non-polar side chains inactivate the signal (59) (Figure 1.6).

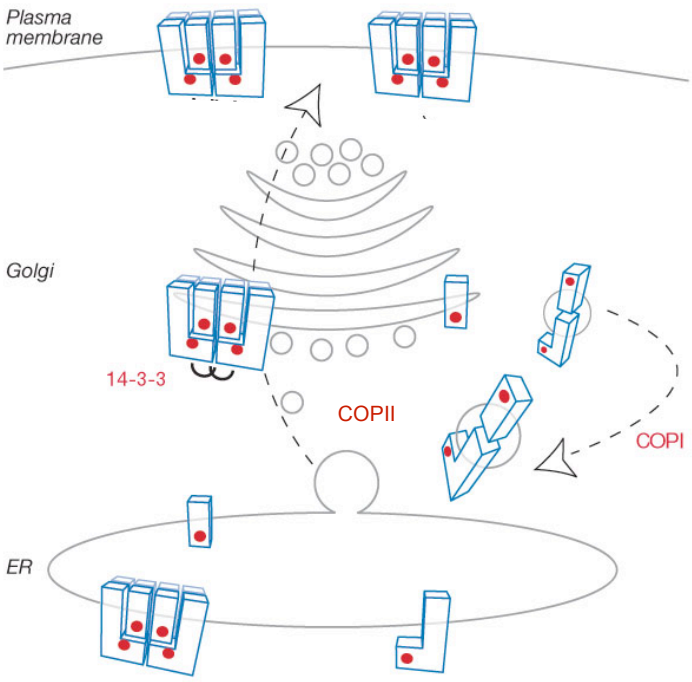

Figure 1.6 Regulated trafficking of inward rectifying potassium channel.

Both Kir6.2 and Sur1 (small and large rectangular shapes, respectively) have di-arginine retention signal (red dot). These proteins are retrieved back from the Golgi via COPI vesicles if they do not form a correct assembly. The correct assembly of the channel shields the di-arginine ER retention signals and results in exit from the ER by COPII vesicles. Furthermore, with the contribution of 14-3-3 proteins, which may mask the retention signals, channel can travel to cell surface. Taken from and modified after (50).

1.3 Interaction of ER with the plasma membrane

The ER forms contact sites with the plasma membrane (PM) in order to fulfil various cellular functions, such as lipid transfer and Ca^{2+} signalling. These contact sites are found both in yeast and in mammalian cells (60, 61, 62). In the next sections, some of the proteins that are involved in formation of ER-PM contact sites will be described.

1.3.1 OSBP proteins

The sterol concentration in cellular membranes is tightly controlled; for instance, the ER has around 5 mol% cholesterol (63) whereas the PM has 30-50 mol% (64). In both yeast and mammalian cells, sterols are synthesized *de novo* in the ER and transported to the PM via non-vesicular transport pathway. This trafficking is Brefeldin A (BFA) insensitive and requires ATP-dependent carrier proteins (65). BFA is a drug that blocks the trafficking through the Golgi (66). This non-vesicular transport of sterols between membranes is mediated by OSBPs and OSBP-related proteins (ORPs). These proteins are a conserved family of soluble proteins and are also called sterol-binding lipid transfer proteins (LTPs). The OSBP and ORPs are not only capable of binding oxysterols, which are the regulators of cholesterol metabolism, but also phosphoinositides and many other sterol derivatives, including cholesterol (67, 68, 69).

All ORPs, including the *Saccharomyces cerevisiae* Osh (OSBP homologue) proteins, harbors an OSBP-related domain (ORD). The budding yeast has seven OSBP homologues (Osh). Four Osh proteins (from Osh4 to Osh7) consist of only an ORD, whereas the other three contain additional domains such as phosphoinositide-binding pleckstrin homology (PH) domain (70). Osh family proteins function in trafficking of cholesterol from the ER to the PM, since *in vitro* studies demonstrated that Osh proteins could transfer sterols between the membranes (71, 72).

In addition to their function in sterol transport, the Osh proteins are recently shown to have the function of regulating phosphoinositide metabolism at ER-PM contact sites (73). The PH-domain containing family member, Osh3, is found to localize at the ER-PM contact sites and this localization is dependent on the levels of PI4P at the PM, suggesting a role for Osh3 as sensor of PI4P of PM and activator of Sac1 (73). Sac1 is a lipid phosphatase, which hydrolyzes PI4P. In addition to Osh3, the ER VAP proteins, Scs2/Scs22 control the PI4P levels and the activity of Sac1. Osh3, in addition to its lipid-binding PH domain, contains a protein-protein interaction domain (FFAT) that binds Scs2/Scs22 (74). Therefore, a proposed model for the formation of ER-PM contact sites would be as following: In the presence of high concentrations of PI4P at the plasma membrane, the PH domain of Osh protein binds PI4P of the PM whereas the FFAT domain binds Scs2/Scs22 in the ER. As a consequence, ER is brought to a close proximity of the PM. Following recruitment of the ER to the PM, the ER resident Sac1 binds to PI4P and thus regulates the phosphoinositide metabolism (73) (Figure 1.7).

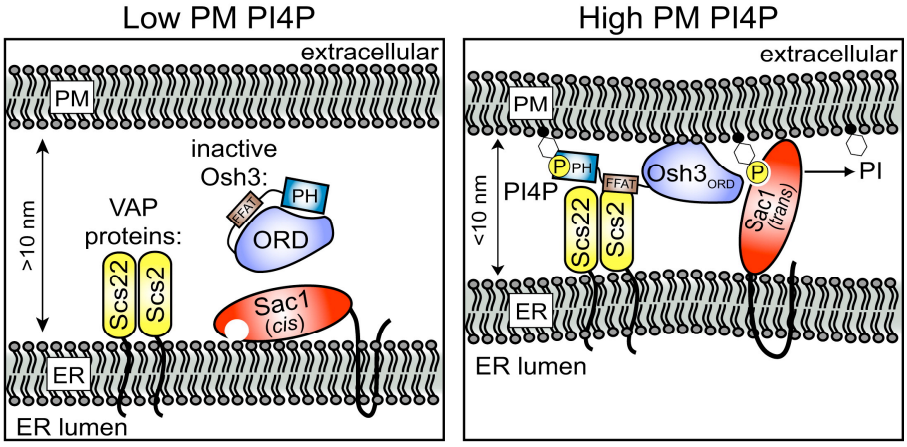

Figure 1.7 PI4P turnover at ER-PM contact sites.

High PM PI4P levels recruit and activate Osh3 at ER-PM contact sites. Osh3 interacts with VAP proteins Scs2/Sc22 at the ER membrane by FFAT domain and binds to PM via its PH domain. Sac1 is recruited at these contact sites and there it regulates the phophoinositide metabolism. Taken from (73).

1.3.2 Junctophilin proteins

In excitable cell types, such as muscle cells, the junctions between the endo/sarcoplasmic reticulum (ER/SR) and PM are frequently formed and they are named as junctional membrane complexes (75). This ER/SR-PM contact sites formation is a prerequisite for a cross talk between the Ca^{2+} channels, which localize in either ER/SR (Ryanodine Receptors- RyR) or PM (voltage-gated Ca^{2+} channels- VGCC) (76). The formation of SR-PM contact site is mediated by junctophilins (JPHs), which are consistently expressed in excitable cells (75, 77). The JPHs function to transmit the Ca^{2+} influx signal to the Ca^{2+} release signal. Upon influx of Ca^{2+} from VGCC, which is in the PM, the RyR releases Ca^{2+} that is stored in ER/SR. This cross talk of these two channels is achieved by JPHs (Figure 1.8). This process is crucial for contraction of muscles, release of insulin from pancreatic β-cells and synaptic plasticity in neurons (78, 79).

There are four JPH isoforms in mammals and they all are single-pass type 2 membrane proteins. Primary sequence analysis suggests that all JPH isoforms contain “membrane occupation and recognition nexus” (MORN) motifs clustered near the N-terminus, which faces the cytosol (80). The MORN motifs are suggested to mediate association with the PM, either directly by interacting with lipids or indirectly through membrane-bound adapter proteins (81). The α-helical domain, which follows the MORN domain, is believed to determine the distance between the PM and the ER/SR. Electron microscopy studies showed that the distance between the ER/SR and PM is around 12 nm (75, 82). Moreover, genetic deletion of *JPH2* in mice resulted in the formation of fewer and improperly aligned junctional membrane complexes in cardiac muscle (75). Intriguingly, overexpression of *JPH1* in amphibian embryonic cells promoted the generation of 12 nm junctions between the ER/SR and PM (83).

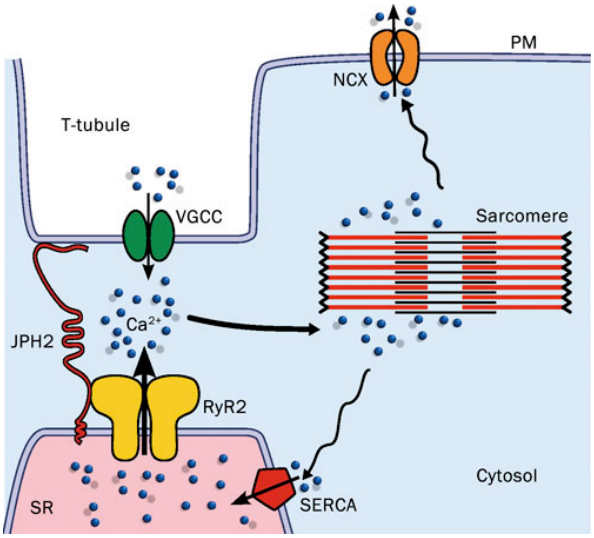

Figure 1.8 Proposed function of Junctophilin-2 in cardiac myocytes.

PM depolarization results in the opening of voltage-gated Ca^{2+} channels (VGCC), which promote influx of Ca^{2+}. Following the Ca2+ influx, ryanodine receptors (RyR2) release a greater amount of Ca^{2+} from the sarcoplasmic reticulum (SR). This results in Ca^{2+}-induced contraction of the sarcomere. For relaxation of the myocyte Ca^{2+} is pumped back into the SR by sarco/endoplasmic reticulum Ca^{2+} ATPase (SERCA) or removed from the myocyte by the Na^{+}/Ca^{2+} exchanger (NCX). For the proper excitation-contraction coupling in cardiac myocytes, proper function of junctophilin-2 (JPH2) is required (Taken from (84)).

1.3.3 Ist2 protein

Physical contacts between the cortical ER and the PM also play a role in the sorting of the polytopic membrane protein Ist2 in budding yeast. Ist2, which is synthesized from a bud-localized mRNA, travels to the PM-associated cortical ER (85). From there the protein may travel further to domains of the PM independently of the function of the classical secretory (sec) pathway (86, 87). The cortical ER of the yeast lies in close proximity to the PM and forms contacts with a distance of 30 nm or even less (60, 88, 89). Therefore, in yeast it is very difficult to distinguish whether the localization of a protein is at the cortical ER or the PM. In the case of Ist2, cell fractionation and protease protection experiments suggested that it reaches the PM (86).

1.3.3.1 Transport of Ist2 to ER-PM contact sites in yeast

In case *IST2* mRNA is not transported, Ist2 is translated at the perinuclear ER, from where the protein diffuses quickly to the cortical ER. This transport of Ist2, which is the accumulation at PM-associated ER, is mediated by the C-terminal region of 69 amino acids (878–946) (90). This region is defined as the cortical sorting signal of Ist2 (CSS^{Ist2}). This signal has two functionally important regions. The N-terminal region consists of single amino acid repeats of threonine, histidine and serine residues (T/H/S-cluster). This T/H/S-cluster functions most likely as a multimerization domain, since its function can be replaced by another multimerization domain.

In addition, the length of T/H/S-cluster (50 amino acids) is important for the function of of the CSS^{Ist2} (90). This T/H/S cluster provides the necessary distance between the ER and the PM for the function of the CSS^{Ist2}.

The C-terminal region of CSS^{Ist2} (last 18 amino acids) is rich in lysine residues and capable of forming a short amphipathic α-helix (85). This amphipathic α-helix formation is predicted to cover the last 11 amino acids. The N terminal region of the helix is rich in basic residues and they are important for the localization of Ist2. The mutation of four lysine and one histidine (K931A/K933A/H934A/K935A/K936A) was shown to cause a weak perinuclear accumulation of Ist2. This suggests that multiple basic residues are required for the function of CSS^{Ist2}.In addition, the mutational analysis of the Ist2 sorting signal revealed that positions of hydrophobic residues (L938, L939 and L942) at one side of the amphipathic α-helix are also required for sorting of Ist2 (85) (Figure 1.8)

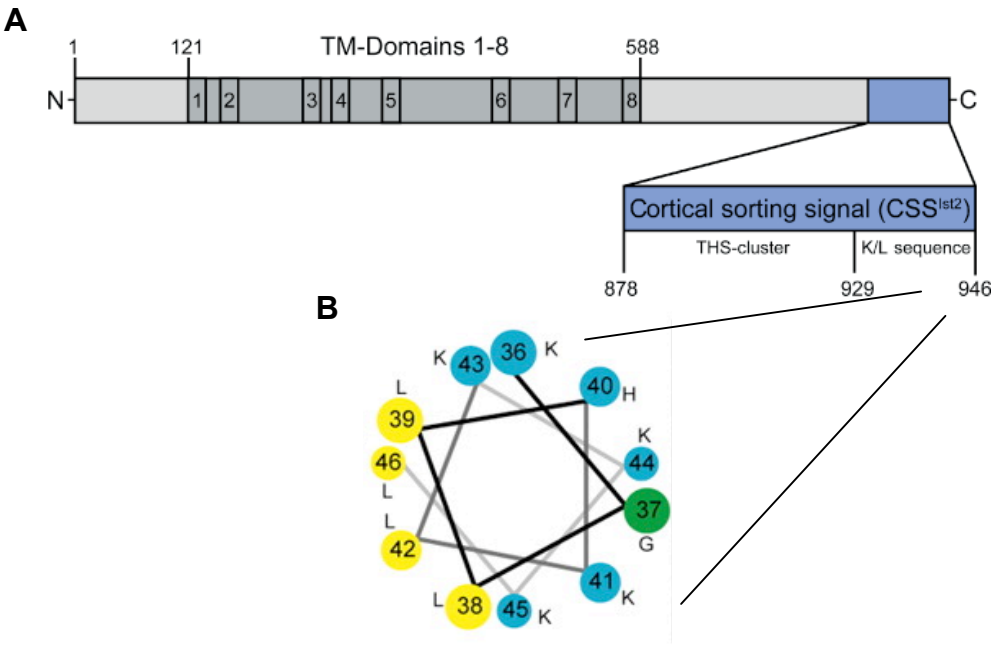

Figure 1.9 Domain structure of yeast Ist2.

(A) Ist2 has eight transmembrane (TM) domains. Its N- and C-terminus faces the cytosol. Last 69 amino acids of Ist2 forms the cortical sorting signal (CSS^{Ist2}). CSS^{Ist2} has two functionally important domains, T/H/S-cluster for multimerization, and K/L sequence (K-rich domain) for binding PM-lipids. Taken from (91) (B) Last 11 amino acids of K-rich domain forms amphipathic α-helix, which has a hydrophobic patch on one basic patch on the other side. Taken from (85).

Since the *IST2* mRNA localizes to the bud, the role of mRNA localization in trafficking of Ist2 was investigated. The mRNA-binding protein She2 recognizes the stem loop of *IST2* mRNA, which functions as mRNA localization signal (92, 93). This signal is part of the sequence encoding the CSS^{Ist2}. However, it was found that the function of the CSS^{Ist2} is independent of *IST2* mRNA localization. The disruption of the secondary structure of the stem-loop mRNA sequence and the experiments performed in *she2*Δ mutants did not change the localization of the protein (90).

As it was shown for the recruitment of soluble proteins from the cytosol to the PM, the sorting of the polytopic protein Ist2 depends on interaction with PM lipids (85). Basic residues and the amphipathic α-helix are required for binding of the CSS^{Ist2} to $PI(4,5)P_2$-containing PM-like liposomes, suggesting that this interaction is necessary and sufficient for efficient transport of Ist2 from the perinuclear to the cortical ER (85, 91). *In vivo*, it was shown that the CSS^{Ist2} can be functionally replaced by a *bona fide* $PI(4,5)P_2$-specific lipid-binding domain from phospholipaseC-δ1 (PLC-δ1) but not by other lipid-binding domains, which recognize PI3P (phosphoinositide 3 phosphate) or PI4P. Attached to other integral ER membrane proteins, the CSS^{Ist2} targeted these proteins to the cortical ER. Thus, interaction of CSS^{Ist2} with lipids serves as a dominant and a novel mechanism for sorting of integral membrane proteins to the ER-PM contact sites (91).

1.3.3.2 CSS^{Ist2}-tagged membrane proteins form ER-PM contact sites in mammalian cells

Since yeast is not suitable for the investigation of exact localization of Ist2, due to its cell wall and constitutive cortical ER, additional localization studies were performed in mammalian cells. In this work, I attached the CSS^{Ist2} to the integral ER-membrane proteins, such as CD4, MHC Class I, TAP1, Kir6.2. Interestingly the resulting chimeras were recruited to peripheral ER structures, which are in close proximity to the PM (94, 95). The formation of these patches was achieved by direct interaction of CSS^{Ist2} with the phosphoinositides of the PM. In my thesis, I show that the peripheral ER patches are stable and immobile structures that are in continuity with the rest of the ER. In parallel to my study, another group showed by siRNA experiments that the CSS^{Ist2}-induced peripheral ER formation was dependent on both COPI and the microtubule (+)-end binding protein EB1 (95).

1.3.3.3 Possible function of Ist2 at the ER-PM contact sites

Ist2 is the yeast member of the mammalian ANO/TMEM16 family, which shares approximately 20% sequence similarity and a similar membrane topology (96). TMEM16A and TMEM16B were recently identified as calcium-activated chloride channels of the PM (97, 98, 99). These channels are expressed in multiple tissues and play important roles in cellular physiology,

including epithelial secretion of electrolytes and water, sensory transduction, regulation of neuronal and cardiac excitability, and regulation of vascular tone (98, 99).

A more recent study on other member of TMEM16 family, TMEM16F, revealed that this protein, which is located at the PM, functions as phospholipids scramblase. It mediates the translocation of phosphatidylserine from the inner leaflet to the outer leaflet. Moreover, this function of TMEM16F is dependent on cytosolic Ca^{2+} levels and the increase of cytosolic Ca^{2+} activates the protein (100).

Although Ist2 cannot react to the cell surface in mammalian cells, it may function as chloride channel or as phospholipids scramblase at the cortical ER. Nevertheless, the function of Ist2 still remains to be elusive.

1.3.4 STIM proteins

Interestingly, the phenomenon of Ist2 transport to the cortical ER in yeast shares some similarities with the intracellular distribution of stromal interaction molecule 1 (STIM1) and 2 (STIM2) in mammalian cells. STIM1 was originally described as a PM protein of bone marrow stromal cells, hence the original name stromal interaction molecule (101), and of the chronic myeloid leukemia cell line K562 (102). Further studies showed that STIM1 localizes predominantly in the ER (61, 103, 104, 105), with its N-terminus localized in the ER lumen. The N-terminus of STIM1 has a size of approximately 22 kDa after cleavage of its signal sequence.

STIM1 has a crucial role in Ca^{2+} signalling during T cell activation. It basically carries out two functions in order to activate CRAC (Ca^{2+} release-activated Ca^{2+}) channels. STIM1 first senses the ER Ca^{2+} store depletion and second, activates the Ca^{2+} channels in the PM. This process is called store-operated Ca^{2+} entry (SOCE), where the store is the ER (106-108).

Activation of T cells

The stimulation of immune cells and many other non-excitable cell types involves the opening of CRAC channels in the PM. As a consequence, the cytosolic Ca^{2+} concentration increases from approximately 100 nM at resting state to more than 1000 nM (109). Ca^{2+} entry into the cytosol is critical for responses of all immune cells. In T cells, a sustained Ca^{2+} uptake regulates proliferation and cytokine production. SOCE is the primary mechanism of Ca^{2+} influx in T cells. The SOCE is initiated by ligand binding to the T cell receptors (TCR). This ligand binding results in generation of a cascade of signaling events. This cascade starts with the activation of tyrosine kinases (such as Itk), which phosphorylate and activate phospholipase C. The phospholipase C hydrolyzes $PI(4,5)P_2$ (phosphoinositide 4,5 bisphosphate) in the PM to IP_3 (inositol 1,4,5 triphosphate) and diacylglycerol. IP_3 then binds to IP_3 receptors (IP_3R) in the ER membrane and the binding results in release of Ca^{2+} to the cytosol. The depletion of ER Ca^{2+}

stores leads to the oligomerization of STIM proteins, which in turn form ER-PM contact sites. At these sites, STIM proteins interact with and open the PM Ca^{2+} channels (CRAC or Orai1). As a result of Ca^{2+} uptake into the cytosol, the calmodulin (CaM)-dependent phosphatase calcineurin is activated. Calcineurin then dephosphorylates the transcription factor NFAT (nuclear factor of activated T cells), which translocates into the nucleus and initiates the transcription of cytokines (reviewed in (110) and (108)) (Figure 1.9).

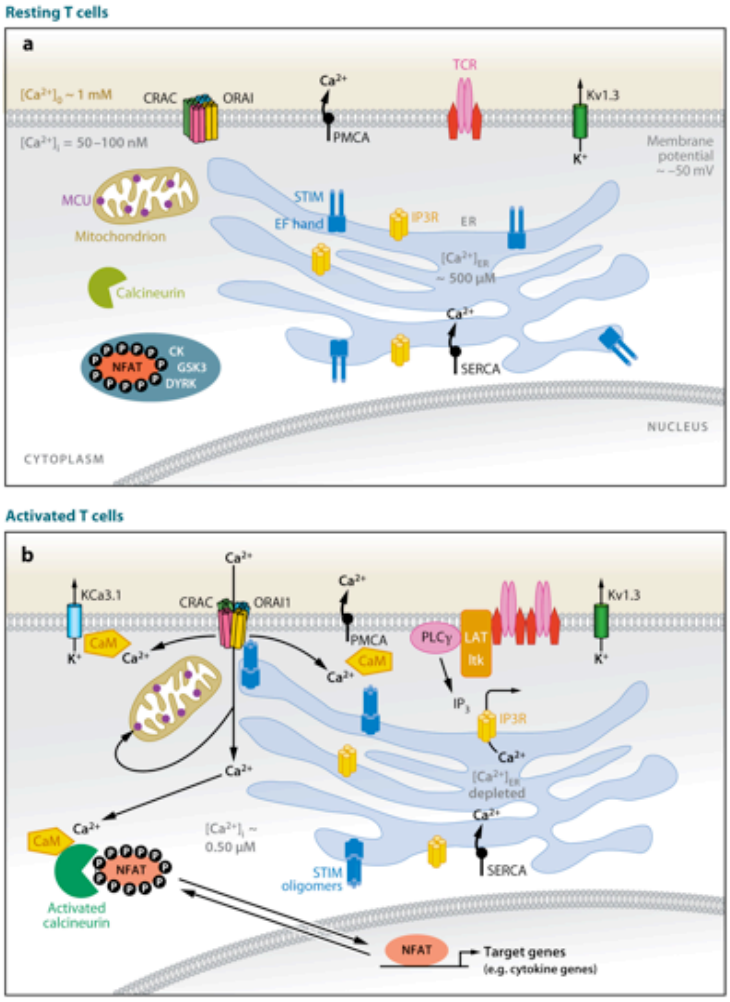

Figure 1.10 Signaling pathway that connects SOCE with NFAT-dependent gene transcription in T cells.

(A) Resting T cells have intracellular free Ca^{2+} concentrations of 50–100 nM that are maintained by the PM Ca^{2+} ATPase (PMCA), the SERCA that pumps Ca^{2+} into the lumen of the endoplasmic reticulum (ER), and Na^{+}-Ca^{2+} exchangers (NCX, not shown). Immunoreceptors include antigen receptors on T cells (TCR). The concentration of free Ca^{2+} in the ER is several hundred μM; hence the EF-hand of STIM1 is saturated with Ca^{2+}, and STIM1 does not form higher-order oligomers. The transcription factor NFAT is heavily phosphorylated and localized to the cytoplasm. (B) Activated T cells. T cell receptors assemble into signaling complexes that contain scaffold proteins such as LAT, tyrosine kinases such as Itk, and phospholipase C (PLC)γ (not all of which are shown). IP_3 produced by PLCγ binds to IP_3 receptors in the ER membrane, causing the release of Ca^{2+} from the ER. As a result of the depletion of ER Ca^{2+} stores, Ca^{2+} dissociates from EF-hand of STIM1 and causes a conformational change that leads to oligomerization. The STIM oligomers move to ER–PM contact sites, recruit Orai1 proteins to these sites, and cause CRAC channels to open. The resulting increase in cytosolic Ca^{2+} promotes binding of CaM to phosphatase calcineurin, which dephosphorylates NFAT and causes its nuclear translocation, thus activating NFAT-dependent transcription of cytokines. Taken from (108)

1.3.4.1 STIMs sense the ER Ca^{2+} concentration

The lumenal N-terminus of STIM1 is responsible for Ca^{2+} sensing. NMR studies demonstrated that human STIM1 (58–201) fragment is composed of two EF-hands and a sterile α motif (SAM) domain (111). Only the first EF-hand is capable of binding Ca^{2+}, whereas the other makes interactions with the SAM domain. This EF-SAM protein fragment is monomeric, when it is bound Ca^{2+}. As shown by biophysical studies, in the absence of Ca^{2+}, the protein shows a substantial unfolding and starts to form dimers and aggregates (111, 112).

Since the concentration of Ca^{2+} in the ER lumen is hundreds of micromolar (μM), STIM1 should have a low affinity for Ca^{2+} in order to function as a sensor. The experiments that are performed by a recombinant STIM1 luminal domain revealed that a K_d of STIM1 for Ca^{2+} is around 500–600 μM (112). On the other hand, STIM2 was shown to be more sensitive upon changes of Ca^{2+} in the ER, suggesting a function as a basal regulator. This suggests that STIM2 function is not only related to signal amplification but also to refilling the ER Ca^{2+} stores (113).

1.3.4.2 Oligomerization and distribution of STIMs

The activation of STIM1 by decrease of ER Ca^{2+} levels drives its oligomerization, which starts with an aggregation of the Ca^{2+}-binding EF-hand- and SAM domains in the N-terminus (107). The conformational changes upon the oligomerization of the N-terminal domains of STIMs spread into their cytosolic domain. The cytosolic domains of STIMs are comprised of two coiled-coil domains, a serine/proline rich domain and a lysine (K)-rich domain. Recent studies showed that a region covering the second coiled-coil domain is important for the interaction with the CRAC channel at the PM (Orai1). This domain is named as CAD (CRAC activation domain, residues 342-448) or SOAR (STIM1 Orai-activating domain, residues 344-442) (114, 115) (Figure 1.10).

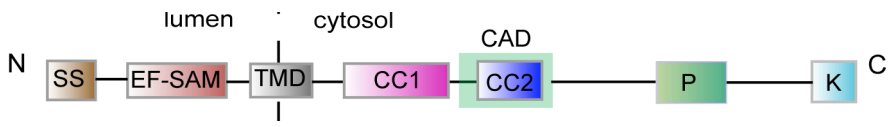

Figure 1.11 Domain structure of STIM proteins.

STIM proteins are type 1 membrane proteins. SS, signal sequence, EF-SAM, consists of two EF-hands and a SAM domain, TMD, transmembrane domain, CC, coiled-coil domain, P, proline-rich domain, K, K-rich domain.

Additionally, STIM1 has been shown to associate with microtubules by binding to the microtubule plus end tracking protein EB1 through a TxIP motif in STIM1 (25, 116). Time-lapse studies showed that EB1 binds and recruits STIM1 to ER-PM contact sites through growing

microtubule (117). In HeLa cells it was shown that the knockdown of EB1, which suppresses microtubule growth, or treatment with taxol to shorten microtubules, destroyed the STIM-microtubule colocalization, but did not affect store-operated Ca^{2+} entry (25).

1.3.4.3 Localization of STIM1 to the ER-PM contact sites and CRAC activation

Depletion of ER Ca^{2+} drives the oligomerization of STIM proteins, which move to ER structures located proximal to the PM, called puncta. At puncta, STIM proteins recruit Orai1, which is the CRAC channel of the PM (61, 103, 118, 119). Recruitment of Orai1 depends on its C-terminal cytoplasmic tail, since Orai1 lacking its C-terminal tail fail to colocalize with STIM1 (120, 121). The positive residues in the CAD of STIM1, binds the acidic amino acids at the C-terminal domain of Orai1 (residues 272-291) and therefore activates the CRAC channel (114, 115, 122, 123). Studies addressing the stoichiometry of STIM1 and Orai1 showed that a STIM1 dimer, or two independent STIM1 molecules, gates a tetrameric Orai1 channel. This multimer formation is necessary for CRAC current activation (119). Furthermore, the cytosolic coiled-coil domains of STIM1 may correlate with the ability to activate the CRAC channel (122).

The studies in order to investigate the interactions that retain STIM1 at the ER–PM contacts revealed that the short polybasic segment at the STIM1 C-terminus, K-rich domain, has a role (114, 124, 125). The K-rich domain was shown to interact with phosphoinositides at the cytosolic face of the PM (94, 126). The depletion of both $PI(4,5)P_2$ and $PI(3,4,5)P_3$ (phosphoinositide 3,4,5 triphosphate) of the PM, abolished STIM1 migration to puncta (126). In consistence with this data, experiments performed in this study revealed that STIM1 C terminus could bind $PI(4,5)P_2$. In the same study, I showed that the STIM2 C-terminus bind to both $PI(4,5)P_2$ and $PI(3,4,5)P_3$ more efficiently than the STIM1 C-terminus (94).

Moreover, in addition to binding PM-lipids, isotermal calorimetry and nuclear magnetic resonance studies revealed that peptides of STIM1 and STIM2 K-rich domains bind to Ca^{2+}/CaM (127). This finding is really important, since it is well known that the Ca^{2+} sensor CaM interacts with many proteins such as phosphatase calcineurin, cytoskeletal proteins and ion transporters and regulates their functions (reviewed in (128)). CaM interacts with target proteins through hydrophobic and electrostatic interactions (129). Binding of CaM to the target peptide might promote formation of an α-helix (130). Nevertheless, how the binding of CaM and PM-lipids to the K-rich domain influences the function of STIMs remains unknown.

1.3.4.4 Control of STIM1 activation

The activity of the CRAC channel is strictly regulated, as Ca^{2+} overload leads to undesirable outcomes such as apoptosis. The activation of STIM1 is controlled by an intra-molecular interaction between an acidic residue-rich auto-inhibitory domain (302-322) and a polybasic region (382-386) in CAD (131, 132). The auto-inhibitory domain of STIM1 is highly homologous

to a domain in the C terminus of Orai1, which also binds to CAD at the polybasic region (123, 131, 132). This intra-molecular interaction therefore masks the interaction surface of CAD and Orai1, thereby functioning as a regulatory switch (114, 115, 132). Additional regulation involves a Ca^{2+}-dependent feedback inhibition of the CRAC channel, where an inactivation domain (475-483) of STIM1 together with Ca^{2+}/CaM inactivates the channel (133, 134). The EF-hand containing protein CRACR2A stimulates STIM1 and Orai1 complex formation at low cytosolic Ca^{2+}, whereas high cytosolic Ca^{2+} dissociates the CRACR2A, STIM1 and Orai1 complex and thereby terminates SOCE (135).

1.3.4.5 Interaction of STIM1 with other Ca^{2+} channels

In addition to Orai1, STIM1 was shown to interact directly with TRPC (transient receptor potential channel) proteins in biochemical and functional assays, suggesting that via a specific mechanism STIM1 can gate TRPC channels (136, 137, 138). There are seven TRPC proteins in mammals. In a study investigating the interplay between STIM1 TRP channels, it was found that STIM1 binds TRPC1, TRPC4 and TRPC5 and determines their function as SOCs. Moreover, STIM1 also regulates TRPC3 and TRPC6. This regulation is not by direct interaction but STIM1 indirectly mediate the heteromultimerization of TRPC3 with TRPC1 and TRPC6 with TRPC4 (137).

STIM1 is also required for activation of the ARC (arachidonate-regulated Ca^{2+}-selective) channel (139). The ARC channel is a hetero-pentameric channel, which is formed by two Orai3 and three Orai1 proteins. The function of the ARC channel in immune cells remains elusive, but in other cell types its activation occurs independent of ER Ca^{2+} stores (140).

1.3.4.6 Localization of STIM1 to the cell surface

Initial studies on immune cells have shown that STIM1 localizes to the cell surface (101, 102). The N-terminal region of the mouse homologue of STIM1 was shown to bind to pre-B cells and this increases their proliferation. In addition to binding pre-B cells it was shown that the N-terminal domain of STIM1, which is expressed in bone marrow stromal cells, binds to mature B lymphocytes and other lympho-haematopoietic cell lineages probably by interactions with the ligands or receptors on these cells (101). These studies provide indirect evidence that STIM1 functions at the cell surface to mediate cell–cell interactions and growth regulation (102).

Moreover, the studies with the activation of ARC channels suggested that the activation of the channel is achieved by STIM1, which localizes to the cell surface (140). It was previously shown that STIM1 couldn't reach to the cell surface if it is tagged at its N-terminus by a tag that exceeds a certain size, such as YFP. Consequently, STIM1 tagged with hexahistidine tag was detected on the cell surface of HEK293 cells (141).

1.4 Aim of the thesis

In yeast, the polytopic membrane protein Ist2 localizes to the cortical ER and this localization depends on its cortical sorting signal (CSS), which directly binds to PM-lipids. Protease protection experiments suggested that Ist2 may reach the cell surface. However, in yeast with localization of the cortical ER beneath the PM, it was difficult to determine the exact localization of Ist2. One of the aims of this work was therefore to investigate the localization of Ist2 in mammalian cells. These cells provide better microscopic resolution of ER and PM, since static peripheral ER structures are rare.

The second aim of this study was to investigate whether the sorting mechanism of yeast Ist2 to the ER-PM contact sites is conserved in mammalian cells. In order to investigate this phenomenon, I tagged mammalian integral membrane proteins with CSS^{Ist2} and observed their localization by fluorescence and confocal microscopy. I explored the structural features of these domains in order to define their mobility and continuity with the rest of the ER.

Thirdly, I analyzed the mammalian integral membrane proteins, STIM1 and STIM2, which show similar localization phenotypes as the integral membrane proteins that are tagged with the CSS^{Ist2}. In order to fulfil their function in store-operated Ca^{2+} entry, STIMs form ER-PM contact sites. Therefore, I analyzed the ER-PM contact site formation mechanism of these proteins. In addition to microscopy approaches, I performed *in vitro* liposome binding experiments with the purified cytosolic C-terminal domains of STIM1 and STIM2 and investigated the requirements of this protein-lipid interaction.

Finally, I focused my studies on the regulation of STIM1 localization. STIM1, in addition to its localization in the ER, was shown to localize to the cell surface. However, in order to function in store-operated Ca^{2+} entry, it must be retained in the ER. Therefore, I investigated the mechanisms, which retain STIM1 in the ER. Moreover, I underlined an alternative function of the cell surface-located STIM1.

2 Materials and methods

2.1 Molecular Biology Methods

Frequently used buffers can be found in the Appendix section.

2.1.1 Polymerase Chain Reaction (PCR)

Materials and Equipment

Pfu polymerase (Agilent Technologies)

Taq polymerase (New England Biolabs - NEB)

10X *Pfu* Polymerase Buffer (Agilent Technologies)

dNTP (NEB)

Primers (ordered from MWG)

PCR tubes (G. Kisker GbR)

T3 Thermocycler (Biometra)

2.1.1.1 Standard PCR

The DNA fragments were amplified by PCR, from a plasmid, which is used as a DNA template. The primers contained restriction sites and 4 extra flanking bases at their 3´-ends. The PCR reaction mixture was prepared as below:

Table 2.1 Standard PCR reaction mixture

Template DNA	100 ng
10 × *Pfu* Buffer	1 ×
dNTP mix	250 μM
Forward primer	0.5 μM
Reverse primer	0.5 μM
Pfu polymerase	1 μl
Taq polymerase	0.5 μl
dH_2O	
Total	50 μl

The amplification was performed according to the conditions described below. The elongation time was calculated as 1.5 minutes per 1 kb of fragment to be amplified. The reaction was repeated for 25 cycles (steps 2-4).

Table 2.2 Standard PCR conditions

Step	Temperature	Time
1	95°C	30 sec
2	95°C	30 sec
3	58-60°C	1 min
4	68°C	1.5 min/kb
5	68°C	5 min
6	4°C	∞

2.1.1.2 Site-directed mutagenesis

In order to create point mutations, site-directed mutagenesis was performed. The primers were designed as having the desired mutation site in the middle and 15 bases long annealing sites on both 3´ and 5´-ends. The PCR reaction mixture for all mutagenesis experiments was as following:

Table 2.3 PCR reaction mixture for site-directed mutagenesis

Template DNA	50 ng
10 × *Pfu* Buffer	1 ×
dNTP mix	250 μM
Forward primer	0.1 μM
Reverse primer	0.1 μM
Pfu polymerase	1 μl
dH_2O	
Total	20 μl

The amplification was performed according to the conditions described below. The elongation time was calculated as 2 minutes per 1 kb of fragment to be amplified. The samples reaction was repeated for 18 cycles (Steps 2-4).

Table 2.4 PCR conditions for site-directed mutagenesis

Step	Temperature	Time
1	98°C	30 sec
2	98°C	30 sec
3	55°C	1.5 min
4	68°C	2 min/kb
5	4°C	∞

2.1.2 Cloning

The PCR amplified fragment (insert) and the vector were cut with same restriction enzymes, followed by purification and ligation. The correct ligation reaction was analyzed by restriction digestion following transformation and plasmid DNA isolation from the transformants.

Materials

Restriction enzymes (NEB)
10X Restriction Enzyme Buffer (NEB)
100X BSA (NEB, B9001S)
T4 DNA Ligase (NEB, M0202S)
T4 DNA Ligase Buffer (NEB, B0202S)
QIAquick Gel Extraction Kit (Qiagen)
Ethidium Bromide Solution (5mg/ml)
Agarose (Biozym Sientific GmbH)
Mini-DNA isolation kit (Qiagen)
Nucleobond Midi-prep kit (Macherey-Nagel)
6X Gel loading dye (NEB, B7021S)
E. coli DH5α strain
LB plates
UV transilluminator (Bio-Rad)

2.1.2.1 Restriction digestion

Digestion reactions were performed in the appropriate buffer and the temperature recommended by the enzyme manufacturer (NEB). For cloning experiments 5-7 μg of vector DNA was digested in a final volume of 50 μl. In order to digest the PCR amplified inserts, the PCR amplified DNA was initially purified by a PCR purification kit (Qiagen) and the DNA fragments were eluted in 40 μl of dH_2O. For digestion reactions, 40 μl of the PCR amplified DNA was used in a final volume of 50 μl reaction.

For control digestions of plasmid Mini-prep DNA, 500 ng of DNA was used in a final volume of 10 μl reaction. The digestions were performed for 2 hours and the samples were run on Agarose gel after addition of 6X gel loading dye.

For the isolation of the insert and the digested vector backbone from the Agarose gel, the QIAquick Gel Extraction Kit was used. The insert DNA was eluted in 30 μl of dH_2O, whereas 40 ml of dH_2O was used for the elution of the vector DNA.

2.1.2.2 Agarose Gel Electrophoresis

1/6 volume gel loading dye was added to the DNA from PCR or restriction digestion. The samples were loaded onto a 1% agarose gel containing 1 ng/ml ethidium bromide. The NEB Quick-Load 1 kb ladder was used as a marker to compare fragment sizes. Gels were run at 50-80 Volts for around 1 hour in TAE buffer. DNA bands were visualised by UV light on a transilluminator.

2.1.2.3 Ligation

In order to produce new plasmids, opened vector and inserts were ligated by using T4 DNA ligase. The ligation was performed either for 1 hour at 37°C or overnight at 16°C. The ligated fragments were then transformed into *E. coli* DH5α strain. The ligation reaction and the control was prepared as shown below:

Table 2.5 Ligation Reaction mixture

		Ligation	Control
10 × Ligation Buffer	1X	✓	✓
Vector (Plasmid DNA)	50-200 ng	✓	✓
Insert (PCR product)	1:3 – 1:6 molar ratio	✓	0
T4 Ligase	1 µl	✓	✓
dH_20		✓	✓
Final Volume	10 µl	10 µl	10 µl

2.1.3 Transformation

The plasmid DNAs or the DNA from the ligation reactions were transformed into *E. coli* DH5α strain. Simply, 250 ng of a plasmid or 10 µl of the ligation reaction was added into 100 µl of competent cells. Cells then were incubated on ice for 30 minutes and heat shocked for 45 seconds at 42°C. After addition of 750 µl of LB medium, the cells were incubated at 37°C heat block for 1 hour shaking. The cells were then plated on LB plates, containing the appropriate antibiotic.

2.1.4 Plasmid DNA Isolation

Plasmid DNA was isolated from *E. coli* cells, which were grown overnight in 5 ml LB with appropriate antibiotic. For the isolation of plasmid DNA the Qiagen plasmid MINI-DNA isolation kit was used according to the manufacturer's protocol. In order to isolate bigger amounts of plasmid DNA, 200 ml *E. coli* culture was grown and the Nucleobond Midi-prep kit was used for isolation.

Table 2.6 Plasmids used in this study

Plasmid	Description	Resistance in *E. coli*	Source
pEE01	GFP-Ist2-HA^{7-8}	Kan	T. Bitew
pEE03	CD4-AAXX	Amp	B.Schwappach
pEE05	GFP-Ist2	Kan	K. Maass
pEE07	CD4-GFP	Amp	This study
pEE08	CD4-GFP-CSS^{Ist2}	Amp	This study

pEE09	CD4-mCherry-CSS^{Ist2}	Amp	This study
pEE10	EGFP	Kan	Clontech
pEE15	Kir6.2-HA-GFP	Amp	This study
pEE16	Kir6.2-GFP-CSS^{Ist2}	Amp	This study
pEE17	Kir6.2-GFP-PH	Amp	This study
pEE18	MHCI-GFP	Kan	F. Momburg
pEE19	MHCI-GFP- CSS^{Ist2}	Kan	This study
pEE20	TAP1-GFP	Kan	F. Momburg
pEE21	TAP1-GFP- CSS^{Ist2}	Kan	This study
pEE23	TAP2-tdimer(12)	Kan	F. Momburg
pEE30	YFP-STIM1$_{EF}$ (D74A)	Kan	T. Meyer
pEE31	YFP-STIM2$_{EF}$ (D80A),	Kan	T. Meyer
pEE32	CD4-GFP-CSS^{Ist2} (K931A, K933A, H934A, K935A, K936A)	Amp	This study
pEE33	CD4-GFP- CSS^{Ist2} (L939P)	Amp	This study
pEE34	CD4-GFP- CSS^{Ist2} (941K-2A-942L)	Amp	This study
pEE35	CD4-GFP- CSS^{Ist2} (L942Q)	Amp	This study
pEE41	Sur1	Amp	B. Schwappach
pEE44	SH4-mCherry	Amp	This study
pEE45	Kir6.2-GFP-STIM1C	Amp	This study
pEE46	Kir6.2-GFP-STIM2C	Amp	This study
pEE47	expression, GFP-STIM1C	Amp	This study
pEE48	expression, GFP-STIM1C ΔCC	Amp	This study
pEE49	expression, GFP-STIM1C ΔK (deletion of last 25 aa, used in lipid binding)	Amp	This study
pEE50	expression, GFP-STIM1 K-rich	Amp	This study
pEE53	expression, GFP-STIM2C	Amp	This study
pEE54	expression, GFP-STIM2C ΔCC	Amp	This study
pEE55	expression, GFP-STIM2 ΔK	Amp	This study
pEE56	expression, GFP-STIM2 K-rich	Amp	This study
pEE57	expression, GFP-STIM2 K-rich (K729P)	Amp	This study
pEE58	expression, GFP-STIM2 K-rich (L726-A-F727)	Amp	This study
pEE60	expression, GFP-STIM2 K-rich (K718,719A)	Amp	This study
pEE62	YFP-STIM1$_{EF}$ ΔK	Kan	This study
pEE63	YFP-STIM2$_{EF}$ ΔK	Kan	This study
pEE64	YFP-STIM2$_{EF}$ (K729P)	Kan	This study
pEE65	YFP-STIM2$_{EF}$ (L726-A-F727)	Kan	This study
pEE66	YFP-STIM2$_{EF}$ (K718,719A)	Kan	This study
pEE68	pIRES-GFP dual promoter, Orai1	Amp	B. Niemeyer
pEE69	pIRES-GFP dual promoter, Orai2	Amp	B. Niemeyer
pEE70	pIRES-GFP dual promoter, Orai3	Amp	B. Niemeyer
pEE71	HA-STIM1	Kan	This study
pEE72	HA-STIM2	Kan	This study
pEE82	GFP-Sec61γ	Kan	H. Lorenz
pEE84	ss-RFP-KDEL	Kan	H. Lorenz
pEE92	HA-STIM1ΔK	Kan	This study

pEE94	HA-ΔN_{ext}-STIM1	Kan	This study
pEE96	HA-STIM1ΔK STIM2 K-rich	Kan	This study
pEE103	TRPC1	Amp	D. Clapham
pEE104	TRPC4	Amp	D. Clapham
pEE127	HA-STIM1 R500A (500RQR to AQA)	Kan	This study
pEE128	HA-STIM1 R500,530A (500RQR and 530RQR to AQA)	Kan	This study
pEE130	HA-STIM1 R311,500,530A	Kan	This study
pEE137	HA-STIM1 R530A	Kan	This study
pEE138	HA-STIM1ΔK, R500A	Kan	This study
pEE139	GFP-Orai1	Kan	This study
pEE142	expression, GFP-STIM1C ΔK (deletion of last 15 aa, used in CaM binding)	Amp	This study
pEE157	expression, GFP-STIM1C ΔK K3A	Amp	This study
pEE158	expression, GFP-STIM1C ΔK $H2_{AA}$	Amp	This study
pEE159	expression, GFP-STIM1C ΔK $H2_{AA}$	Amp	This study
pEE160	expression, GFP-STIM1C ΔK ΔCaMI	Amp	This study
pEE161	expression, GFP-STIM1C ΔK ΔCaMI-II	Amp	This study
pEE162	GFP-NFAT	Kan	R. Kehlenbach
pEE163	GalTase-RFP	Kan	H. lorenz

2.2 Mammalian Cell Culture Methods

Material, Media and chemicals

10 cm dishes (TPP)
Cryo-tubes (NeoLab)
DMEM Glutamax (Gibco, 61965)
DMEM/F12 (Gibco, 21331)
Opti-MEM (Gibco, 31985)
Fetal Bovine Serum (FBS) (Gibco, 10270-106)
Glutamine (Gibco, 25030)
Sodium pyruvate (Gibco, 11360)
0.05% Trypsin-EDTA (Gibco, 25300)
DMSO (Sigma)
Fugene HD (Roche)

2.2.1 Cell lines

Table 2.7 Cell lines used in this study

Cell Line	Description
HEK293	HEK293 cells are human embryonic kidney cells and can either be adherent or suspension cells.
HEK293T	HEK293T cells are human embryonic kidney cells and can either be adherent or suspension cells. The HEK293T cells are transformed with large T antigen of the SV40 virus.
HeLa	HeLa cells are adherent cells derived from human cervix carcinoma.
U2OS	U2OS cells are human osteosarcoma cells and are adherent cells
RPE-1	RPE-1 cells are human retinal-pigmented epithelial cells and are adherent cells. They are telomerase reverse transcriptase immortalized.

2.2.2 Maintaining cells in culture

All cells were grown and maintained at 37°C, 5 % CO_2 in a cell incubator. Culture conditions vary widely for each cell type. Below is shown the cell type specific culturing conditions.

Table 2.8 Culturing conditions of cell lines used in this study

Cell Line	Description
HEK293	DMEM/F12, 10% FBS, 2mM Glutamine
HEK293T	DMEM/F12, 10% FBS, 2mM Glutamine
HeLa	DMEM Glutamax, 10% FBS, 2mM Glutamine, 1mM Sodium Pyruvate
U2OS	DMEM Glutamax, 10% FBS, 2mM Glutamine, 1mM Sodium Pyruvate
RPE-1	DMEM/F12, 10% FBS, 2mM Glutamine

In order to to replenish nutrients and avoid the potentially harmful metabolic byproducts and dead cells, the cells were passaged every 2 or 3 days according to the confluency of the cells.

2.2.2.1 Passaging of the cells

In order to passage the cells, the medium was aspirated and the adharent cells were gently washed once by 10 ml of 1X PBS. PBS was then aspirated and 2 ml of Trypsin-EDTA was added onto cells and distributed all over the plate for the detachment of the cells from the plate. The Trypsin-EDTA was aspirated and the cells were incubated in 37°C incubator for maximum 10 minutes. 10 ml of appropriate medium was added onto cells to resuspend and collect the cells. The number of the cells was calculated by counting with a haemocytometer and they were seeded at a confluency according to the type of experiment that would be performed. For continuation of the cells in culture, 1/10 dilution was done.

2.2.2.2 Freezing and thawing of the cells

For freezing, the cells were harvested at 1000 rpm for 2 minutes and washed once with 1X PBS. After removal of the PBS, the cells were resuspended in freezing medium, which contains 10% DMSO and 90% FBS. 1 ml of the suspension was added into each cryo-tube. In general, from one 10 cm dish with 80% confluency, 2 ml of cell suspension was generated. The tubes containing the cells were then placed in -80°C freezer. For longer storage, the cells were transferred to the liquid nitrogen tanks.

For thawing, the cells taken from liquid nitrogen were placed into 37°C water bath. In order to avoid the toxic effect of DMSO, this process should be performed quickly. As soon as the cells were thawn, they were transferred into 15 ml falcon tubes containing the appropriate medium. In order to get rid of residual DMSO, the cells were washed with the medium for two times. After the last wash, they were resuspended in medium and transferred into 10 cm dishes and placed in 37°C incubator.

2.2.3 Transfection of cells

In order to introduce plasmids into the cells, the Fugene HD transfection reagent was used. For different cell lines, different reaction mixtures were prepared.

Table 2.9 Transfection conditions for different cell lines used in this study

Cell Line	DNA : Fugene HD
HEK 293T HEK293	1 μg : 2.5 μl
HeLa	1 μg : 3 μl
U2OS	1 μg : 3 μl
RPE-1	1 μg : 3 μl

The reaction mixture was prepared as described in manufacturer´s manual. Briefly, the DNA was diluted 1:100 in Opti-MEM (per 1 μg DNA, 100 μl Opti-MEM) and the Fugene HD was added by continuous pipetting 20-30 times.

Table 2.10 Transfection reaction mixture

DNA	1 μg
Opti-MEM	100 μl
Fugene HD	2.5-3 μl

The mixture was kept in RT for 20 minutes and then added onto the pre-seeded cells.

For a better transfection efficiency, the cells were seeded one day before into appropriate dishes according to the type of the experiment.

2.3 Microscopy Techniques

Materials and Chemicals

12-well dishes (TPP)
Round coverslips (12 mm diameter, Peske)
35 mm glass bottom dishes (0.16–0.19 mm) (MatTek)
Formaldehyde (methanol free, Polysciences, 04018)
ER-Tracker Blue-White DPX dye (Invitrogen, E12353)
FURA-2AM (Invitrogen, F1221)
Leibovitz's medium (Gibco, 21083)
Thapsigargin (Tg, Calbiochem, 586005)
DAPI (4′,6-diamidino-2-phenylindole)

Equipment
Olympus CellR inverted microscope
Zeiss Axiovert 200M inverted microscope
Nikon Ti inverted microscope
PerkinElmer UltraView spinning disc confocal on Nikon Ti inverted microscope

2.3.1 Immunofluorescence

Table 2.11 Antibodies used in immunofluorescence experiments

Antibody	Species	Dilution	Source
anti-HA.11 Clone: 16B12	mouse	1:1000	BAbCO
anti-calreticulin	rabbit	1:300	Affinity Bioreagents
anti-calnexin	rabbit	1:50	A. Helenius
anti-Sec61β	rabbit	1:300	B. Dobberstein
anti-Sec61γ	rabbit	1:100	S. High
anti-TRAM	rabbit	1:50	T. Rapoport
anti-PDI	mouse	1:300	Abcam
anti-GRP78/BiP	rabbit	1:100	Abcam
anti-rabbit Alexa Fluor® 546	goat	1:600	Invitrogen
anti-mouse Alexa Fluor® 568	goat	1:600	Invitrogen

Solutions

Fixation Solution-1

Total	dH_2O	10X PBS	10% FA	1 M sucrose
15 ml	8.625 ml	1.5 ml	3 ml	1.875 ml

Fixation Solution-2

Total	dH_2O	10X PBS	10% FA
15 ml	12 ml	1.5 ml	1.5 ml

In order to prepare cells for observation with fluorescence microscopy, the cells were first seeded onto ethanol-washed coverslips, which were placed in 12-well dishes. 300000 HEK293T cells or 100000 U2OS or RPE-1 cells were seeded. The next day, cells were transfected with 0.5-1 μg of desired plasmid. For co-transfection experiments, in total of 1 μg DNA was used. The transfection was done for 14-20 hours. The next day, the immunofluorescence was performed as following:

The medium was aspirated and the adherent cells were washed gently two times by 1X PBS (1 ml per well). In the case of HEK293T cells, after aspiration of the medium, the fixation solution was added directly. After the PBS wash, 1 ml of fixation solution-1 was added onto cells and incubated for 20 minutes at room temperature (RT). The fixation solution-1 was aspirated and the cells were washed two times with 1X PBS. The fixation solution-2 was added and incubated for 10 minutes at RT. After fixation, the cells were washed and for permeabilization of the cells 1 ml of permeabilization solution (0.3% Triton, 0.05% SDS in 1X PBS) was added into each well. The incubation with the permeabilization solution was done for 15 minutes at RT. After permeabilization the cells were washed two times with 1X PBS. In order to get rid of nonspecific

binding of antibodies, the 1 ml of blocking solution (10% FBS in 1X PBS) was added onto cells and incubation was performed for 1 hour at RT.

For incubation with the primary antibody, the desired concentration of the antibody was prepared in 1X PBS, which was containing 5% FBS. 25 μl of the antibody solution was dropped onto a parafilm and the coverslip, cells facing the antibody drop, was placed onto the drop. The primary antibody incubation was done for 1 hour at RT. The coverslips then placed back into the 12-well dish and were washed three times with 1X PBS. The secondary antibody was prepared in the same way and this time the samples were kept in dark for 1 hour. After the incubation with the secondary antibody, the coverslips were placed back in the 12-well dish and washed three times with 1X PBS. In order to mount the coverslips onto the slides, 20 μl of mowiol was used. The fixed cells on the coverslip were dipped into dH_2O prior to mounting on slides. The samples were dried either for 1 hour at 37°C or overnight at 4°C.
The treatments with Tg or EGTA were performed prior to fixation.

2.3.2 Epi-fluorescence microscopy of fixed cells

In order to visualize the localizations of the proteins of interest, either Olympus CellR inverted microscope with Plan-Apo 60X / 1.4 numerical aperture (NA) oil objective or Zeiss Axiovert 200M inverted microscope with Plan Apo 63X / 1.4 NA oil objective with 360, 488 and 561 nm filters were used. The images were then prepared by using either ImageJ and Adobe Photoshop or Metamorph softwares.

2.3.3 Epi-fluorescence microscopy of live cells

For staining the entire ER of the U2OS cells expressing GFP-Ist2-HA[7-8], the cells were seeded in 35-mm glass bottom dishes. The cells were transfected with 1 μg of the DNA for 18 hours. Prior to the microscopy, the cells were incubated 30 minutes at 37°C in 2 ml of Leibovitz's medium, containing 10% FBS and 1 μM ER-Tracker Blue-White DPX dye, which can be imaged by DAPI (4′,6-diamidino-2-phenylindole) filter. Imaging was performed by using a Zeiss Axiovert 200M Plan Apo 63X / 1.4 NA oil objective with 360 and 488 nm filters.

2.3.4 Total Internal Reflection Fluorescence Microscopy (TIRFM)

The U2OS cells were seeded in 35-mm glass bottom dishes. Next day they were co-transfected with the CD4-GFP (0.5 μg) and SH4-mCherry (0.5 μg) or CD4-GFP-CSS^{Ist2} (0.5 μg) and SH4-mCherry (0.5 μg). 18 hours after the transfection, the cells were fixed as explained in part 2.3.1. After fixation, they were kept and imaged in 1X PBS. The images were acquired with a TIRF system on a Nikon Ti inverted microscope with a TIRF 60x/1.49 NA oil objective and 488 and 561 nm laser lines. A Hamamatsu ORCA-AG high-resolution sensitive black and white camera was used to acquire the images. The images were prepared by using ImageJ and Adobe Photoshop.

2.3.5 Confocal Microscopy

The U2OS cells, which were grown in 35-mm glass bottom microwell dishes were transfected with 1 μg of the mentioned constructs for 18 to 20 hours. 30 minutes prior to imaging, the cells were incubated with 1 μM ER-Tracker Blue-White DPX dye in 2 ml of Leibovitz's medium containing 10% FBS. They were washed once with 1X PBS and the images were acquired in 2 ml of Leibovitz's medium containing 10% FBS at 37°C. The live cell confocal images were acquired on a PerkinElmer UltraView spinning disc confocal on Nikon Ti inverted microscope with 405 and 488 nm laser lines and a Hamamatsu EM-CCD camera. The Plan Apo 100x/1.4 NA oil objective was used to acquire z-stack with 150 nm interval spacing. To increase localization precision, z-stacks were deconvolved with Huygens software 3.1 (Scientific Volume Imaging).

2.3.5.1 Fluorescence Recovery After Photobleaching (FRAP) and Fluorescence Loss in Photobleaching (FLIP)

The U2OS or HeLa cells, which were grown in 35-mm glass bottom dishes were transfected with 1 μg of mentioned constructs. For co-transfection, in total of 1 μg DNA was used, e.g. 0.5 μg of Kir-GFP-CSS^{lst2} and 0.5 μg of ss-RFP-KDEL. They were imaged in Leibovitz's medium containing 10% FBS at 37°C. The PerkinElmer UltraView spinning disc confocal system on a Nikon Ti inverted microscope with 60x Plan Apo/1.2 NA water objective was used for imaging. The 488, 514 and 561 nm laser lines were used for photobleaching the specified area with 100% power. For FRAP experiments of full and half patch, after photobleaching, images were acquired at half-second intervals for 300 seconds (n = 6). For FRAP of GFP-Sec61γ that is localized to a patch or to reticular ER was bleached by a 488-nm laser line and the images were acquired in one second intervals for 120 seconds (n = 4). For FRAP of ss-RFP-KDEL, the laser lines 514 and 561 nm were used and the image acquirement was performed in 60 millisecond intervals for 20 seconds (n = 6).

For the FLIP experiment, ss-RFP-KDEL in a full patch was bleached with the laser lines 514 and 561 nm with 100% power. The images were acquired every 60 milliseconds for 600 seconds (n = 4).

For all FRAP and FLIP experiments the fluorescence decrease was normalized according to overall bleach of a neighbouring cell. The background was subtracted. For the analysis of bleaching, the corrected fluorescence intensity (cFI) was calculated according to the formula below and the mean averages of the normalized data for each set of FRAP experiments were plotted and FRAP curves were fitted to a single exponential curve by using Microsoft Excel.

$$cFI = [(FI_{FRAP} - FI_{bg}) / (FI_{FRAPt0} - FI_{BGt0}) \times 100] \times [(100 - FI_{bleach} / FI_{bleacht0}) / 100] + 1$$

FI_{FRAP} = fluorescence intensity of bleached region at any time
FI_{BG} = fluoresce intensity of a background region at any time
FI_{FRAPt0} = fluorescence intensity of bleached region at time zero
FI_{BGt0} = fluoresce intensity of a background region at time zero
FI_{bleach} = fluorescence intensity of a region in neighbouring cell at any time
$FI_{bleacht0}$ = fluorescence intensity of a region in neighbouring cell at time zero

2.3.6 Intracellular Ca^{2+} Imaging

Chemicals

2-Aminoethoxydiphenyl borate (2-APB, Sigma, D9754)

Ringer Solution	Tg Solution	2-APB Solution
155 mM NaCl	155 mM NaCl	155 mM NaCl
4.5 mM KCl	4.5 mM KCl	4.5 mM KCl
1 mM $MgCl_2$	1 mM $MgCl_2$	1 mM $MgCl_2$
10mM D-Glucose	10mM D-Glucose	10mM D-Glucose
5 mM Hepes	5 mM Hepes	5 mM Hepes
2mM $CaCl_2$	1 μM Tg	2mM $CaCl_2$
		50 μM 2-APB

pH adjusted with HCl to 7.4

For the imaging of cytosolic Ca^{2+} levels, the HEK293T cells were seeded in 35 mm glass bottom dishes and transfected with the mentioned STIM1 constructs (0.5 μg) and pIRES-GFP dual promoter Orai1 (0.5 μg) for 18-20 hours. Prior to imaging, the cells were loaded with 4 μM FURA-2AM dye for 30 min in Ringer solution at 37ºC. The cells were then incubated in Ringer solution for an additional 30 min at 37ºC. 5 min prior to imaging, cells were kept in the nominally Ca^{2+} free (NCF) Ringer solution (without $CaCl_2$). During the experiment, the buffers were changed as shown in the graphs at indicated times. Imaging was performed by Nikon Ti inverted microscope with 20X SFluor objective. Images were taken every 5 seconds with 340nm and 387nm excitation wavelengths. The transfected cells according to GFP signal were selected for analysis. The analysis of the images and the calculation of the intensity ratios (F340/F387) were done by the Nikon imaging software (NIS-elements). The averages of at least 150 cells from three independent experiments were calculated and the graphs were plotted in Microsoft Excel.

2.4 Biochemistry Techniques

2.4.1 Expression and purification of 6xHis-GFP-fusion proteins

Materials and Chemicals

Microfluidizer (EmulsiFlex-C5)
Isopropyl-β-D-thiogalactopyranosid (IPTG, Applichem)
E. coli BL21 (DE3) Codon Plus
Spectrophotometer (Pharmacia Biotech)
Ni-NTA (nitrilotriacetic acid) Agarose Beads (Qiagen)
LB Ampicillin (LB+Amp)
Imidazole (Merck)
EDTA-free protease Inhibitor complex (Roche)
Dialysis Membrane (Spectrum, MWCO=12000-14000 kDA)

Buffers

Lysis Buffer

50 mM Tris/HCl pH 7.5
250 mM NaCl
20 mM Imidazole
2 mM EDTA

Dialysis Buffer 1

50 mM Tris/HCl pH 7.5
250 mM NaCl

Dialysis Buffer 2

25 mM Hepes pH 7.5
150 mM KCl
(pH adjusted by KOH)

Elution Buffer

50 mM Tris/HCl pH 7.5
250 mM NaCl
300mM Imidazol

2.4.1.1 Expression of 6xHis-GFP-fusion proteins

For the expression of GFP-fusion constructs, they were transformed into *E. coli* BL21 (DE3) Codon Plus strain. A pre-culture was prepared over day in 50 ml of LB+Amp. The culture was then diluted to 0.1 OD in 500 ml LB +Amp and incubated for additional 1-1.5 hours at 37ºC until the OD reached 0.4-0.6. The cultures were cooled down to RT by incubating for 30 min at RT. After addition of 0.25 mM IPTG to final concentration, they were incubated at 25ºC overnight.

2.4.1.2 Purification of 6xHis-GFP-fusion proteins

Next day cells were spun down at 4000 rpm for 10 minutes and resuspended in 30 ml of ice-cold lysis buffer containing 1mM PMSF, 10 mM β-mercaptoethanol and protease inhibitor complex. The lysis of the resuspended cells was performed by a microfluidizer at a pressure of 15000-20000 bars. The lysate was then centrifuged by using a pre-cooled Ti45 rotor at 32000 rpm for 45 minutes. In the mean time the Ni-NTA beads were washed three times with cold lysis buffer in 50 ml falcon tubes. The centrifugation of the beads was done at 1000 rpm for 1 minute. The supernatant of the lysate was then added onto the pre-washed beads and incubated for 1 hour at 4ºC rotating.

After the incubation for protein binding, the non-specific binding of other proteins were eliminated by several washing (3 to 5 times) steps with 25 ml of lysis buffer. The beads were transffered to 15 ml falcon tube and 2 ml of elution buffer was added. After incubation with the elution buffer for 1 hour at 4ºC rotating, the beads were spun down. The supernatant was loaded into dialysis membrane. Dialysis was performed in dialysis buffer-1 for CaM Binding experiments and in dialysis buffer-2 for liposome binding experiments. A step-wise dialysis was performed by incubation for instance in 500 ml of dialsis buffer-1 contaning 150 mM Imidazole and dialysis buffer-1 contaning 75 mM Imidazole for 1 hour and overnight in 1 L dialysis buffer-1.

Next day, the proteins were transferred into 1.5 ml tubes and stored at -20ºC. Samples were run on 10% SDS-PAGE and analyzed by Coomassie Blue Staining.

2.4.2 Calmodulin binding assay

Materials and Buffers

Calmodulin (CaM) affinity resin (Agilent technologies, 214303-52)

NP-40 (Calbiochem)

CaM binding buffer

25 mM Tris/HCl pH 7.5
150 mM NaCl
1 mM $CaCl_2$ or 0.5 mM EGTA
0.1 % NP-40

2X Sample Buffer

100 mM Tris/HCl pH 6.8
4% SDS
20% glycerol
100 mM DTT
0.1% bromophenol blue

30 μl of the CaM beads were washed with CaM binding buffer. The amount of NP-40 or concentration of NaCl was adjusted according to the type of the experiment. The GFP or GFP-fusion proteins (1 μM) were incubated with CaM beads in 600 μl of CaM binding buffer for 1 h at 4ºC, rotating. The beads were then spun down at 2000 rpm for 1 minute and a sample from the supernatant was taken as unbound fraction. The beads were washed four times with the CaM binding buffer for elimination of non-specific binding of proteins. 2X sample buffer was added to the beads and they were boiled at 95ºC for 5 min. The samples were then run on 10% SDS-PAGE. Blots were developed with a GFP antibody (1:5.000, SantaCruz).

2.4.3 Liposome binding assay

Materials and Equipment

Round-bottom flask (±10ml volume)
Pipettes (Hamilton)
Methanol (Sigma-Aldrich Fluka)
Chloroform (Sigma-Aldrich Fluka)
HEPES (Roth)
KCl (Calbiochem)
Lipids (Avanti Polar Lipids)
Spectrofluormeter (Jasco FP-6500)
Mini Extruder (Avanti Polar Lipids)
1000 nm filters (Avanti Polar Lipids)
Dynamic Light Scattering (Zetasizer 1000HS_A; Malvern Instruments)
NanoDrop (ND1000 Spectrophotometer)

Table 2.12 Lipids used for preparation of liposomes

Lipid	Ordering Number	Source
Phosphatidylcholine (PC)	840055	Bovine liver
Phosphatidylethanolamine (PE)	840026	Bovine liver
Phosphatidylserine (PS)	840032	Porcine brain
Phosphatidylinositol (PI)	840042	Bovine liver
Sphingomyelin (SM)	860061	Poultry eggs
Cholesterol (CL)	700000	Ovine wool
Rhodamine-phosphatidylethanolamine (Rhod-PE)	810158	synthetic
Phosphatidylinositol-4,5-bisphospahe ($PIP(4,5)P_2$)	840046	Porcine brain
Phosphatidylinositol-3,4,5-triphospahe ($PIP(3,4,5)P_3$)	850166P	synthetic

HK-buffer
25mM HEPES
150mM KCl
pH 7.4 (with KOH)

2.4.3.1 Preparation of liposomes

The lipids were added one by one in a methanol and chloroform washed round-bottom flask by using Hamilton pipettes. The mixture of the lipids was dried with a rotary evaporator (350mPa and down, 150rpm, 37˚C water bath) and after evaporation of the chloroform, the drying was continued at 20mPa for at least 20 minutes. The dried pellet was resuspended by continues shaking in HK-buffer containing 10% sucrose resulting in liposomes with 4mM concentration. In order to have 4mM concentration of liposomes, initially prepared 1 ml lipid mixture (3mM) was dissolved in 750 μl of HK-buffer containing 10% sucrose. The sucrose is necessary to pellet liposomes during centrifugation in further steps. The resuspended liposomes were homogenized by 10 freeze thaw cycles. The freezing was performed in a box containing some dry ice and isopropanol. The frozen liposomes were thaw in 37˚C water bath. During freezing and thawing, flasks were rotated so that the liposomes freeze in a more homogeneously distributed way on the surface of the flask- thin layer like. After this homogenization step, liposomes were sized by using a mini-extruder and a filter membrane, which has a pore size of 40-1000 nm. This extrusion was performed 21 times and the liposomes were transferred into 1.5 ml tubes. They were stored in 4˚C fridge for 3-5 days. Table 2.13 shows an example for 1 ml of $PI(4,5)P_2$ containing PM like liposome preparation.

The sizes of the liposomes were checked by dynamic light scattering to be around 200 nm (roughly 180 nm to 230 nm) in diameter.

Table 2.13 PM-$PI(4,5)P_2$ -like liposome preparation (1 ml of lipid mixture)

Lipid	MW (Da)	mol%	conc. (mg/ml)	Volume (μl)
PC	786.12	12.5	25	24
PE	768.06	9	10	41
PS	810.03	5	10	24
PI	909.12	5	10	27
$PIP(4,5)P_2$	1098.19	5	1	329
SM	703.44	12.5	10	53
CL	386.66	50	10	116
Rhod-PE	1233.04	1	1	74
		100		
Average MW	589.52		**Sum (μl)**	689
			Chloroform (ml)	1.31

2.4.3.2 Liposome binding

In the case of having two different types of liposomes, such as PC or PM-like, the ratios were arranged according to their rhodamine signals. The readings were done by spectrofluormeter. The 488 nm excitation and 585/20 nm emission was used for rhod-PE.

In order to calculate the concentrations of the GFP-fusion recombinant proteins, the amount of GFP alone was calculated by Nanodrop. The GFP signals of the other fusion proteins, which were detected by spectrofluometer were normalized to GFP alone. The 488 nm excitation and 530/20 nm emission was used for GFP. The ratio between the fluorescence of GFP-fusion protein and GFP alone was then multiplied with the concentration of GFP alone.

Prior to incubation of the protein with the liposomes, the 25 μl of liposomes were blocked in 100 μl of HK-buffer containing 4% of BSA in Thermomixer for 1 hour at 25˚C shaking at 400 rpm. The liposomes were washed with 1 ml of HK-buffer and centrifuged down at 15000 xg for 10 min at 25˚C. The supernatant was aspirated and 1 or 3 μM of protein diluted in 100 μl of HK-buffer was added to the liposomes. The incubation was done in Thermomixer for 3-4 hours at 25˚C and 400 rpm.

After incubation, the liposomes were washed with 1 ml of HK-buffer and spun down at 15000 xg for 10 min at 25˚C. The pellet was resuspended in 300 μl of HK-buffer and the binding was analyzed by flow cytometry as described in section 2.5.2.

2.4.4 Preparation of yeast membranes and proteinase K treatment

Materials and Buffers

Glass beads 0.425-0.6 mm (Sigma)
Proteinase K (Merck)

Lysis Buffer
20 mM Hepes
50 mM Potassium Acetate
5 mM Magnesium Acetate
pH was adjusted to 7.6 by KOH

HU Buffer
8 M Urea
5% SDS
200 mM Tris/Hcl pH 6.8
1 mM EDTA
0.025% Bromophenol blue
4% β-mercaptoethanol

*Ist2*Δ cells (MATa *ist2*Δ*::HIS3MX* by C. Jüschke-CJY3) expressing either GFP- HA^N-Ist2 or GFP-Ist2-HA^{7-8} were grown in selective medium containing 2% (w/v) raffinose. Expression was induced by the addition of 2% (w/v) galactose for 2 hours. Cells from 5 OD_{600} units were spun down and resuspended in 1 ml of a Lysis Buffer. Lysis was performed on ice with glass beads and vortexing. The beads were centrifuged at 1200 xg, for 2 minutes, at 4°C. The supernatant was then transferred into new tube and centrifuged for 20 minutes at 25000 xg and the resulting pellets was resuspended in Lysis Buffer and incubated at 37°C for 30 minutes with 5 μg/μl proteinase K.

After addition of HU buffer to the samples, they were heated in 50°C heat-block for 20 minutes prior to loading on 15% SDS-gel.

2.4.5 SDS-PAGE and Immunoblotting

Materials and Equipment

Mini Protean Gel System (BioRad)
Nitrocellulose membrane (0.45 μM pore size, Protran, Whatman)
Luminescent Image Analyzer LAS-4000 (FUJIFILM)
ColorPlus Prestained protein Ladder (NEB, P7711S)
Acrylamide 37.5 :1 (rotiphorese gel 30, Roth)
TEMED (Sigma)
APS (Sigma)
SDS (Roth)
Tween-20 (Sigma)
Chemiluminescence Blotting Substrate (Roche)

2.4.5.1 SDS-PAGE

Protein samples were separated under denaturing conditions by SDS-PAGE. Mini gels (0.75 mm or 1 mm) were prepared according to the following scheme:

Table 2.14 Solution mixture for polyacrylamide gel preparation

	Separating Gels (10 ml)		Stacking Gel (5 ml)
	10 %	15 %	4 %
30 % Acrylamide 37.5 : 1	3.3 ml	5 ml	670 μl
dH_2O	4.5 ml	2.8 ml	3 ml
2 M Tris-HCl pH 8.8	2 ml	2 ml	-
0.5 M Tris-HCl pH 6.8	-	-	1.25 ml
10 % SDS	100 μl	100 μl	50 μl
10 % APS	50 μl	50 μl	50 μl
TEMED	5 μl	5 μl	5 μl

Samples were loaded on polyacrylamide gels and run at 25 mA for approximately 1 hour in SDS-PAGE running buffer. ColorPlus prestained broad range protein marker was used to compare protein sizes.

2.4.5.2 Immunoblotting

Table 2.15 Antibodies used in immunoblotting experiments

Antibody	Species	Dilution	Source
anti-HA.11	mouse	1:5000	BabCo
anti-GFP	rabbit	1:5000	SantaCruz
anti-Kar2	rabbit	1:20000	M. Seedorf
anti-Ist2	rabbit	1:10000	M. Seedorf

Proteins were transferred onto nitrocellulose membranes by semi-dry blotting. The standard blotting conditions were 110 mA per blot for 2 hours. Proteins on nitrocellulose membranes were stained with Ponceau S solution (1 % (v/v) acetic acid, 0.5 % (w/v) Ponceau S) for 5 min washed with H_2O.

In general, blots were blocked in 5 % dry skimmed milk dissolved in 1X PBS containing 0.05 % (w/v) Tween (PBS-T) for 30 minutes at RT. The blots were incubated at 4 °C overnight with the primary antibody in 5% milk in PBS-T. Next day the blots were washed three times with 1XPBS-T. After washing, they were incubated with the secondary antibody coupled to horseradish peroxidase in 5% milk in PBS-T for up to 1 hour at RT. The blots were washed three times with PBS-T. After incubation with the Chemiluminescence Blotting Substrate, light emission was acquired by LAS-4000.

2.5 Flow cytometry

Materials, Buffers and Equipment

6-welldishes (TPP)
FACS tubes (NeoLab)
Enzyme-free PBS-based cell dissociation buffer (Gibco, Cat. 13151-014)
FACSFlow buffer (BD, 342003)
Propidium iodide (Invitrogen, P3566)
Brefeldin A (BFA) (Sigma, B7651)
FACScan (Becton Dickinson)
FACS Calibur (Becton Dickinson)

2.5.1 Flow cytometry of cells

Table 2.16 Antibodies used in flow cytometry experiments

Antibody	Species	Dilution	Source
anti-CD4-R-phycoerythrin (PE)	mouse	1:100	Dianova, (OMA1-03301)
anti-HA.11	mouse	1:200	BabCo
anti-mouse PE-conjugated AffiniPure F(ab')2 fragment	goat	1:200 1:150	Dianova (115-116-146) Invitrogen (P852)

Cells were grown in 6-well dishes. HEK293, HeLa and U2OS cells were transiently transfected with 1 μg of GFP-Ist2-HA$^{7-8}$, CD4-GFP or CD4-GFP-CSS^{Ist2} constructs for 18 hours. For the analysis of the surface expression of HA-tagged STIMs, the HEK293T cells were transfected with 0.5 μg of HA-STIM construct with 0.5 μg GFP or pIRES-GFP dual promoter Orai1. HeLa and U2OS cells were collected by using enzyme-free PBS-based cell dissociation buffer, HEK293 and HEK293T cells were simply collected by resuspension in their medium and transferred in pre-chilled 1.5 ml tubes. Cells were then spun down in a 4ºC centrifuge at 2,000 rpm for 2 minutes. After washing once with 1 ml FACSFlow buffer they were incubated with CD4-PE or HA.11 antibodies in 100 μl of FACSFlow buffer on ice for 30 minutes for surface staining. Cells were then washed once with FACSFlow buffer. The secondary antibody incubation for HA-tagged constructs was performed with PE-conjugated AffiniPure F(ab')2 fragment goat anti-mouse IgG antibody (1:200 Dianova or 1:150 Invitrogen) in 100 μl of FACSFlow buffer on ice for 30 min. Cells were then washed with ice-cold FACSFlow buffer and resuspended in 300 μl of FACSFlow buffer containing 1 μg propidium iodide (PI). Fifteen thousand HEK293 and HeLa, 10000 U2OS and 30000 HEK293T cells were gated for PI-negative population and the CD4 or HA surface signal was measured by using FACScan. The cut offs for GFP-positive cells were set according to cells either nontransfected and stained with antibodies or transfected with CD4-AAXX and not stained with antibodies. The cut offs for HA and CD4 surface signals were set according to cells transfected with GFP.

The percentage of the cells expressing HA-tagged or CD4 protein on the cell surface was calculated according to the ratio of PE-positive cells to PE- and GFP-positive cells. For the EGTA or Tg treatment, 2 mM EGTA or 1 μM Tg was added to the cells in medium for 1 hour prior to experiment. To block the secretory pathway, after transfection for 12 hours, the cells were treated with 1 μg/ml BFA for 6 hours. Three independent sets of experiments were done and the averages of the experiments were plotted in Microsoft Excel. The standard error of the mean (s.e.m.) was calculated for the error bars.

2.5.2 Flow cytometry of liposomes

The setup of the flow cytometry of liposomes was previously done as described in (142). FACS Calibur was used to count the rhodamine-positive liposomes. The GFP signal cutoff was done by liposomes contaning no protein. 30000 liposomes were counted and the data were processed with CellQuest Pro software. The background binding of GFP alone was substracted. In addition, shape index factor of the rhodamine signal was calculated by dividing the rhodamine signal of GFP-fusion protein to rhodamine signal of GFP alone. Briefly the formula below was used to determine the corrected fluorescence units (cFU), thus binding.

$$cFU = \frac{(FU_{GFP\text{-}fusion} - FU_{GFP\text{-}alone})}{(FU\ Rhodamine_{GFP\text{-}fusion} / FU\ Rhodamine_{GFP\text{-}alone})}$$

The data of three independent experiments were prepared and the graphs were plotted in Microsoft Excel.

3 Results

In yeast, Ist2 protein predominantly localizes to the cortical ER and makes contact with the PM through an interaction between its cortical sorting signal (CSS^{Ist2}) and the lipids of the PM. Protease protection experiments showed that Ist2 could also reach to the cell surface independently of Golgi function. However, the cortical ER beneath the PM makes it difficult to determine the exact Ist2 in yeast. This led me to investigate this drawback in mammalian cells. The ER of mammalian cells is also capable of forming contacts with the PM, however it does not accumulate beneath the PM as yeast cortical ER does. Mammalian cells, which are larger in size, give higher microscopic resolution and were therefore suitable to study the localization of Ist2. Moreover, it was of interest to gain information on the conservation of the novel trafficking pathway of Ist2 in mammalian cells. Since the CSS^{Ist2} is not conserved in mammalian homologues of Ist2 (TMEM16 family), I attached CSS^{Ist2} to the cytosolic C-termini of mammalian integral proteins and investigated the localizations of these chimeras in detail.

Moreover, by *in silico* analysis, we identified that the K-rich region of CSS^{Ist2} shows similarity with the K-rich domain of mammalian STIM2 protein. This led me to investigate the molecular mechanism that lies behind the localization of STIM proteins. I showed that both STIM1 and STIM2 are capable of forming ER-PM contact sites via their K-rich domain by binding to PM lipids as K-rich region of CSS^{Ist2} does.

Furthermore, STIM1, which dominantly stays in the ER, was initially shown to travel to the cell surface. I was therefore interested in the regulation of STIM1 localization, which is either to ER-PM contact sites or to the cell surface. I identified two types of signals that retain STIM1 in the ER. One of these signals is the di-arginine based ER retention signal and the other is the K-rich domain, which I showed that is regulated by cytosolic Ca^{2+} levels. I furthered my studies on the cell surface function of STIM1 and found Orai1 as likely interacting Ca^{2+} channel.

3.1 Yeast Ist2 forms ER-PM contact sites in mammalian cells

Initial experiments in yeast showed that a pool of Ist2 may reach to the cell. This trafficking of Ist2 to the cell surface was independent of the Golgi function, suggesting that Ist2 follows an unconventional trafficking pathway. In order to investigate whether Ist2 reaches to the cell surface and whether this unconventional transport is conserved in mammalian cells, I investigated the localization of Ist2 in different cell lines, such as human embryonic kidney cells (HEK293), human cervix cancer cells (HeLa) and human bone osteosarcoma cells (U2OS). For detection at the cell surface, a hemagglutinin (HA) tag between the predicted transmembrane domains (TMD) 7 and 8 of Ist2 were inserted, resulting in GFP-Ist2-HA^{7-8} (cartoon, Figure

3.1A). In order to predict the TMDs, TMHMM server (http://www.cbs.dtu.dk/services/TMHMM-2.0/) was used. Moreover, treatment of isolated membranes from yeast expressing green fluorescence protein GFP-Ist2-HA$^{7-8}$ with proteinase K (PK) generated a major HA fragment of approximately 15 kDa (Figure 3.1B, lane 4). On the other hand treatment of membranes expressing GFP-Ist2 with an HA tag at the N-terminus of Ist2, however, resulted in digestion of the N-terminally located HA tag (Figure 3.1B, lane 2). This indicates that the N-terminus of Ist2 and the loop between TMDs 7 and 8 are located on opposite sides of the membrane. In the same experiment, a fraction of Kar2, which is present in the ER lumen, was protease protected, whereas the C-terminal domain of Ist2 was completely digested (Figure 3.1B, lanes 2 and 4). As the Ist2 N- and C-terminus are oriented toward the cytosol (87), these results confirmed that the loop between TMDs 7 and 8 faces either the ER lumen or the exterior of the cell.

If Ist2 reaches the cell surface of cells, the HA epitope will be exposed toward the exterior and one can measure the amount of GFP-Ist2-HA$^{7-8}$ on the cell surface with HA-specific antibody staining. The experimental setup was controlled by co-expression of a GFP-tagged version of the ATP-sensitive potassium channel subunit Kir6.2 and its subunit SUR1 (51). Kir6.2 contains two TMDs, cytosolically orientated N- and C-termini, and exposes a di-arginine ER-retention signal. Between the two TMDs, Kir6.2 contains an HA epitope (see cartoon, Figure 3.1C). Interaction with SUR1 inactivates the di-arginine signal of Kir6.2 and the correctly assembled channel travels to the cell surface (51). After cotransfection, many of the GFP-positive HEK293 cells exposed HA on their surface as shown by flow cytometry (Figure 3.1C).

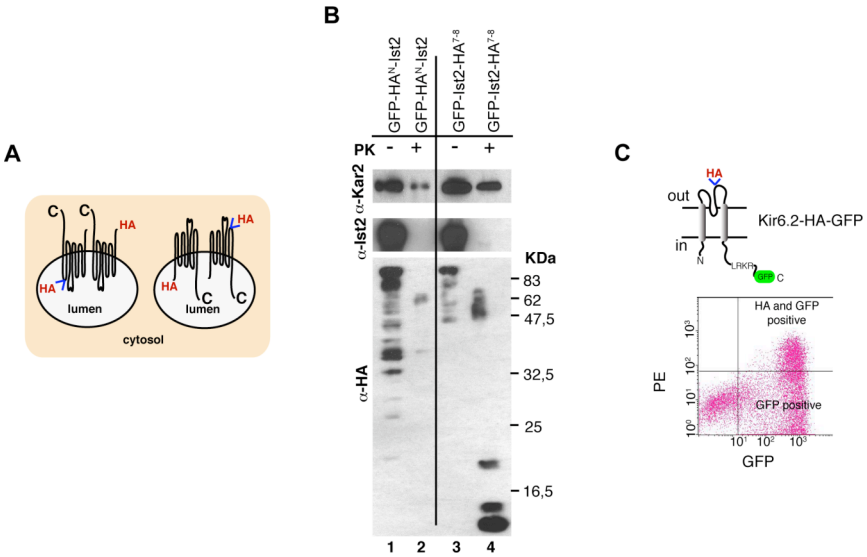

Figure 3.1 The HA tag in GFP-Ist2-HA$^{7-8}$ faces the ER lumen and/or extracellular space.

(A) Cartoon of different topologies of Ist2 in membrane vesicles with an engineered HA epitope between TM domains 7 and 8 or at the N-terminus. **(B)** Western blot of membranes from *ist2*Δ yeast cells expressing GFP-HA^{N}-Ist2 or GFP-Ist2-HA$^{7-8}$. After treatment of membranes from GFP-HA^{N}-Ist2 and GFP-Ist2-HA$^{7-8}$ expressing yeast cells with PK, Kar2, Ist2 and Ist2 with the HA tag were detected with specific antibodies. For detection of the C-terminal domain of Ist2, we used an antibody raised against GST-Ist2 residues 589-946. **(C)** Cartoon of the topology of Kir6.2-GFP with a HA tag positioned between the two TM domains (Kir6.2-HA-GFP). FACS diagram of HA surface staining of GFP-positive HEK293 cells cotransfected with Kir6.2-HA-GFP and SUR1.

3.1.1 Yeast Ist2 localizes at intracellular patch-like structures

After showing that the HA tag faces the ER lumen and/or extracellular space, I tested the localization of GFP-Ist2-HA$^{7-8}$ by immunofluorescence and flow cytometry. In both nonpermeabilized and permeabilized HEK293 cells, which were transfected with GFP-Ist2-HA$^{7-8}$ a peripheral GFP fluorescence was observed (Figure 3.2A). In permeabilized cells a perfect overlap between the GFP and the HA signals was observed. However, in nonpermeabilized cells, these structures were not recognized by the HA antibody. This indicates that the engineered HA tag is not recognized at the cell surface, suggesting that Ist2 resides at peripheral intracellular structures.

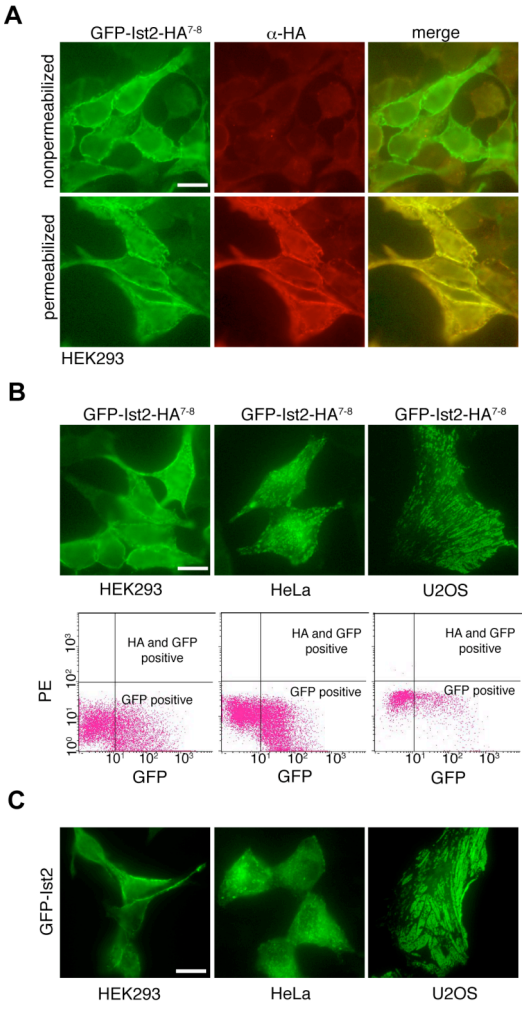

Figure 3.2 Ist2 localizes to intracellular structures in different cell types.

(A) Epifluorescence microscopy of HEK293 cells after transfection with GFP-Ist2-HA$^{7-8}$. GFP fluorescence (green) and antibody staining of HA (red) at the surface of nonpermeabilized cells and in permeabilized cells are shown. The scale bar in this figure and all following figures corresponds to 10 µm, if not mentioned otherwise. **(B)** GFP fluorescence of HEK293, HeLa and U2OS cells expressing GFP-Ist2-HA$^{7-8}$ and FACS diagrams of HA surface staining of GFP-positive cells. **(C)** Localization of GFP-Ist2 in different cell types. GFP fluorescence of HEK293, HeLa and U2OS cells expressing GFP-Ist2 visualized by epifluorescence microscopy.

In order to obtain better spatial resolution of these peripheral structures and to analyze whether their formation is a general phenomenon, localization studies of GFP-Ist2-HA$^{7-8}$ was carried on in different cell lines, such as epithelial HeLa and U2OS cells. Epifluorescene microscopy revealed that HeLa and U2OS cells express GFP-Ist2-HA$^{7-8}$ in morphologically different patch-like structures, changing from dot-like appearance to large rectangular-shaped ones (Figure 3.2B). In addition to the patches, HeLa cells often showed a diffuse intracellular GFP signal, suggesting that some of the GFP-Ist2-HA$^{7-8}$ remained at reticular ER structures. This was different from the situation in U2OS cells, which developed patches without any apparent reticular localization of GFP-Ist2-HA$^{7-8}$. Different transfection methods (lipid- or Ca_2PO_4-mediated transfection) had no impact on the formation of patches (data not shown). Quantification of the HA surface signal by flow cytometry in GFP-Ist2-HA$^{7-8}$-transfected HEK293, HeLa and U2OS cells showed that the HA tag was not accessible for antibodies added from the outside (Figure 3.2B). This suggests that Ist2 does not localize to the surface of all tested cells. Moreover, the HA tag had no influence on the intracellular distribution of Ist2, since the GFP-Ist2-HA$^{7-8}$ and GFP-Ist2 without the HA tag localized similarly (Figure 3.2C and B).

Together, these results revealed that Ist2 in mammalian cells resides at peripheral but intracellular membranes.

3.1.2 Yeast Ist2 localizes at peripheral ER structures

The next question was to identify these peripheral intracellular structures. Localization studies in living U2OS cells by epifluorescence microscopy revealed that some of the ER co-localized with GFP-Ist2-HA$^{7-8}$ patches (Figure 3.3). In this experiment, the entire ER was stained with the ER-specific lipid dye ER-Tracker™.

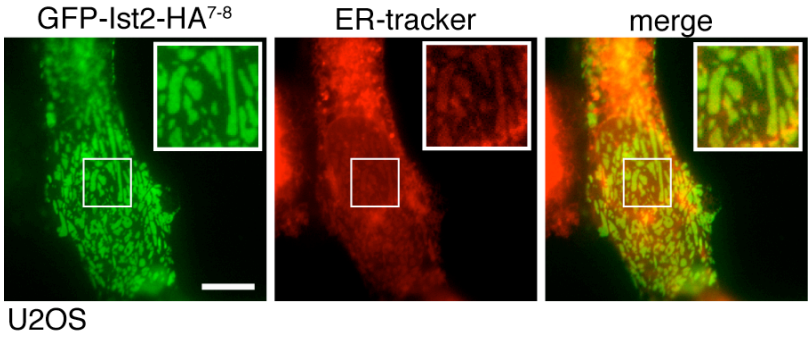

Figure 3.3 Yeast Ist2 localizes to patch-like ER structures in U2OS cells.

Co-localization of GFP-Ist2-HA$^{7-8}$ (green) and ER-tracker (red) in U2OS cells. The inserts show patch formation of GFP-Ist2-HA$^{7-8}$ and recruitment of some of the ER to these patches.

3.1.3 The CSS^{Ist2} targets integral membrane proteins to PM-associated domains of the ER

As it does in yeast cells (85, 91), the CSS in GFP-Ist2 may bind to PI(4,5)P_2 and/or other PIPs in the mammalian PM. This interaction may result in the recruitment of ER to the PM and explain why GFP-Ist2-HA$^{7-8}$ was not detected at the cell surface. To test whether this recruitment of ER to the PM is achieved by the function of the CSS^{Ist2}, the CSS^{Ist2} was attached to the cytosolically oriented C-terminus of the T-cell surface glycoprotein CD4 (Figure 3.4A). Staining with an antibody that recognizes the N-terminus of CD4 in nonpermeabilized HEK293 cells showed that 76% of the GFP-positive cells express CD4-GFP at the cell surface. On the other hand, quantification of CD4-GFP-CSS^{Ist2} in GFP-positive HEK293 cells showed that only 26% of these cells had CD4 at the cell surface (Figure 3.4B).

Furthermore, I investigated whether this small amount of surface expression of CD4-GFP-CCS^{Ist2} is dependent on the function of the Golgi. For this purpose, I treated the cells with brefeldin A (BFA) 6 hours prior to measurement of the surface-located CD4 by flow cytometry. Trafficking of CD4-GFP-CSS^{Ist2} to the surface was BFA sensitive, indicating that a certain fraction of CD4-GFP-CSS^{Ist2} reached the surface of HEK293 cells via transport along the classical secretory pathway (Figure 3.4B).

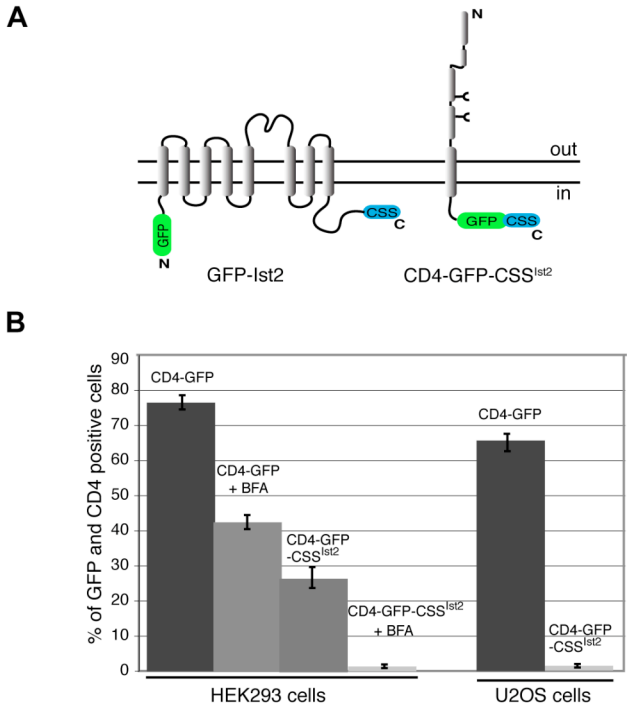

Figure 3.4 The CSS^{Ist2} traps CD4 at intracellular structures.

(A) Cartoon of the topology of GFP-Ist2 and CD4-GFP tagged with CSS^{Ist2}. The position of two N-linked glycosylation sites in CD4 is indicated. **(B)** Quantification of HEK293 and U2OS cells expressing CD4 on their cell surface by flow cytometry after transfection with CD4-GFP and CD4-GFP-CSS^{Ist2}. HEK293 cells were treated for 6 h with BFA (+BFA). The data represents the average of three independent experiments and the error bar of this and all following flow cytometry quantifications show the standard error of the mean (s.e.m.)

Moreover, I tested the localization of CD4-GFP-CSS^{Ist2} in U2OS cells and found that the vast majority of these cells had no CD4-GFP-CSS^{Ist2} on their surface. This suggests that the CSS^{Ist2} retains the majority of CD4 in U2OS cells at intracellular structures. In U2OS cells, CD4-GFP-CSS^{Ist2} fluorescence appeared as distinct patches at the cell periphery (Figure 3.5A, middle panel and insert), while CD4-GFP alone was distributed over the entire cell. CD4-GFP was enriched in the region of the Golgi with GFP signal visible at cell edges corresponding to CD4-GFP at the PM (Figure 3.5A, left panel). Detection of the ER marker calreticulin by antibody staining in CD4-GFP-CSS^{Ist2} expressing U2OS cells revealed that the formation of CD4-GFP-CSS^{Ist2} containing patches had a dramatic impact on the distribution of calreticulin. Instead of an ER-like reticular staining, as in CD4-GFP expressing cells, calreticulin showed a clear co-localization with peripheral CD4-GFP-CSS^{Ist2} (Figure 3.5B).

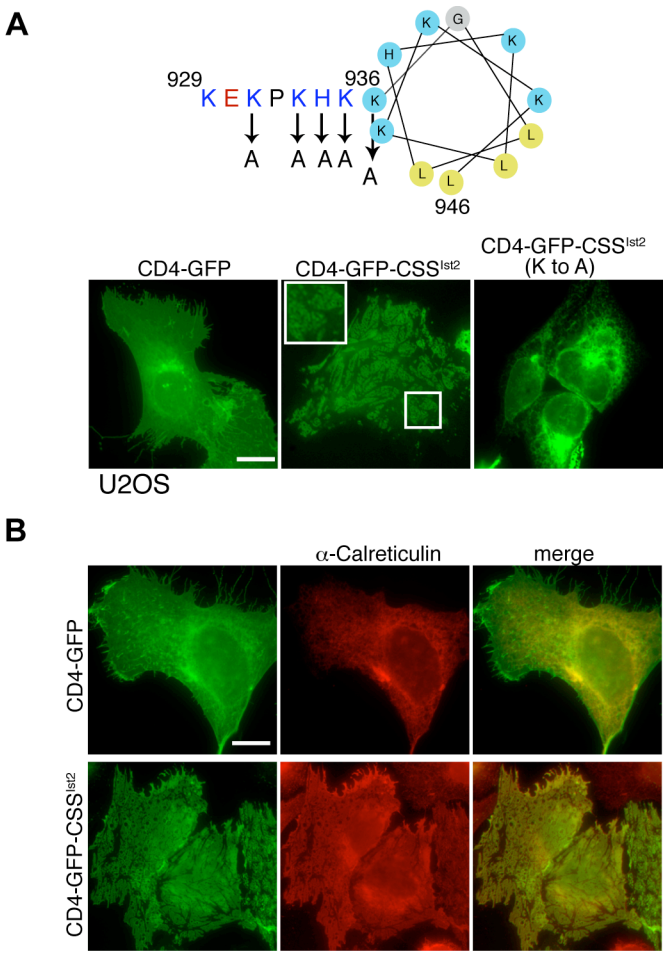

Figure 3.5 CSS^{Ist2} drags CD4 into patch-like ER structures.

(A) Sequence of the last 18 residues of yeast Ist2. According to the prediction program 'AmphipaSeek', the last 11 residues are shown as α-helical wheel projection (143). The arrows indicate mutations into alanine. GFP fluorescence detected by epifluorescence microscopy of U2OS cells expressing CD4-GFP, CD4-GFP-CSS^{Ist2} and CD4-GFP-CSS^{Ist2} with K931, K933, H934, K935 and K936 to A mutations (K to A). **(B)** GFP fluorescence of U2OS cells after transfection with CD4-GFP (green) and CD4-GFP-CSS^{Ist2} (green) and antibody staining of calreticulin (red) visualized by epifluorescence microscopy.

This suggests that the majority of CD4-GFP-CSS^{Ist2} localized at specific ER domains and that the expression of CD4-GFP-CSS^{Ist2} resulted in a dramatic reorganization of the ER.

As the CSS^{Ist2} signal can drive CD4-GFP into distinct patch-like structures, which seem close but on the cytosolic side of the PM, I further investigated the responsible residues of this signal that result in this patch-like localization of the ER. Previous *in vitro* experiments showed that the positively charged residues of the CSS^{Ist2} and an amphipathic α-helix of 11 residues with hydrophobic side chains on one side of the helix are essential for the binding to PI(4,5)P_2-containing PM-like liposomes (85, 91). This indicates that an interaction between positive residues of the CSS^{Ist2} and lipids at the PM recruits yeast Ist2 to PM-associated domains of the cortical ER. In yeast, the efficient transport of Ist2 from the perinuclear to the cortical ER was diminished by mutation of K931, K933, H934, K935 and K936 to alanine (85). In the context of CD4-GFP-CSS^{Ist2} in U2OS cells, this mutation (denoted as K to A) abolished the formation of patches. Mutated CD4-GFP-CSS^{Ist2} localized at structures resembling the general ER (Figure 3.5A, right panel), suggesting that mutation of K931, K933, H934, K935 and K936 abrogates the function of the CSS^{Ist2} as a strong signal for sorting to the cell periphery. Moreover, these results suggest that this mutation most likely interferes with the α-helical structure of the CSS^{Ist2} C-terminus and as a result leads to the exposure of a linear KKKL sequence, which then functions as ER-retention signal.

3.1.4 Mutations in CSS^{Ist2} changes the morphology of the ER

In order to study the structural requirements of this lipid-protein interaction, additional mutations were created in the K-rich region of CSS^{Ist2}. One of the mutations was L939P, which is expected to destroy the amphipathic α-helix structure due to introduction of the proline. As expected, the patch formation was demolished and instead, a more tubular ER forms were created (Figure 3.6). Another mutation was created to destroy the amphipathic behavior of the helix. In this mutation two alanine residues were inserted in between K941 and L942. This mutation gave a similar phenotype as the L939P mutation. The exaggerated formation of ER-tubules in both mutants might be due to either interaction of the mutant CSS^{Ist2} with ER-lipids or an increased association with microtubules. Indirect immunofluorescence experiments showed that these structures co-localize with tubulin, supporting the latter possibility (data not shown). Another mutation was created in order to reduce the hydrophobicity of the α-helix. In this case leucine residue was mutated into a glutamine residue (L942Q). This mutation resulted in more reticular localization. As seen in figure 3.6, all mutations destroyed the formation of ER-PM contact sites, suggesting the importance of the basic, hydrophobic and the α-helical structure in binding to PM lipids.

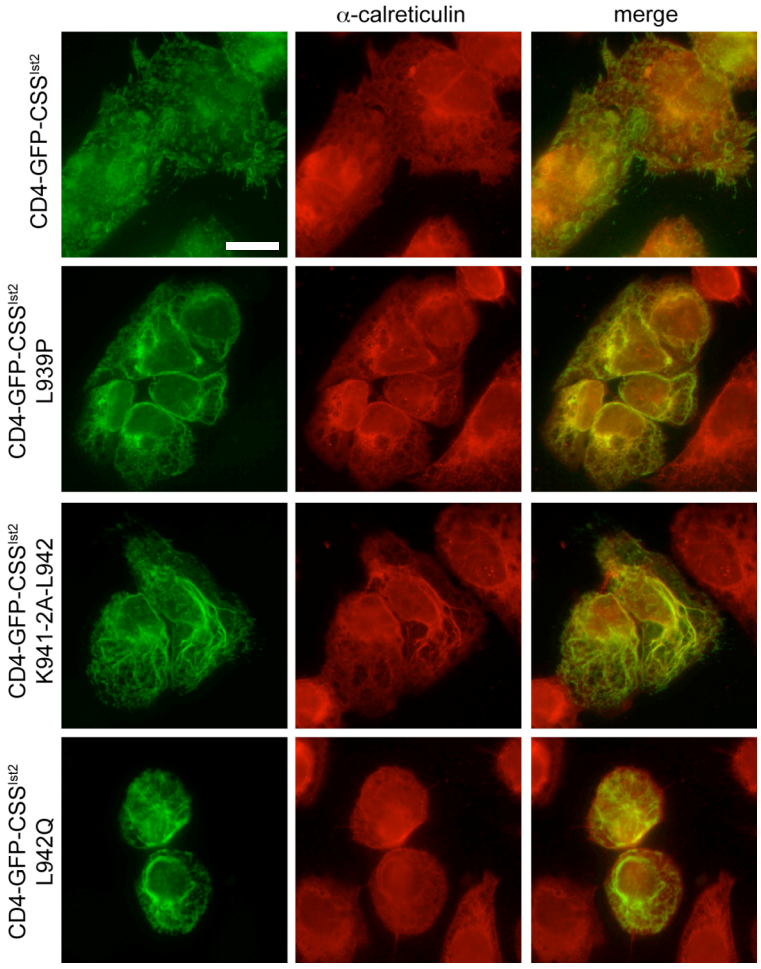

Figure 3.6 Mutations in CSS^{lst2} abolish the binding to PM lipids.

First row shows the localization of CD4-GFP-CSS^{lst2} (green) and the other rows show the mutants of CSS^{lst2} (green). The calreticulin was stained in order to visualize the ER (red).

3.1.5 The peripheral ER structures are in close proximity to PM

The localization of both GFP-lst2-HA$^{7-8}$ and CD4-GFP-CSS^{lst2} revealed that, the CSS^{lst2} promotes formation of specialized ER domains. In order to study the localization of these domains in detail, I performed more advanced microscopy experiments.

In order to visualize the peripheral and perinuclear ER in cells expressing CD4-GFP-CSS^{lst2} in more detail, confocal microscopy was applied. An *xy*-view of a CD4-GFP-CSS^{lst2} expressing cell showed the formation of patches at a position, where this cell is in contact with the coverslip (Figure 3.7A, bottom view). The corresponding *z*-plane from the middle of this cell revealed a weaker staining of CD4-GFP-CSS^{lst2} at perinuclear and reticular ER structures, which were stained with ER-Tracker (Figure 3.7A, middle views). The arrows indicate staining of CD4-GFP-CSS^{lst2} at perinuclear ER. A reconstruction of the *z*-view of a CD4-GFP-CSS^{lst2} expressing U2OS cell showed that the majority of CD4-GFP-CSS^{lst2} accumulated in patches, which were

distributed over the entire cell surface (Figure 3.7B). These patches seemed to be continuous with perinuclear and intracellular structures, without a disruption of the perinuclear ER.

The limited axial resolution of the confocal microscope (approximately 500 nm) does not allow exact statements about the position of the patches with respect to the PM. Therefore; total internal reflection fluorescence microscopy (TIRFM) was applied. By this approach fluorophores within 100 nm of the PM are selectively excited, allowing to resolve the structures, which are in close proximity to the PM (144). At many positions at the bottom of a U2OS cell, the staining of CD4-GFP overlapped with the PM marker SH4-mCherry, indicating that these proteins localize to the PM within the resolution of TIRFM (Figure 3.7C, second row). The dark spots in SH4-mCherry expressing cells correspond to parts of the cells that are not attached to the coverslip. In TIRFM, fluorophores at these positions are not excited, which results in their dark appearance. Co-localization of CD4-GFP-CSS^{Ist2} and SH4-mCherry at the PM with TIRFM showed that CD4-GFP-CSS^{Ist2} patches are in close proximity to the PM (Figure 3.7D, bottom row). Epifluorescence images of the corresponding cells are shown in figure 3.7C and D (upper rows).

Taken together, the expression of CD4-GFP-CSS^{Ist2} induces peripheral calreticulin-positive ER domains, which are aligned close to the PM.

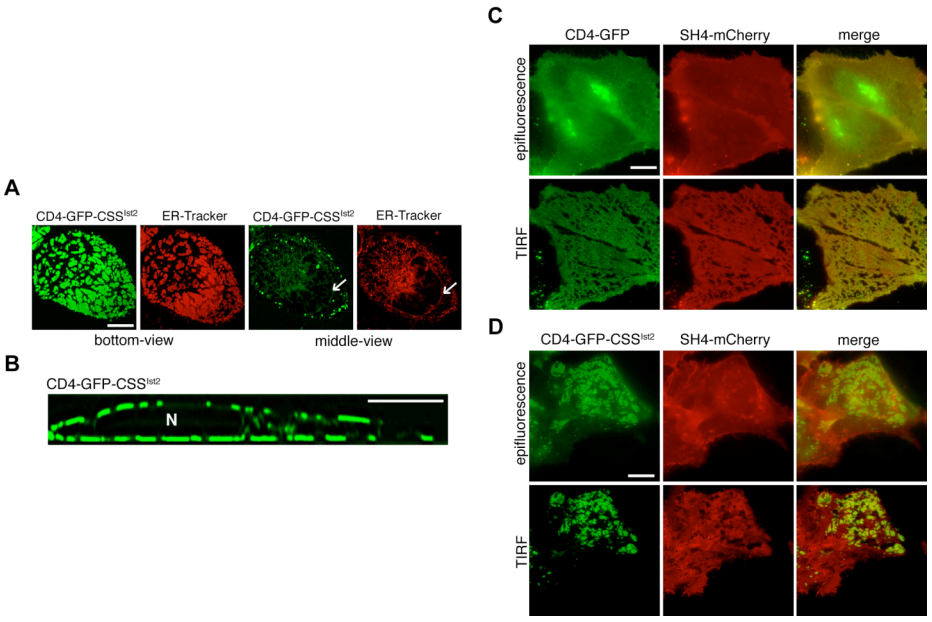

Figure 3.7 CD4-GFP-CSS^{Ist2} localizes at PM-associated ER patches.

(A) U2OS cells after transfection with CD4-GFP-CSS^{Ist2} visualized by confocal microscopy. CD4-GFP-CSS^{Ist2} localization is shown in green and ER-Tracker staining in red. The bottom view shows the *z*-plane where the cell is in contact with the coverslip and the middle view shows co-staining of CD4-GFP-CSS^{Ist2} and ER-Tracker at the perinuclear ER (indicated by arrows). **(B)** Reconstruction of a *z*-view from a cell expressing CD4-GFP-CSS^{Ist2}. N denotes the nucleus. **(C)** Co-localization of CD4-GFP (green) and SH4-mCherry (red) by epifluorescence and TIRF microscopy. **(D)** Co-localization of CD4-GFP-CSS^{Ist2} (green) and SH4-mCherry (red) by epifluorescence and TIRF microscopy.

3.1.6 The CSS^{lst2} functions as dominant sorting signal in mammalian cells

Next, I investigated whether the formation of peripheral ER patches is a general process, and occurring independently of features of the membrane protein that contains the CSS^{lst2}. For this purpose CSS^{lst2} was attached to the cytosolically oriented C-termini of three different integral membrane proteins: the major histocompatibility complex class I heavy chain H-2K^{b} (MHCI), Kir6.2 and the ATP-dependent transporter associated with an antigen presentation subunit TAP1. MHCI has a similar topology and localization as CD4, but it requires the MHCI light chain β_2-microglobulin as well as the TAP peptide transporter and associated molecules for efficient peptide loading and trafficking to the PM (145). TAP1 is an ER-resident multi-spanning membrane protein, which forms a heterodimeric peptide transporter with TAP2 and is strictly retained in the ER (146). In U2OS cells, which lack β_2-microglobulin and SUR1, transfection of either MHCI-GFP or Kir6.2-GFP or TAP1-GFP resulted in an expression at the reticular ER (Figure 3.8A). The attachment of the CSS^{lst2} to these three proteins led to a patch-like localization of the corresponding chimeras at positions where these cells are in contact with the coverslip (Figure 3.8A, bottom views). Moreover, the ER-Tracker co-localized with these peripheral patches, confirming these structures are the domains of the ER. The corresponding *z*-planes from the middle of these cells revealed a weaker staining of the chimeras (Figure 3.8A, middle views). These data suggest that the CSS^{lst2} overrides the endogenous sorting signals of CD4 (Figure 3.5), MHCI, Kir6.2 and TAP1 (Figure 3.8A).

Since TAP1 and TAP2 form a stable complex, I examined whether TAP1-GFP-CSS^{lst2} targets the assembled TAP heterodimer into patches. This was analyzed by co-expression of TAP1-GFP-CSS^{lst2} and TAP2-tdimer2(12) in U2OS cells. The heterodimer showed the identical localization in patches as the TAP1-GFP-CSS^{lst2} monomer (Figure 3.9A). This indicates that TAP1-GFP-CSS^{lst2} forms a complex with TAP2 and that the CSS^{lst2} functions as dominant signal for the TAP1-TAP2 heterodimer.

To further characterize the PM-associated ER patches, I investigated their protein composition. I performed antibody staining of different ER proteins in CD4-GFP-CSS^{lst2} expressing U2OS cells. Peripheral patches contained calnexin in addition to calreticulin but not Sec61γ (Figure 3.9B, C). This suggests a specific protein composition of the peripheral patches: CD4-GFP-CSS^{lst2} recruited calreticulin and calnexin, whereas the translocon component Sec61γ remained separated from the patches. Since the two lectin-like chaperones calnexin and calreticulin interact with and assist the folding of proteins that carry monoglucosylated N-linked glycans (43), I studied whether the recruitment of these two chaperones depends on the presence of N-linked glycans in CD4.

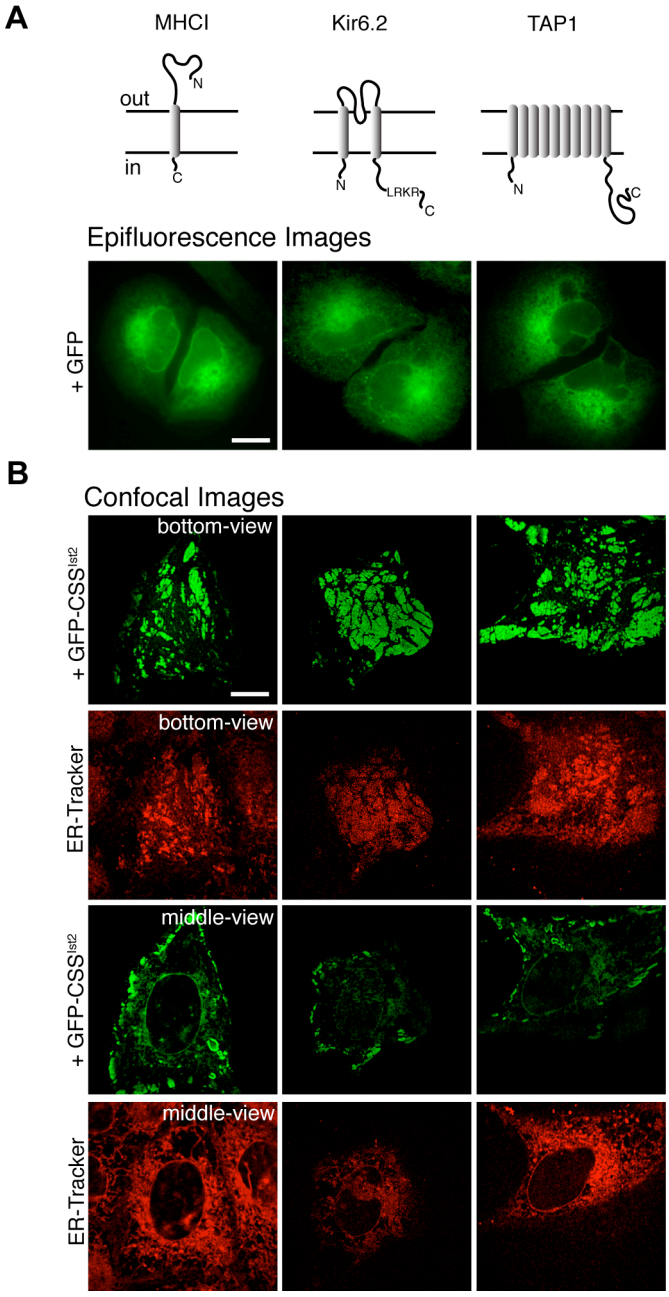

Figure 3.8 The CSS^{lst2} sorts different membrane proteins into peripheral ER patches.

(A) Topology of MHCI, Kir6.2 and TAP1. Epifluorescence microscopy of U2OS cells after transfection with the indicated proteins tagged with GFP (top row). **(B)** Confocal microscopy of U2OS cells after transfection with the indicated proteins tagged with GFP-CSS^{lst2} (green) and co-staining with ER-Tracker (red). Shown are bottom and middle *z*-planes.

Expression of MHCI-GFP-CSS^{lst2}, which also receives an N-linked glycan, resulted in the recruitment of calnexin and calreticulin into peripheral patches. However, the expression of TAP1-GFP-CSS^{lst2}, which does not contain an N-linked glycosylation site, did not recruit calnexin and calreticulin (Figure 3.9B; Table 3.1). In addition to calnexin and calreticulin, the presence of protein disulfide isomerase (PDI), translocon-associated protein Sec61β, translocating chain-associating membrane protein TRAM, ER luminal Hsp70-like chaperone BiP

(Binding immunoglobulin Protein) and TAP2 was tested (Table 3.1). Translocon components and BiP were not enriched in patches, arguing that the induced peripheral ER domains are separated from the rough ER. TAP2 is an example for another ER protein that is not enriched in CD4-GFP-CSS^{lst2} and MHCI-GFP-CSS^{lst2} containing peripheral ER. The peptide transporter subunit TAP2 is unstable in the absence of TAP1 and not expected to be redirected to the ER periphery by MHCI-GFP-CSS^{lst2} (147, 148).

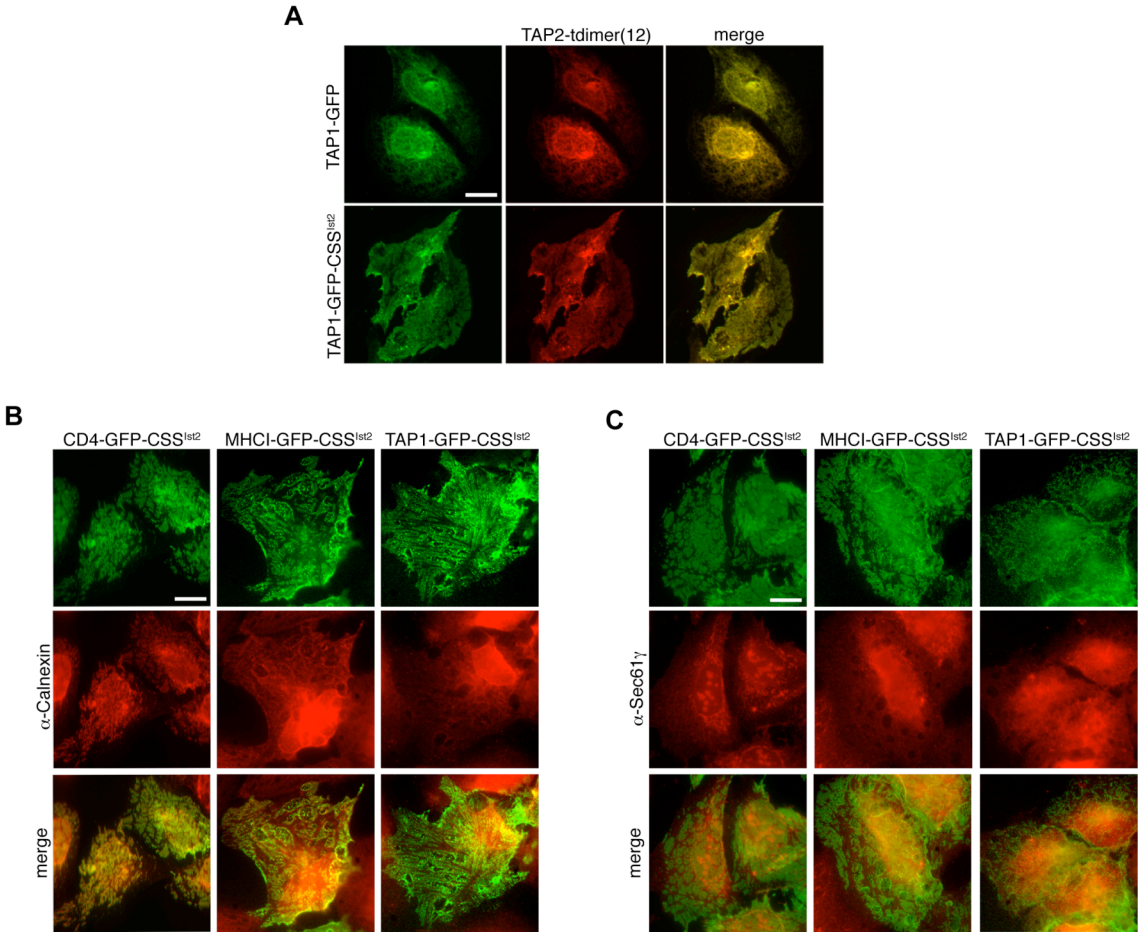

Figure 3.9 CSS^{lst2} functions as a strong signal.

(A) Epifluorescence microscopy of U2OS cells after transfection with TAP2-tdimer2(12) (red), and co-transfection with TAP1-GFP (green) or TAP1-GFP-CSS^{lst2} (green). **(B)** Epiflouresence microscopy of cells after transfection with CSS^{lst2} tagged proteins (green) and co-staining of ER with either calnexin or **(C)** Sec61γ.

In summary, the presence of a specific set of proteins suggests that the induced peripheral ER represents a subdomain of the smooth ER. Moreover, the properties of the different reporter proteins with CSS^{lst2} influence the composition of these peripheral ER domains.

Table 3.1 Accumulation of the indicated ER proteins at peripheral patches induced by expression of CD4-GFP-CSS^{lst2}, MHCI-GFP-CSS^{lst2} and TAP1-GFP-CSS^{lst2} in U2OS cells.

ER markers	CD4-GFP-CSS^{lst2}	MHCI-GFP-CSS^{lst2}	TAP1-GFP-CSS^{lst2}
Calreticulin	Yes	Yes	No
Calnexin	Yes	Yes	No
PDI	Yes	Yes	No
Sec61β	Yes	No	No
Sec61γ	No	No	No
TRAM	No	No	No
GRP78/BiP	No	No	No
TAP2	No	No	Yes

3.1.7 The CSS^{lst2}-dependent peripheral ER formation does not alter the function of the ER

In order to investigate the effect of ER-PM contact site formation on the function of ER, the anterograde trafficking from ER to Golgi was investigated. For this reason, I used red fluoresence protein (RFP)-tagged GalTase, which localizes to Golgi (Figure 3.10B). I performed a fluorescent recovery after photobleaching (FRAP) experiment, where I bleached the Golgi localized GalTase-RFP and checked the recovery of the Golgi fluorescence. If the peripheral ER formation abolishes the trafficking from ER to Golgi, the recovery of GalTase-RFP in Golgi would not be similar as in the control cells. In order to induce the peripheral ER formation, I co-expressed GalTase-RFP and Kir-GFP-CSS^{lst2}. As a control, I analyzed cells co-expressing Kir6.2-GFP and GalTase-RFP. In Hela cells, Kir6.2-GFP-CSS^{lst2} localized to patch-like ER structures (Figure 3.10A). Both in control cells, co-expressing Kir6.2-GFP and GalTase-RFP, and cells expressing Kir6.2-GFP-CSS^{lst2} and GalTase-RFP, the recoveries of Golgi fluorescence were identical (Figure 3.10B and C).

This suggests that the trafficking from the ER to the Golgi was not affected by the formation of CSS^{lst2}-dependent ER-PM contact sites.

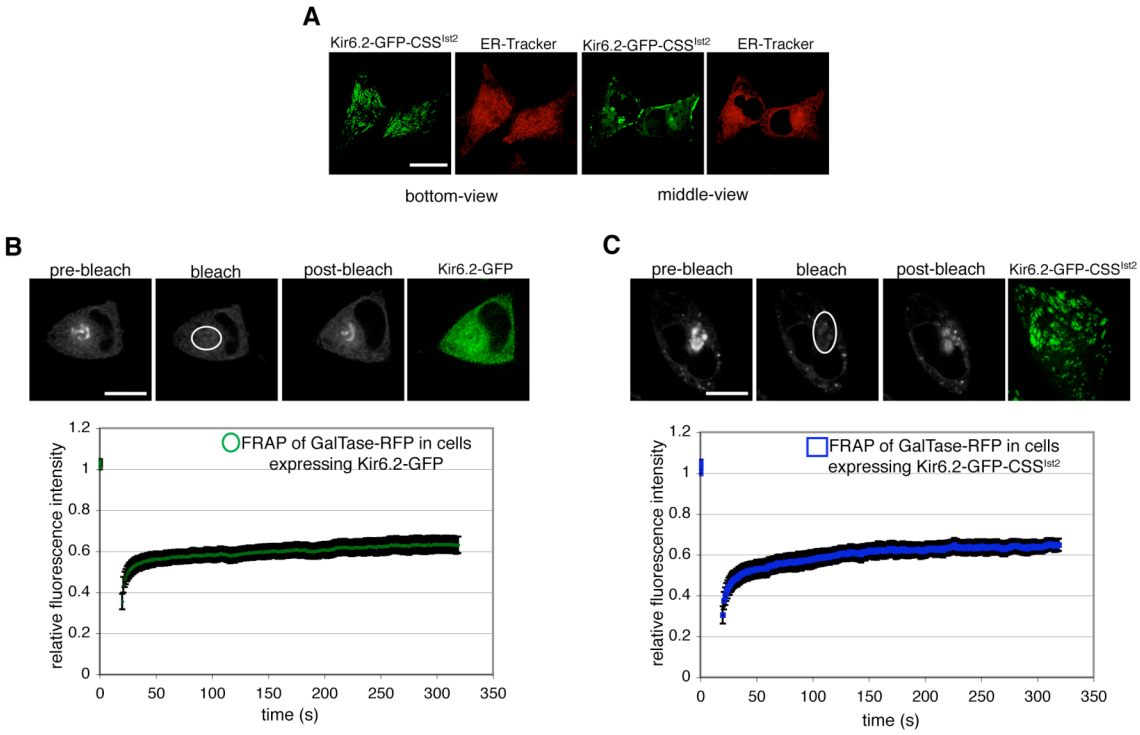

Figure 3.10 CSS^{lst2}-dependent ER-PM contact site formation does not alter the trafficking from ER to Golgi

(A) Fluorescence of Kir6.2-GFP-CSS^{lst2} (green) and ER-tracker (red) in living HeLa cells. **(B)** The left image shows the fluorescence before (pre-bleach), the middle images show 1 second after (bleach) and 300 seconds after photobleaching (post-bleach) of Golgi. The right image shows the localization of Kir6.2-GFP in the same cell. The bottom part shows the quantitation of FRAP analysis of Golgi during the first 300 seconds (n = 6). All bleached areas are indicated and the scale bars of all FRAP experiments correspond to 2 µm. **(C)** The left image shows the fluorescence before (pre-bleach), the middle images show 1 second after (bleach) and 300 seconds after photobleaching (post-bleach) of Golgi. The right image shows the localization of Kir6.2-GFP-CSS^{lst2} in the same cell. The bottom part shows the quantitation of FRAP analysis of Golgi during the first 300 seconds (n = 6).

3.1.8 CSS^{lst2}-induced PM-associated ER domains are stable structures

In order to further investigate the properties of the peripheral ER patches, I analyzed the mobility of the CSS^{lst2}-tagged protein in these patches. Confocal laser scanning microscopy of living U2OS cells expressing Kir6.2-GFP-CSS^{lst2} revealed that most of the patches were static. Only occasionally, fission and fusion events were observed (data not shown).

Photobleaching of a complete Kir6.2-GFP-CSS^{lst2} patch (of approximately 3 µm diameter) revealed that the recovery of fluorescence in this area was extremely slow. Five minutes after photobleaching, the signal of the bleached area remained low (Figure 3.11A, post-bleach image). On the other hand, within a patch, Kir6.2-GFP-CSS^{lst2} displayed mobility. When a region corresponding to approximately 50% of a patch was bleached, fluorescence of the bleached area recovered to 40% of the pre-bleach intensity with a $t_{1/2}$ recovery of 26 seconds (Figure 3.11A, lower panel). These experiments indicate that individual patches can be

considered as stable units with little exchange of Kir6.2-GFP-CSS^{lst2} between individual patches. However, the protein is mobile within a patch.

Next, I studied whether the lumen of these patches is continuous with the rest of the ER. For this purpose, the Kir6.2-GFP-CSS^{lst2} was co-expressed with an artificial luminal ER marker comprising of a signal sequence, RFP and the ER-retention signal KDEL (ss-RFP-KDEL). FRAP of a complete Kir6.2-GFP-CSS^{lst2} patch revealed a $t_{1/2}$ recovery of ss-RFP-KDEL of 1.4 seconds (Figure 3.11B, blue curve). This $t_{1/2}$ recovery was similar to the $t_{1/2}$ recovery of ss-RFP-KDEL (0.8 seconds) at reticular ER (Figure 3.11B, green curve) and $t_{1/2}$ recovery, which was similar to what has been observed for ss-GFP-KDEL in the ER of CHO cells (149). These data indicate that the diffusion of this lumenal ER reporter between general ER and peripheral ER patches is similar to its diffusion within the reticular ER.

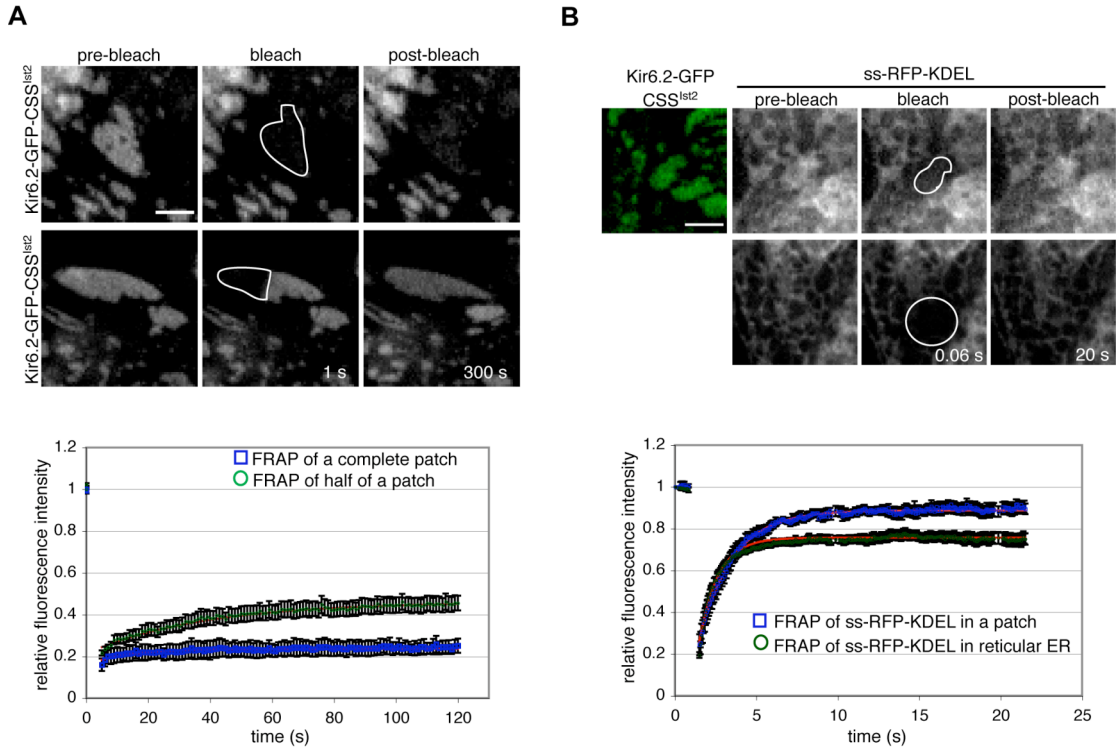

Figure 3.11 PM-associated ER domains are stable structures.

(A) Fluorescence of Kir6.2-GFP-CSS^{lst2} in living U2OS cells. The left image shows the fluorescence before (pre-bleach), the middle image 1 second after (bleach) and the right image 300 seconds after photobleaching (post-bleach) of an entire patch (top panels) or one half of a patch (bottom panels). The bottom part shows the quantitation of FRAP analysis of complete patch compared to half patch during the first 120 seconds (n = 6). All bleached areas are indicated and the scale bars of all FRAP experiments correspond to 2 µm. The time-points of the bleach and the post-bleach images are indicated. **(B)** Fluorescence of ss-RFP-KDEL in cells transfected with Kir6.2-GFP-CSS^{lst2}. The first image of the top row shows Kir6.2-GFP-CSS^{lst2} (green). The bottom row shows ss-RFP-KDEL fluorescence in a cell without transfection of Kir6.2-GFP-CSS^{lst2}. The bottom part shows the quantitation of these FRAP experiments (n = 6).

This is consistent with the results from fluorescence loss in photobleaching (FLIP) analysis with repeated bleaching of a Kir6.2-GFP-CSS^{Ist2} patch, which resulted in loss of ss-RFP-KDEL fluorescence at the entire ER (Figure 3.12A). In addition to the lumenal ER protein ss-RFP-KDEL, I investigated whether an integral membrane protein (Sec61γ) can diffuse into a peripheral ER patch. Compared to endogenous Sec61γ (Figure 3.9C), the overexpressed GFP-Sec61γ was localized at peripheral ER patches. Photobleaching of CD4-mCherry-CSS^{Ist2} patches revealed a $t_{1/2}$ recovery of 14.5 seconds (Figure 3.12B, blue curve). This was similar to the $t_{1/2}$ recovery of 11 seconds of GFP-Sec61γ to reticular ER (Figure 3.12, green curve).

Taken together, these FRAP and FLIP data show that CSS^{Ist2}-induced peripheral ER patches are in continuity with the rest of the ER.

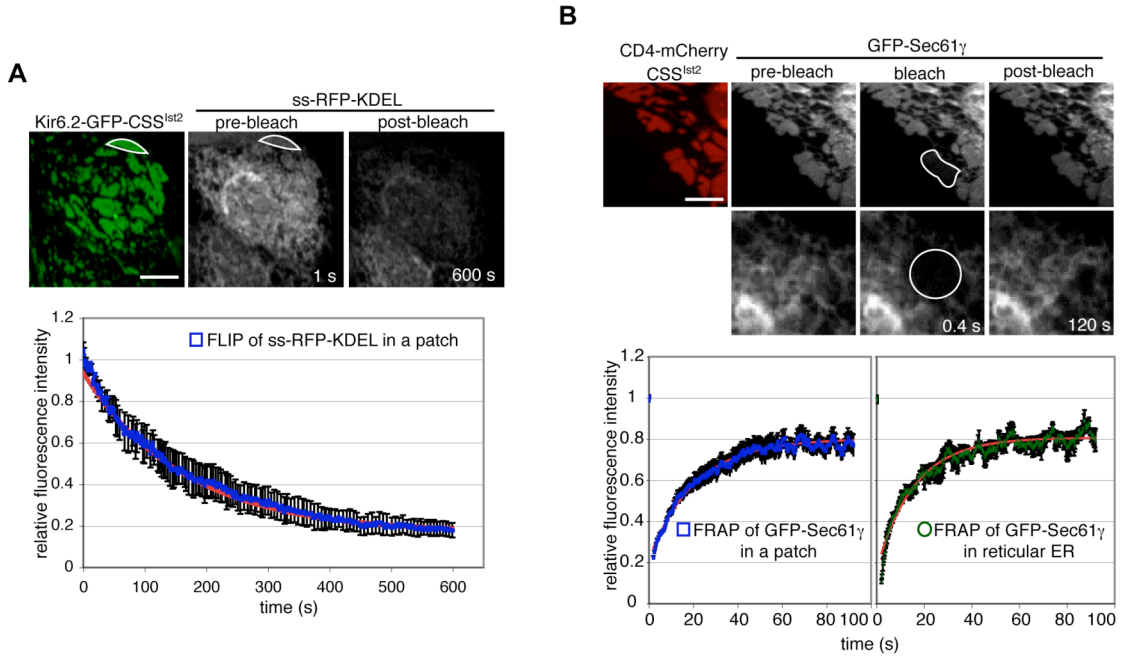

Figure 3.12 CSS^{Ist2}-driven peripheral patches are in continuity with the ER.

(A) Co-expression of Kir6.2-GFP-CSS^{Ist2} and ss-RFP-KDEL and repeated photobleaching (FLIP) of ss-RFP-KDEL in the indicated area. The bottom part shows the quantitation of the loss of ss-RFP-KDEL fluorescence (n = 4). **(B)** Fluorescence of GFP-Sec61γ in cells transfected with CD4-mCherry-CSS^{Ist2}. The first image of the top row shows CD4-mCherry-CSS^{Ist2} (red). The bottom row shows GFP-Sec61γ fluorescence in a cell without transfection of CD4-mCherry-CSS^{Ist2} after similar photobleaching. The bottom part shows the quantitation of these FRAP experiments (n = 4).

3.1.9 The CSS^{Ist2} binds PI(4,5)P$_2$ at the PM

Next, I asked whether different proteins containing CSS^{Ist2} are targeted to similar regions of the PM. To address this question, I expressed Kir6.2-GFP-CSS^{Ist2} with CD4-mCherry-CSS^{Ist2}. Both proteins localized in overlapping patches (Figure 3.13A), suggesting that they are targeted to similar domains of the PM. Since in yeast the CSS^{Ist2} could be functionally replaced by the PI(4,5)P$_2$-binding PH domain from phospholipase C-δ1 (PLC-δ1-PH) (91), I investigated whether this domain targets Kir6.2-GFP in a similar manner. The PH domain was fused to the

C-terminus of Kir6.2-GFP resulting in Kir6.2-GFP-PH. Expression of this chimera resulted in localization in patches (Figure 3.13B), indicating that they represent physical contacts between the ER and PI(4,5)P_2 at the PM. To test whether these domains are similar to those targeted by the CSS^{Ist2}, Kir6.2-GFP-PH was co-expressed with CD4-mCherry-CSS^{Ist2}. These proteins shared a large degree of co-localization (Figure 3.13C), suggesting that CSS^{Ist2} binds PI(4,5)P_2 at the PM.

In summary, I found that interaction of a lipid-binding signal in an ER-membrane protein with PM lipids, targets ER to the PM.

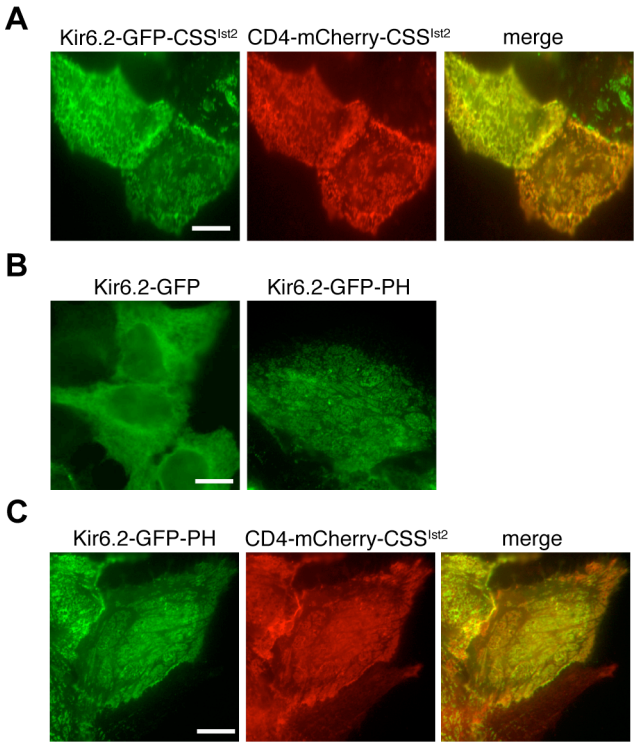

Figure 3.13 The CSS^{Ist2} interacts with PI(4,5)P_2 at the PM.

(A) Co-localization of Kir6.2-GFP-CSS^{Ist2} (green) and CD4-mCherry-CSS^{Ist2} in U2OS cells analyzed by epifluorescence microscopy. **(B)** Localization of Kir6.2-GFP and Kir6.2-GFP-PH in U2OS cells. PH denotes the PI(4,5)P_2-binding PH domain from phospholipase C-δ1. **(C)** GFP and mCherry fluorescence of U2OS cells expressing Kir6.2-GFP-PH (green) and CD4-mCherry-CSS^{Ist2} (red).

3.2 Mammalian STIM proteins form Ist2-like ER-PM contact sites

The formation of ER-PM contact sites occurs naturally in mammalian cells in order to uptake Ca^{2+} from outside into the cytosol. The ER-PM contact site formation is initiated by depletion of Ca^{2+} in the ER and this process is called Store Operated Ca^{2+} entry (SOCE). STIM proteins are the molecular players of this process, which is crucial for the activation of immune cells (see Introduction).

Both STIM1 and STIM2 are single-pass ER membrane proteins. The C-terminus faces the cytosol and the luminal N-terminus is comprised of Ca^{2+} sensing EF-hand and a SAM domain. The cytosolic C-terminus has two coiled-coil (CC) domains and an extreme K-rich domain (Figure 3.14A).

In order to investigate whether the ER-PM contact site formation is conserved in mammalian proteins, I analyzed the features of STIM1 and STIM2 C-terminal domains in binding to PM lipids.

3.2.1 Comparison of features of CSS^{Ist2} with STIM1 and STIM2 C-termini

Sequence comparison between the C-termini of STIM1, STIM2 and Ist2 shows that these sequences are rich in basic residues (Figure 3.14B). Within the last 18 residues of STIM1, STIM2 and Ist2, there are eight to nine lysine or arginine residues and only one (Ist2 and STIM2) or none (STIM1) acidic residue (Figure 3.14B). Another feature of the extreme C-terminus of Ist2 is the formation of an amphipathic α-helix with four hydrophobic leucine residues forming a hydrophobic patch on one side of the helix (Figure 3.14C). Circular dichroism spectroscopy with a 14 amino acid peptide corresponding to Ist2 933-946 in trifluoroethanol confirmed that this sequence has the propensity to adopt an α-helical structure (85). Whether the extreme C-termini of STIM1 and STIM2 can adopt an α-helical fold as well remains open. The presence of a proline at the extreme C-terminus of STIM1 K-rich region makes it unlikely to form a helix (Figure 3.14C).

To investigate whether the STIM1 and STIM2 have similar activities as CSS^{Ist2}, the entire C-terminal domains of STIM1 and STIM2 were attached to the C-terminus of Kir6.2-GFP (Figure 3.15A). Kir6.2-GFP-STIM1C showed a similar reticular ER localization as Kir6.2-GFP, whereas the attachment of the STIM2 C-terminal domain led to the recruitment of Kir6.2-GFP-STIM2C into dot- and patch-like structures (Figure 3.15A).

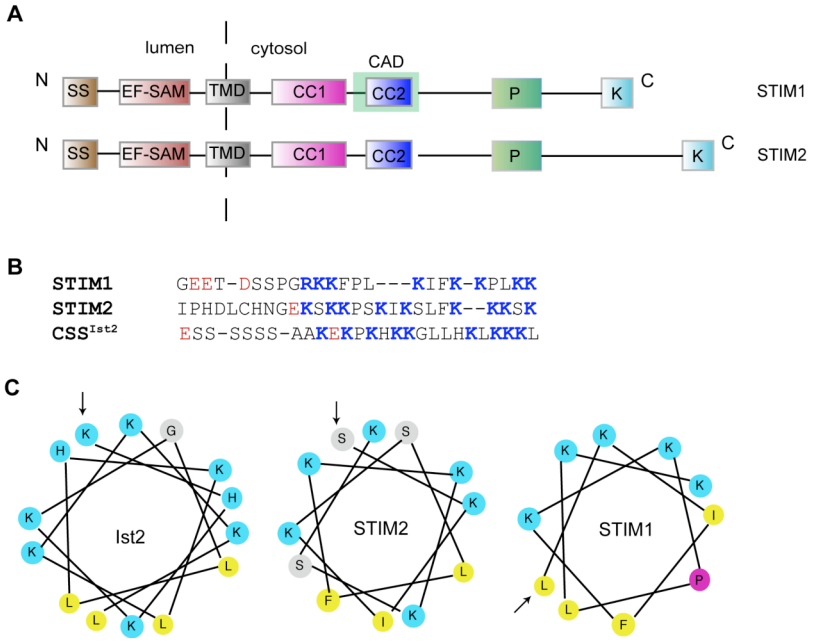

Figure 3.14 The domain structure of STIMs and comparisons of their K-rich domains with the K-rich region of CSS^{Ist2}.

(A) Cartoon of STIM1 and STIM2. EF indicates the N-terminal EF-hand domains, TM the transmembrane domains, CC the two coiled-coil domains, CAD the CRAC channel activation domain of STIM1, P the proline-rich domains and K the lysine-rich domains. **(B)** C-terminal sequences of STIM1 (aa 640 to 663 of the mature protein, without counting the signal sequence of 22 residues), STIM2 (aa 706 to 732 of the mature protein, without counting the signal sequence of 14 residues) and Ist2 (aa 920 to 946, the protein does not have a cleaved signal sequence). Basic residues are shown in bold blue and acidic residues in red. **(C)** The α-helices of Ist2 (last 14 residues), STIM2 (last 12 residues) and STIM1 (last 10 residues) according to the HeliQuest program (http://heliquest.ipmc.cnrs.fr/).

Comparison of different U2OS cells expressing Kir6.2-GFP-STIM2C showed a variable number of dots and patches and staining of reticular ER-like structures (Figure 3.15B). Moreover, similar to CSS^{Ist2}, the C-terminal domain of STIM2 did not change the morphology of the peripheral ER (Figure 3.15C).

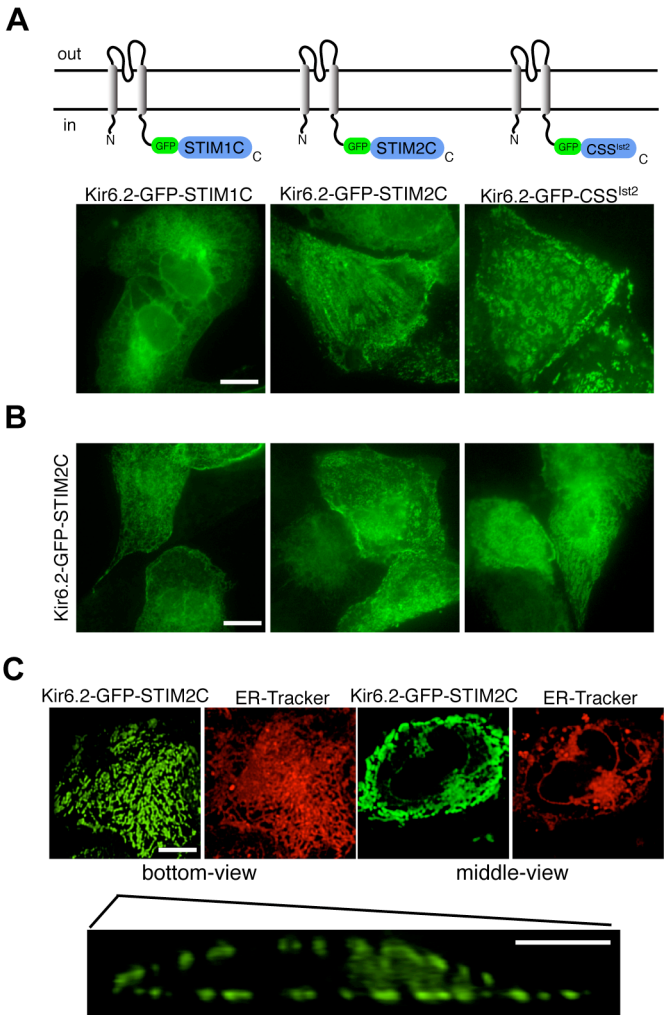

Figure 3.15 STIM2C targets Kir6.2-GFP to similar peripheral structures as CSS^{lst2} with dot- or patch-like appearance.

(A) Cartoon of topology of Kir6.2-GFP with the C-terminal domains of STIM1 and STIM2 and the CSS^{lst2} attached to its C-terminus. Epifluorescence microscopy of U2OS cells transfected with these constructs. **(B)** GFP fluorescence of different U2OS cells expressing Kir6.2-GFP-STIM2C visualized by epifluorescence microscopy. **(C)** Confocal microscopy of a cell expressing Kir6.2-GFP-STIM2C (green) and co-staining with ER-Tracker (red). Shown are a bottom and a middle *z*-plane and reconstruction of an *xz*-section of Kir6.2-GFP-STIM2C localization.

Moreover, co-localization of Kir6.2-GFP-STIM2C and CD4-mCherry-CSS^{lst2} in U2OS cells showed that both proteins accumulated at overlapping peripheral domains, whereas co-expression of Kir6.2-GFP-STIM1C and CD4-mCherry-CSS^{lst2} did not lead to such co-localization (Figure 3.16). Taken together, these results suggest that the CSS^{lst2} and the C-terminal domain of STIM2 have similar properties with respect to the formation of ER-PM contacts.

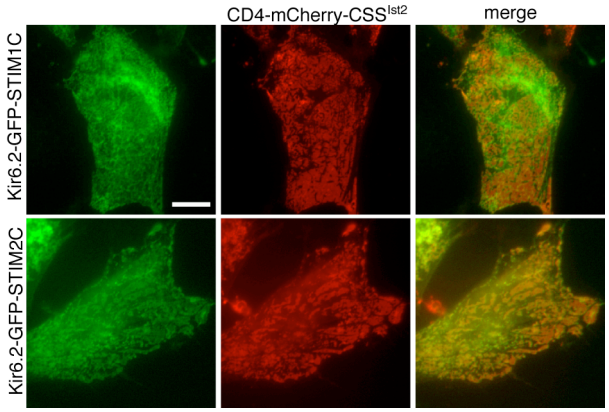

Figure 3.16 STIM2C and the CSS^{lst2} interact with similar domains at the PM.

GFP and mCherry fluorescence of U2OS cells expressing CD4-mCherry-CSS^{lst2} (red) with Kir6.2-GFP-STIM1C (green) or Kir6.2-GFP-STIM2C (green).

3.2.2 The C-termini of STIM1 and STIM2 interact with PM lipids

As Kir6.2-GFP-STIM2C patches overlapped with CD4-mCherry-CSS^{lst2}, I investigated whether STIM proteins bind to membrane lipids as CSS^{lst2} does. In order to address this question, a FACS-based liposome-binding assay was performed (142). With this approach, the ability of GFP-tagged recombinant C-termini of STIM1 (GFP-STIM1C) and STIM2 (GFP-STIM2C) to interact with PIP-containing liposomes was explored. As previously shown (85, 91), recombinant GFP-CSS^{lst2} interacts with PM-like liposomes (50 mol% cholesterol, 12.5 mol% sphingomyelin, 12.5 mol% phosphatidylcholine, 9 mol% phosphatidylethanolamine, 5 mol% phosphatidylserine, 5 mol% phosphatidylinositol) containing 5 mol% PI(4,5)P_2, whereas GFP did not (Figure 3.17A). This binding of GFP-CSS^{lst2} was set arbitrarily to 100 to normalize all data. The binding of GFP-CSS^{lst2} to PM-like liposomes required PI(4,5)P_2, whereas PC liposomes containing 5 mol% PI(4,5)P_2 showed an eightfold reduction of GFP-CSS^{lst2} binding.

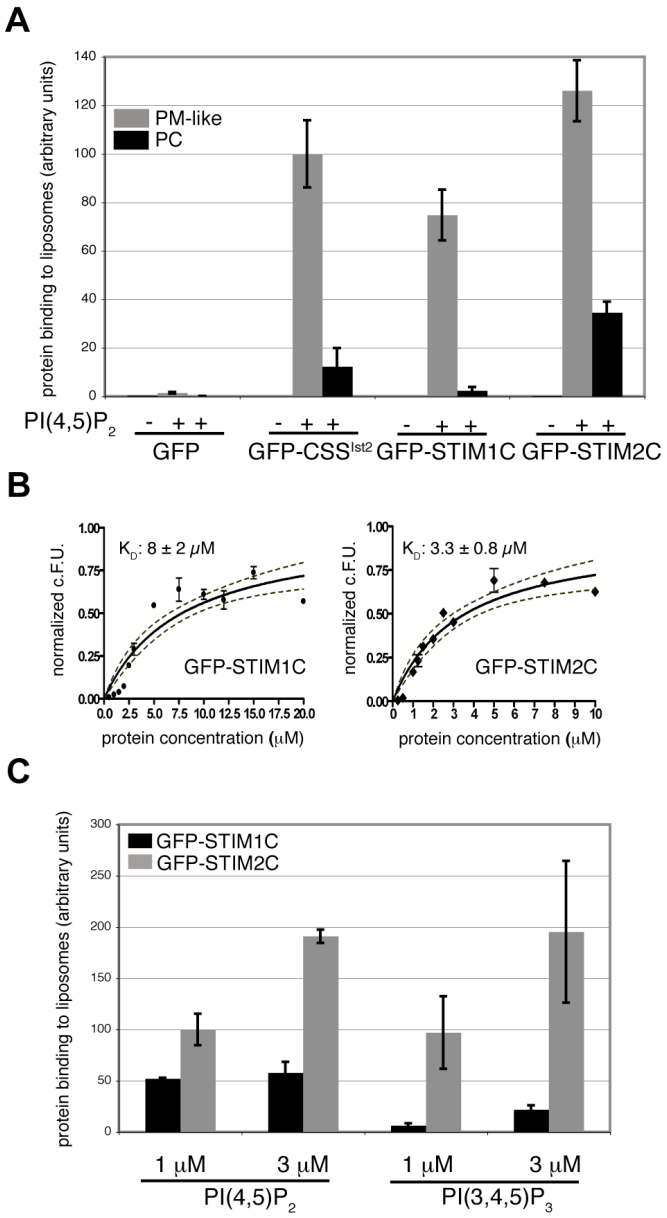

Figure 3.17 Binding of the C-terminal domain of STIM1 and STIM2 to liposomes.

(A) Relative binding of recombinant GFP, GFP-CSS^{lst2}, GFP-STIM1C and GFP-STIM2C to PM-like liposomes with or without 5 mol% PI(4,5)P_2 and to PC liposomes with 5 mol% PI(4,5)P_2. Binding of GFP-CSS^{lst2} to PM-like liposomes with 5 mol% PI(4,5)P_2 was set to 100 (shown as arbitrary units). **(B)** Relative binding of the indicated concentrations of GFP-STIM1C and GFP-STIM2C to PM-like liposomes containing 5 mol% PI(4,5)P_2. The dashed line shows the 95% confidence line and c.F.U. indicates the corrected fluorescence units. **(C)** Relative binding of 1 and 3 µm recombinant GFP-STIM1C (black bars) and GFP-STIM2C (gray bars) to PM-like liposomes containing either 5 mol% PI(4,5)P_2 or PI(3,4,5)P_3. The error bars in all graphs show the standard error of the mean (*n* = 3).

GFP-STIM1C and GFP-STIM2C did also bind to PI(4,5)P_2-containing PM-like liposomes, with more efficient binding of GFP-STIM2C and less binding of GFP-STIM1C as compared to the binding of GFP-CSS^{lst2} (Figure 3.17A). With PC liposomes that contain 5 mol% PI(4,5)P_2, binding of GFP-STIM1C and GFP-STIM2C was reduced 40- and 4-fold, respectively, as

compared to their binding to PM-like liposomes containing 5 mol% $PI(4,5)P_2$. This suggests that other lipids than $PI(4,5)P_2$ of the PM are absolutely essential for the binding of the STIM1 C-terminus to the PM, whereas the STIM2 C-terminus is less selective with respect to PM lipids.

In order to compare the affinities of the C-terminal domains of STIM proteins and CSS^{Ist2} for $PI(4,5)P_2$-containing PM-like liposomes, the K_D values were measured. GFP-STIM1C had a K_D of 8 ± 2 μM and GFP-STIM2C of 3.3 ± 0.8 μM (Figure 3.17B). Under similar conditions, a K_D value for GFP-CSS^{Ist2} was previously determined to be 12 ±3 μM (91).

Many other proteins with polybasic clusters, e.g. small guanosine triphosphatases from the Ras, Rho, Arf and Rab subfamilies interact with $PI(4,5)P_2$ and $PI(3,4,5)P_3$ at the PM, arguing that these lipids play a ubiquitous role in regulating cellular signaling events (150). Therefore, the binding of GFP-STIM1C and GFP-STIM2C to PM-like liposomes containing 5 mol% $PI(4,5)P_2$ or $PI(3,4,5)P_3$ was compared. At 1 and 3 μM protein concentration, GFP-STIM1C had a clear preference for $PI(4,5)P_2$-containing liposomes, whereas GFP-STIM2C showed similar binding to $PI(4,5)P_2$- and $PI(3,4,5)P_3$-containing PM-like liposomes (Figure 3.17C). Overall, the binding of GFP-STIM2C to PIP-containing liposomes was consistently stronger than the binding of GFP-STIM1C under all conditions tested.

The binding of STIM1C and STIM2C to PM lipids, and domains of the STIM C-termini, which are responsible for binding to liposomes were further investigated. For the CSS^{Ist2}, it was previously found that multimerization, which is mediated by the N-terminal part (90), is a prerequisite for binding to $PI(4,5)P_2$-containing PM-like liposomes (91). Therefore, both coiled-coil domains of GFP-STIM1C and GFP-STIM2C were deleted (see cartoon, Figure 3.18A). This deletion abolished binding of GFP-STIM1C completely, whereas the corresponding deletion in GFP-STIM2C had no effect (Figure 3.18B). GFP-STIM2C-ΔCC showed 62% more binding than GFP-STIM2C. In order to test whether the K-rich domains alone interacts with PM lipids, the coiled-coil and the P-rich domains were deleted. The resulting constructs contained GFP, the K-rich domains and 10 additional N-terminal residues (GFP-STIM1 K-rich and GFP-STIM2 K-rich). Similar to GFP-STIM1C-ΔCC, no binding for GFP-STIM1 K-rich was observed, suggesting that multimerization of STIM1C is necessary for binding to $PI(4,5)P_2$ at the PM. Surprisingly, GFP-STIM2 K-rich showed 48% more binding than GFP-STIM2C (Figure 3.18B). This indicates that multimerization of STIM2 via the coiled-coil domains is not required for the interaction with PM lipids. On the other hand, the presence of the proline residue at the extreme C-terminus of the STIM1 K-rich domain may abolish the helix formation, thus binding to PM-lipids. In order to overcome this drawback, STIM1 may need to multimerize through its coiled-coil domains.

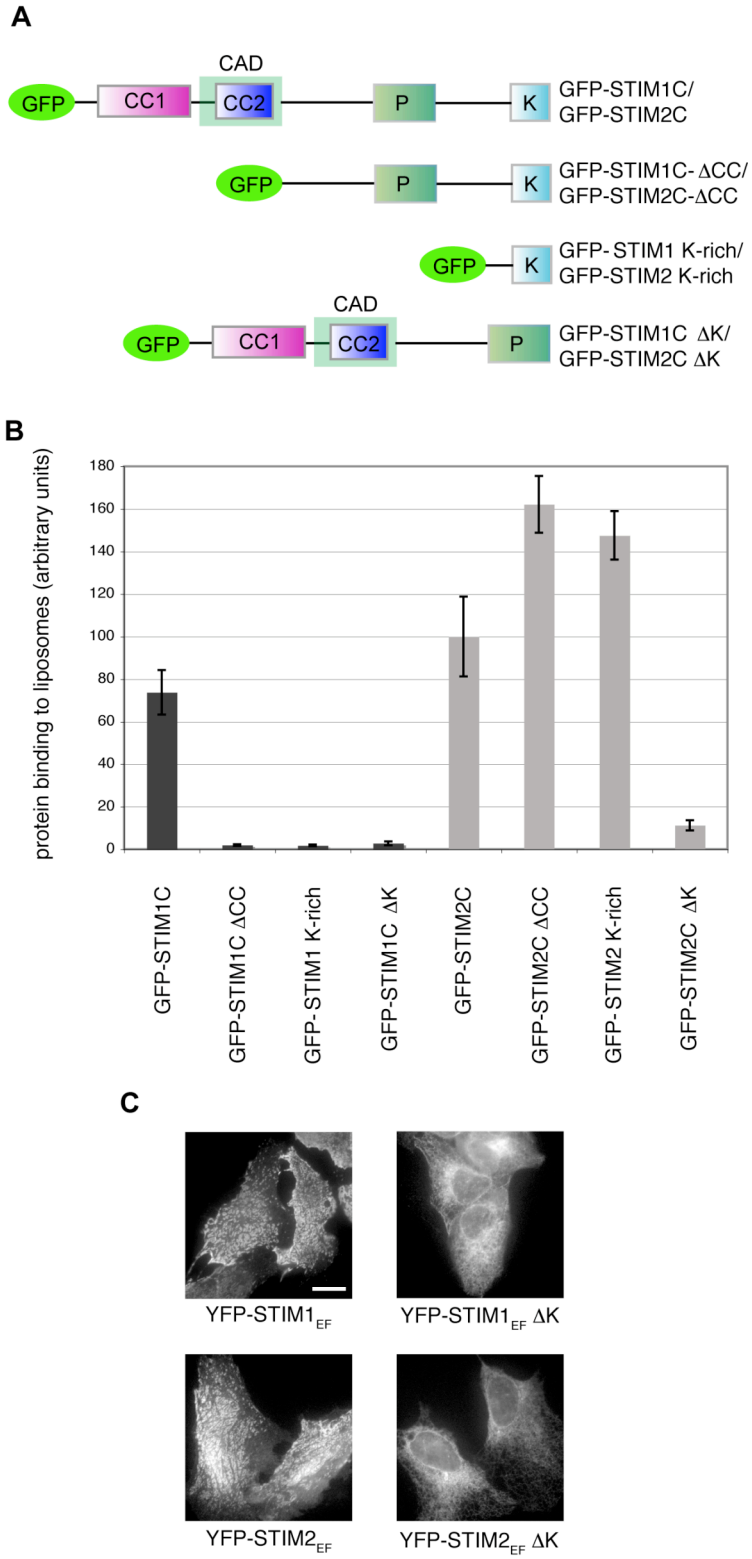

Figure 3.18 Contribution of different domains STIM1 and STIM2 to the lipid binding.

(A) Cartoon of the general domain structure of the C-termini of STIM1 and STIM2. The top row shows the coiled-coil domains (CC), the CAD domain of STIM1 overlapping with the second CC, the proline-rich domain (P) and the lysine-rich domain (K). The bottom rows indicate which domains were deleted from GFP-STIM1C and GFP-STIM2C. **(B)** Relative binding of these constructs to PM-like liposomes containing 5 mol% PI(4,5)P_2. **(C)** YFP fluorescence of U2OS cells after transfection with YFP-STIM1$_{EF}$, YFP-STIM1$_{EF}$ ΔK, YFP-STIM2$_{EF}$ and YFP-STIM2$_{EF}$ ΔK visualized by epifluorescence microscopy.

The K-rich domains of STIM1 and STIM2 are required for binding to $PI(4,5)P_2$-containing PM-like liposomes. GFP-STIM1C ΔK showed only background binding and the binding of GFP-STIM2C ΔK was 10-fold reduced (Figure 3.18B). To test the function of the K-rich domains for recruitment of the ER to the PM *in vivo*, the contribution of these domains to the formation of ER-PM contacts was analyzed. As an assay, the localization of overexpressed and mutated versions of yellow fluorescent protein (YFP)-tagged STIM1 and YFP-STIM2 were analyzed. These proteins carry single point mutations in their EF-hand Ca^{2+}-binding domains (YFP-$STIM1_{EF}$ and YFP-$STIM2_{EF}$), which result in their constitutive localization at puncta and patch-like ER–PM contacts (113). Deletion of the K-rich domains of YFP-$STIM1_{EF}$ and YFP-$STIM2_{EF}$ abolished the formation of these ER-PM contacts and YFP-$STIM1_{EF}$ ΔK and YFP-$STIM2_{EF}$ ΔK remained at reticular ER (Figure 3.18C), confirming the results of the *in vitro* lipid binding data.

3.2.3 Basic and hydrophobic residues are required for the function of the STIM2 lipid binding signal

Previous experiments with Ist2 revealed that different lipids contribute to the interaction with the PM (91). Moreover, experiments showed that the function of the CSS^{Ist2} depends on multimerization, basic residues and an amphiphatic α-helix with a hydrophobic patch of bulky side chains on one side of the α-helix (85). To test whether the basic residues and/or the hydrophobic patch contribute to the interaction of the STIM2 K-rich domain with lipids, the effect of different mutations in GFP-STIM2 K-rich in binding to $PI(4,5)P_2$- or $PI(3,4,5)P_3$-containing PM-like liposomes was analyzed. In order to analyze the effect of basic residues on lipid binding, two lysine residues were mutated into alanine. The mutations K718A and K719A had the strongest effect and reduced binding to $PI(4,5)P_2$ and $PI(3,4,5)P_3$ liposomes by 44 and 74%, respectively (Figure 3.19A). This reduction of binding suggests an electrostatic interaction between the K-rich domain of STIM2 and the negatively charged PIPs at the PM.

By the insertion of an alanine residue in between L726 and F727 (L726-A-F727), the hydrophobic patch of the putative amphipathic α-helix was destroyed. This mutation conserved the helical structure but destroyed the amphipathic feature. In this case, the binding to $PI(4,5)P_2$ and $PI(3,4,5)P_3$ liposomes reduced by 33 and 56%, respectively. This suggests that the positions of hydrophobic residues on one side of an α-helix contribute to the interaction between K-rich domain of STIM2 and lipids (Figure 3.19A).

Moreover, if the K-rich domain of STIM2 forms an amphipathic α-helix, introduction of a proline residue is expected to interfere with helix formation. Therefore, the K729P mutation was created in GFP-STIM2 K-rich. Moreover, this mutation would mimic the sequence of the extreme C-terminus of STIM1 K-rich domain (PLKK). With $PI(4,5)P_2$-containing liposomes, this mutation reduced binding by 22% and with $PI(3,4,5)P_3$ liposomes by 48% (Figure 3.19A).

Overall, these data show that the K-rich domain of STIM2 recognizes $PI(4,5)P_2$ and $PI(3,4,5)P_3$ at the PM and that the two distinct features of the STIM2 K-rich domain are important for

recognition of PM lipids. These features are a cluster of basic residues and a patch of hydrophobic residues located on one side of an amphipathic α-helix.

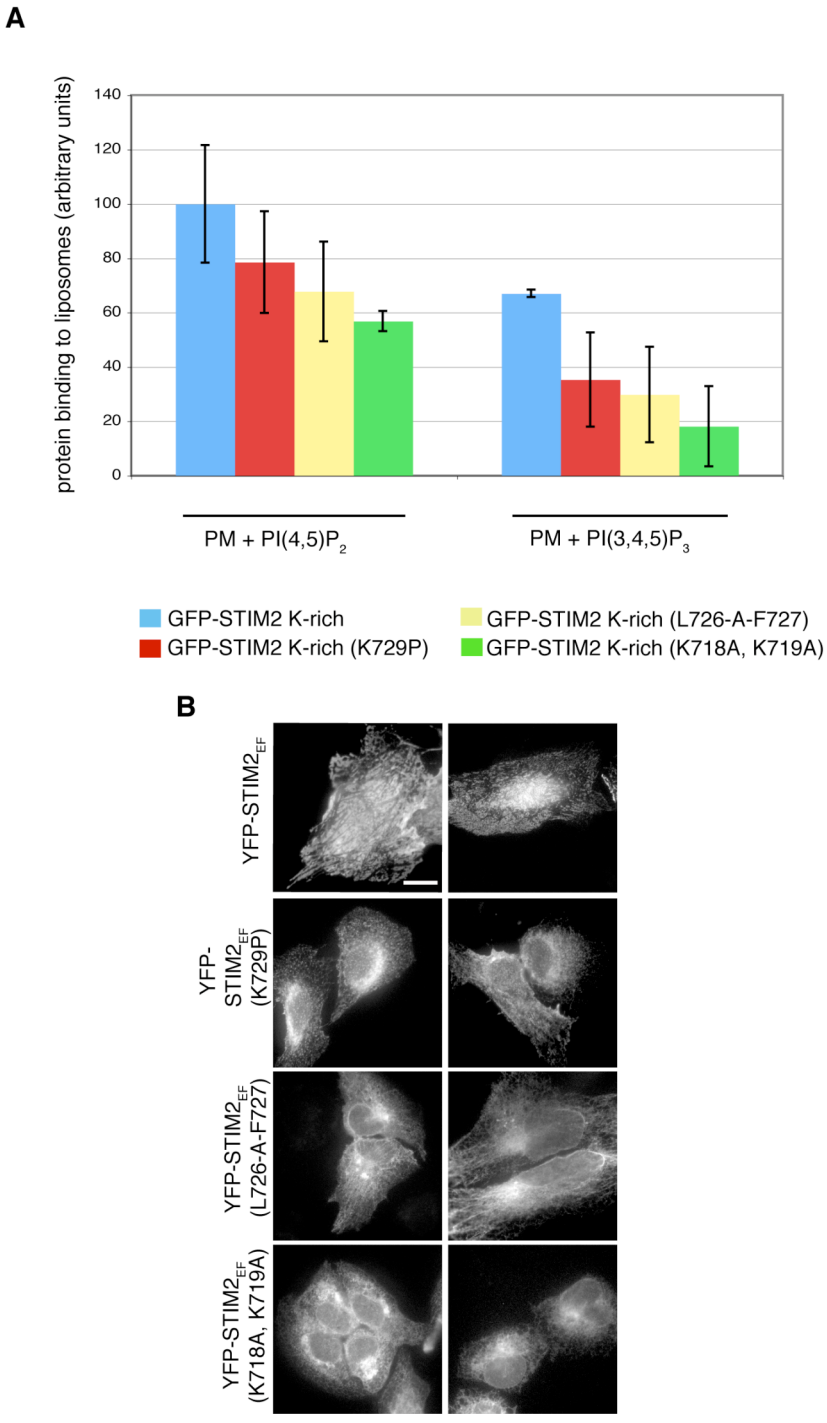

Figure 3.19 Effect of mutations in the K-rich domain of STIM2 on lipid binding and localization at ER–PM contacts.

(A) Relative binding of recombinant GFP-STIM2 K-rich and of GFP-STIM2 K-rich carrying the indicated mutations to PM-like liposomes with 5 mol% $PI(4,5)P_2$ or $PI(3,4,5)P_3$. **(B)** YFP fluorescence of U2OS cells after transfection with $YFP\text{-}STIM2_{EF}$ and $YFP\text{-}STIM2_{EF}$ carrying the indicated mutations visualized by epifluorescence microscopy. Representative cells for each phenotype are shown.

Finally, the effect of these mutations on the localization of YFP-STIM2$_{EF}$ was tested. Compared to YFP-STIM2$_{EF}$, which localized at puncta and larger patches (Figures 3.18C and 3.19B), YFP-STIM2$_{EF}$ (K729P) accumulated in smaller puncta with less patch formation. Interference with the postulated hydrophobic patch of the amphiphatic α-helix by the L726-A-F727 mutation had a stronger effect and led to a complete loss of patch formation, while the localization of YFP-STIM2$_{EF}$ (L726-A-F727) changed into reticular ER (Figure 3.19B). A similar reticular localization was seen with YFP-STIM2$_{EF}$ (K718A, K719A).

Taken together, these data suggest that the STIM1 and STIM2 K-rich domains bind lipids at the PM and thereby contribute to the formation of ER-PM contacts.

3.3 Trafficking of STIM1 to the cell surface is regulated by multiple signals

Initial studies on STIM1 localization revealed that, STIM1 localizes to the cell surface of the stromal and mast cells (101, 102). However, the majority of the protein resides in the ER and functions during the SOCE by sensing the Ca^{2+} levels of the ER and forming ER-PM contact sites to activate Ca^{2+} channels at the PM.

Unlike STIM2, STIM1 does not contain a di-lysine ER-retention signal at its extreme C-terminus (Figure 3.14B). It is therefore unclear what kind of mechanisms retains STIM1 in the ER. I was interested in the regulation of STIM1 localization and the mechanisms that retain the protein in the ER. I found two types of signals that retain STIM1 in the ER. One of these signals is an arginine-based ER-retention signal, and the other is the K-rich domain, which is regulated by cytosolic Ca^{2+}. Moreover, I further investigated the additional function of STIM1 on the cell surface.

3.3.1 Di-arginine signals retain STIM1 in the ER

In order to gain insight into the ER-retention mechanism of a STIM1, the protein was N-terminally tagged with one HA epitope (Figure 3.20B). Previous studies showed that STIM1 cannot reach the cell surface when a tag at the N terminus exceeds a certain size, e.g. that of GFP (141). Therefore, this small HA tag was chosen. If HA-STIM1 travels to the cell surface, the protein can be detected on the surface of nonpermeabilized cells, whereas detection of the ER-located pool requires membrane permeabilization (Figure 3.20B). Cotransfection of HEK293T cells with GFP and HA-STIM1 encoding plasmids revealed that under nonpermeabilizing conditions 26% of the GFP positive cells showed HA-STIM1 surface localization by fluorescence microscopy (Figure 3.20C lower panel). Under permeabilized conditions HA-STIM1 was detected in all GFP-cotransfected cells, which is consistent with its predominant ER localization (Figure 3.20C upper panel). Analysis by flow cytometry confirmed that 1% of the GFP-positive cells expressed HA-STIM1 on their surface (Figure 3.20D, left panel). To ensure specific surface localization, a conservative gating was chosen. This may explain the apparent differences in surface localization between immunofluorescence and flow cytometry data.

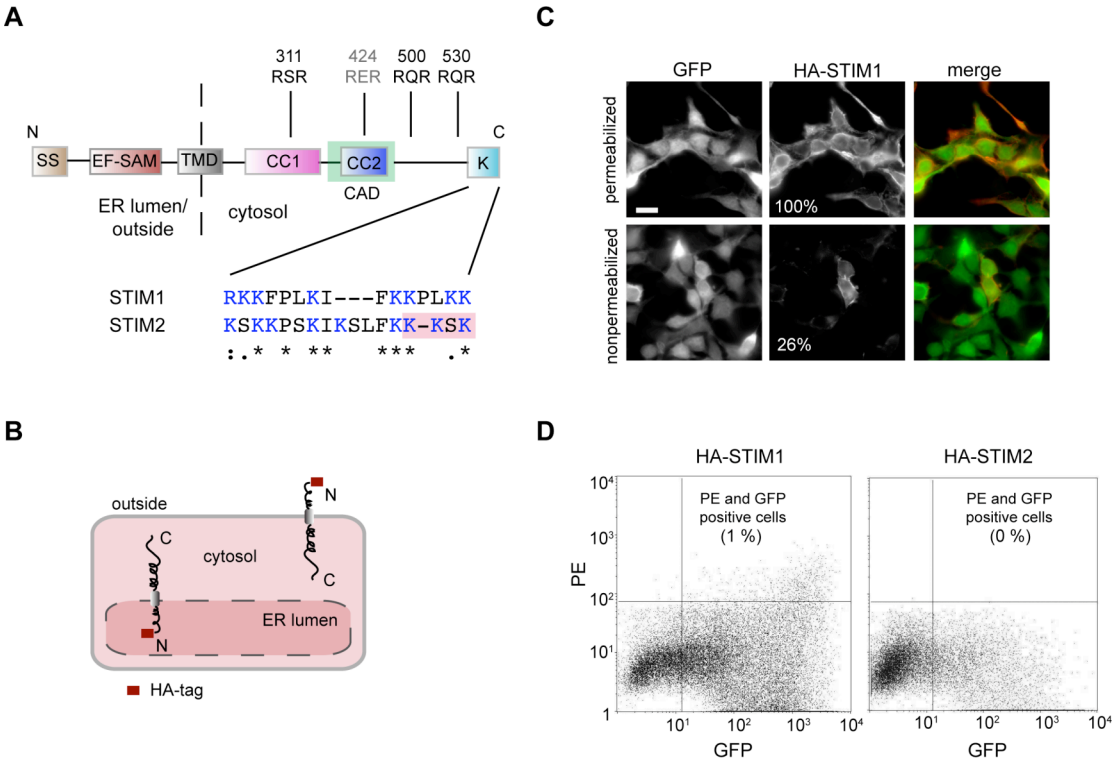

Figure 3.20 HA-STIM1 can reach the surface of HEK293T cells.

(A) The domain structure of STIM1 (SS, signal sequence; EF-SAM, EF-hand and SAM domain; TMD, trans-membrane domain, CC, coiled-coil domain; CAD, CRAC activation domain; K, K-rich domain). Putative di-arginine signals are depicted and alignment of the K-rich region of human STIM1 and STIM2 is shown. Basic residues are shown in blue and the di-lysine ER-retention signal of STIM2 is high lighted. **(B)** Cartoon of membrane topology and intracellular distribution of STIM1. The HA-tag at the N terminus is shown as a red box. **(C)** Immunofluorescence of HEK293T cells co-expressing GFP (green) and HA-STIM1 (red). The number of GFP-positive cells (in %) with HA-STIM1 staining under permeabilized and nonpermeabilized conditions are shown. **(D)** FACS profiles of HA-STIM1 (PE (R-Phycoerythrin)) and GFP (left) or HA-STIM2 and GFP (right) co-transfected HEK293T cells. The cut off for HA surface signal was set according to cells transfected with GFP and stained with HA antibodies.

In comparison to HA-STIM1, HA-STIM2 was remained intracellular in all cells (Figure 3.20D, right panel). This is consistent with the presence of a di-lysine ER-retention signal at the extreme C terminus of STIM2. The function of the STIM2 K-rich domain as an ER-retention signal was further demonstrated by its transplantation to the C terminus of HA-STIM1, lacking its own K-rich domain (HA-STIM1ΔK). This transplantation led to intracellular retention of HA-STIM1ΔK STIM2K (Figure 3.21).

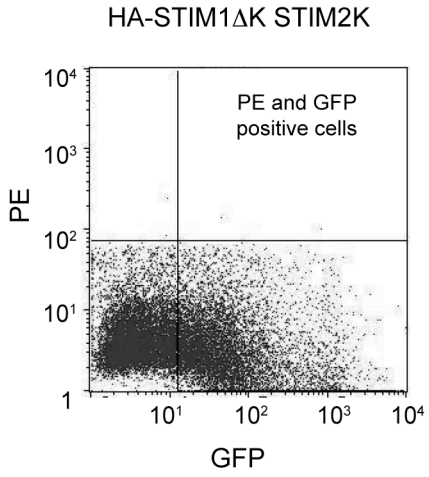

Figure 3.21 STIM2 K-rich region prevents the surface expression of HA-STIM1.
FACS profile of HEK293T cells co-expressing GFP and HA-STIM1ΔK STIM2K.

In a search for additional retention signals, four di-arginine consensus sites located in the cytosolic C terminus of STIM1 were found (Figure 3.20A). One di-arginine signal resides in the first coiled-coil domain (RSR311-313), one in the CAD (RER424-426), and two C-terminal of the CAD (RQR500-502 and RQR530-532). Since previous studies suggested that RER does not function as an efficient di-arginine retention signal (59), the analysis was performed on the other three signals. For this purpose, the critical two basic R residues were mutated to non-polar A residues. Mutation of RQR500-502 showed the strongest effect on retention, where 20% of the transfected cells expressed HA-STIM1 R500A on the cell surface (Figure 3.22A). Under nonpermeabilized conditions, HA-STIM1 R500A was detected in almost all cells at the surface by immunofluorescence (Figure 3.22B). Mutation of RSR311-313 and RQR530-532 had only minor effects with a two-fold increase of cells with HA-STIM1 on the surface as determined by flow cytometry. The combination of mutations did not enhance surface localization when compared to the single R500A mutation (Figure 3.22C).

This suggests that the retention of STIM1 in the ER is achieved by multiple di-arginine signals with RQR500-502 being the most active signal.

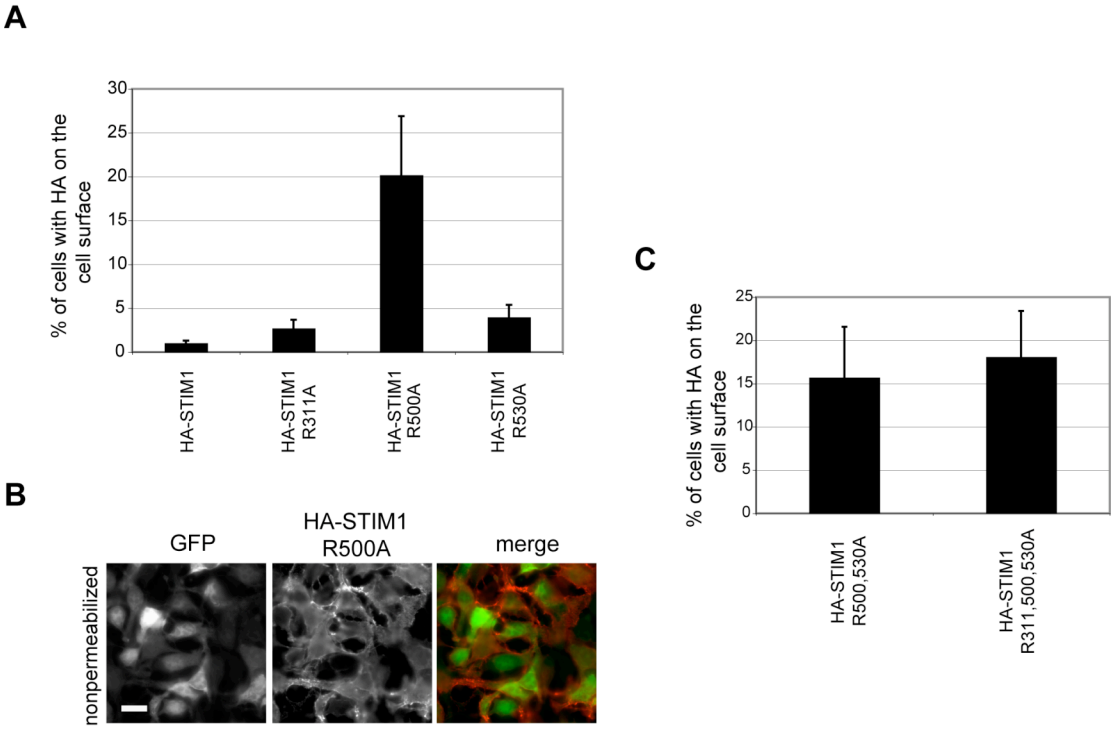

Figure 3.22 Di-arginine signals retain STIM1 in the ER.

(A) Quantification of the number of cells with HA-STIM1 and mutant HA-STIM1 on the cell surface analyzed by flow cytometry. Di-arginine signals were mutated (RXR to AXA) and the position of the first mutated R residue is indicated (R311A, R500A, R530A). **(B)** Immunofluoresence of nonpermeabilized HEK293T cells co-expressing GFP (green) and HA-STIM1 R500A (red). **(C)** Quantification of the number of cells with HA-STIM1 R500,530A and HA-STIM1 R311,500,530A on the cell surface analyzed by flow cytometry.

Next, I investigated the effect of RQR500-502 mutation on formation of ER-PM contact sites. In order to investigate this effect, the ER Ca^{2+} stores were depleted by a drug, Thapsigargin (Tg), which blocks the Sarco/endoplasmic Reticulum Ca^{2+} ATPase (SERCA) that uptake the cytosolic Ca^{2+} into the ER (151). The depletion of Ca^{2+} stores by addition of Tg resulted in co-localization of HA-STIM1 and GFP-Orai1 in puncta (Figure 3.23A). Similarly, addition of Tg created puncta in cells co-expressing HA-STIM1 R500A and GFP-Orai1 (Figure 3.23B). This indicates that the mutation of RQR500-502 in STIM1 did not interfere with the recruitment of Orai1 into puncta.

Moreover, I investigated the effect of R500A mutation on SOCE (Figure 3.23C). This was analyzed by Ca^{2+} imaging in HEK293T cells co-expressing HA-STIM1 R500A and Orai1. These cells were loaded with the Ca^{2+}-sensitive dye FURA-2AM (acetoxymethyl ester) prior to imaging. The addition of 2 mM Ca^{2+} to Tg-treated cells resulted in rapid influx of extracellular Ca^{2+}. As typically observed in SOCE, the addition of 50 µM 2-Aminoethyldiphenyl borate (2-APB) abolished this Ca^{2+} influx (152). 2-APB is a drug that blocks SOCE by inactivating IP_3 receptors that release Ca^{2+} from the ER to the cytosol (153). It was also observed that the co-expression of Orai1 reduced the amount of HA-STIM1 R500A at the cell surface (Figure 3.23D).

Taken together, this data suggests that R500A mutation does not affect the ER-PM contact site formation and SOCE.

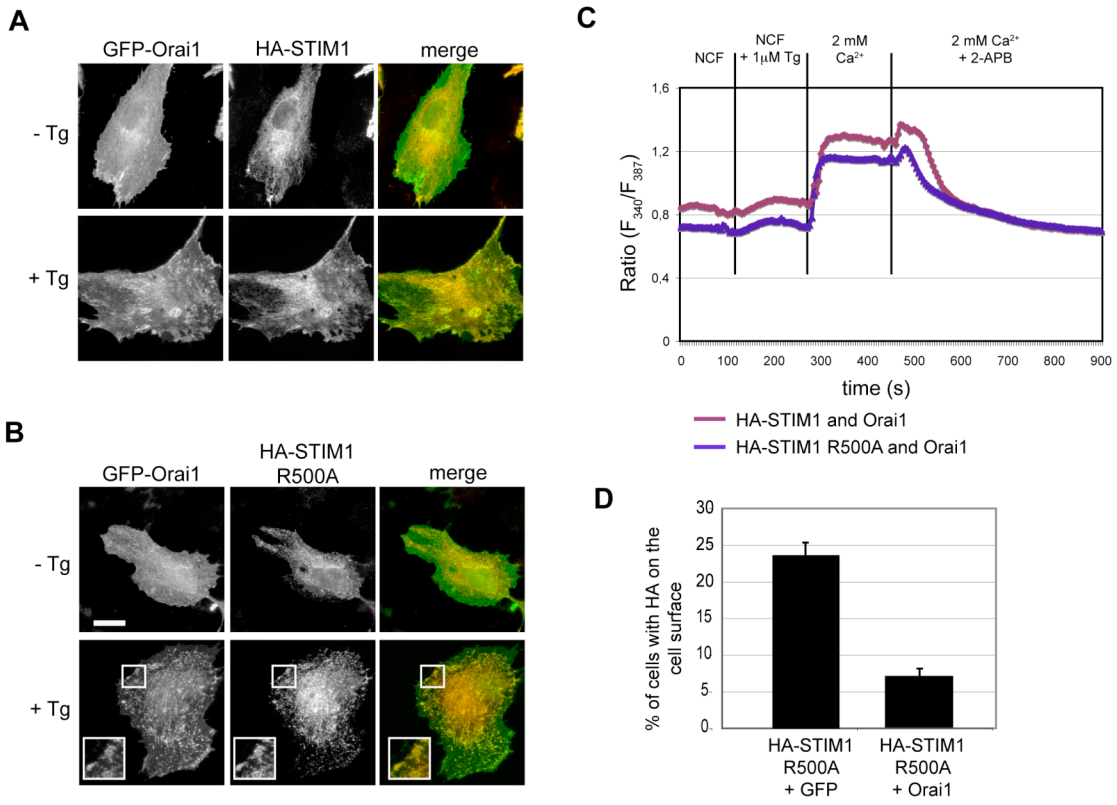

Figure 3.23 R500A mutation does not interfere with the function of STIM1.

(A) Co-localization of GFP-Orai1 (green) and HA-STIM1 (red) or **(B)** HA-STIM1 R500A (red) in RPE-1 cells without treatment or 10 min after addition of 0,5 μM Tg. The insert shows three-fold magnification of the indicated region. **(C)** FURA2-AM loaded HEK293T cells expressing Orai1 and HA-STIM1 or Orai1 and HA-STIM1 R500A were kept for 5 min in Ringer solution without Ca^{2+} (NCF, nominally Ca^{2+} free) before imaging. The ER-stores were depleted for 3 min by 1 μM Tg and the influx of Ca^{2+} was observed by adding Ringer solution containing 2 mM Ca^{2+}. SOCE was blocked by adding 50 μM 2-APB in 2 mM Ca^{2+} containing Ringer solution. Images were acquired every 5 s for 15 min. **(D)** Quantification of the number of cells with HA-STIM1 R500A on the cell surface after co-transfection with GFP or Orai1.

3.3.2 The flexible extreme N-terminus of STIM1 interferes with its localization to the cell surface

Another difference between STIM1 and STIM2 in sequence structure was shown for their extreme N-termini. This region has been previously characterized as a flexible domain (111). In order to study the role of extreme N-terminus in trafficking of STIM1 to the cell surface, I generated a construct lacking this corresponding region, which is from amino acid L23 to H57 (HA-ΔN_{ext}-STIM1). Strikingly, the cell surface expression of STIM1 was abolished as observed in flow cytometry analysis (Figure 3.24A). On the other hand, this deletion did not interfere with the formation of ER-PM contact sites. Upon addition of Tg, the protein was capable of forming puncta as similar as wild-type STIM1 (Figure 3.24B).

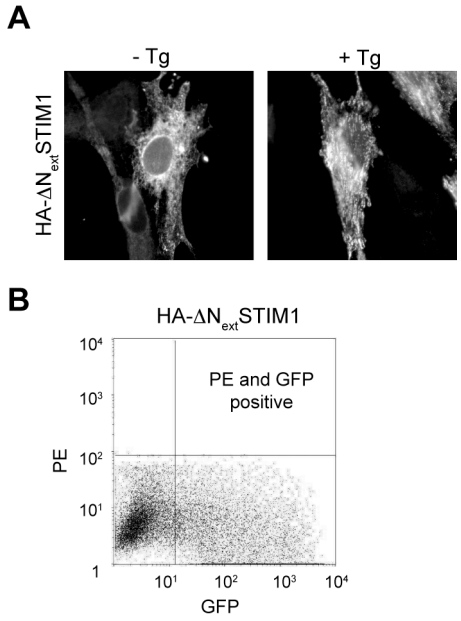

Figure 3.24 Deletion of extreme N-terminus of STIM1 abolishes its surface localization.

(A) Immunofluorescence of RPE-1 cells expressing HA-ΔN_{ext}-STIM1 with and without the treatment of Tg. **(B)** FACS profile of HEK293T cells co-expressing GFP and HA-ΔN_{ext}-STIM1.

3.3.3 The K-rich domain of STIM1 functions as an additional ER-retention signal, which is regulated by Ca^{2+}/calmodulin

As shown in aforementioned experiments, the K-rich domain of STIM1 can bind to PM-lipids. Moreover, independently, it was shown that the K-rich region of both STIM1 and STIM2 are capable of binding Ca^{2+}/CaM *in vitro* (127). I was therefore interested in whether the K-rich region contribute to the ER-retention albeit having no KKXX signal.

In order to test the effect of K-rich domain, I generated a construct lacking this domain (from R671 to K685) (HA-STIM1ΔK). Deletion of the K-rich domain resulted in an increased number of cells with STIM1 localization at the cell surface (Figure 3.25A and 3.26A). In nonpermeabilized conditions, 49% of HEK293T cells expressed HA-STIM1ΔK on the cell surface. Compared to the mutation of the di-arginine signal at position 500-502, the deletion of the K-rich domain had a weaker effect, however the combination of both mutations resulted in strong surface localization. Both in flow cytometry and immunofluoresence experiments this strong surface localization of HA-STIMΔK R500A was observed (Figure 3.25 B and C and 3.26A).

Based on ER retention via the K-rich region and its interaction with Ca^{2+}/CaM (127), I hypothesized that changes in cytosolic Ca^{2+} levels regulate the intracellular distribution of STIM1. In order to challenge this hypothesis, I depleted the cytosolic Ca^{2+} by addition of 2 mM EGTA to the media of the cells and incubated for one hour before the detection of HA-STIM1 at the surface by flow cytometry. This time would allow trafficking of HA-STIM1 to the cell surface. Addition of EGTA led to a two-fold increase of cells with HA-STIM1 on the surface (Figure

3.26B). This Ca^{2+}-dependent increase in the number of cells with HA-STIM1 on the surface depends on the K-rich domain. Addition of EGTA to cells expressing HA-STIM1ΔK did not significantly change the number of cells with surface expression (Figure 3.26B).

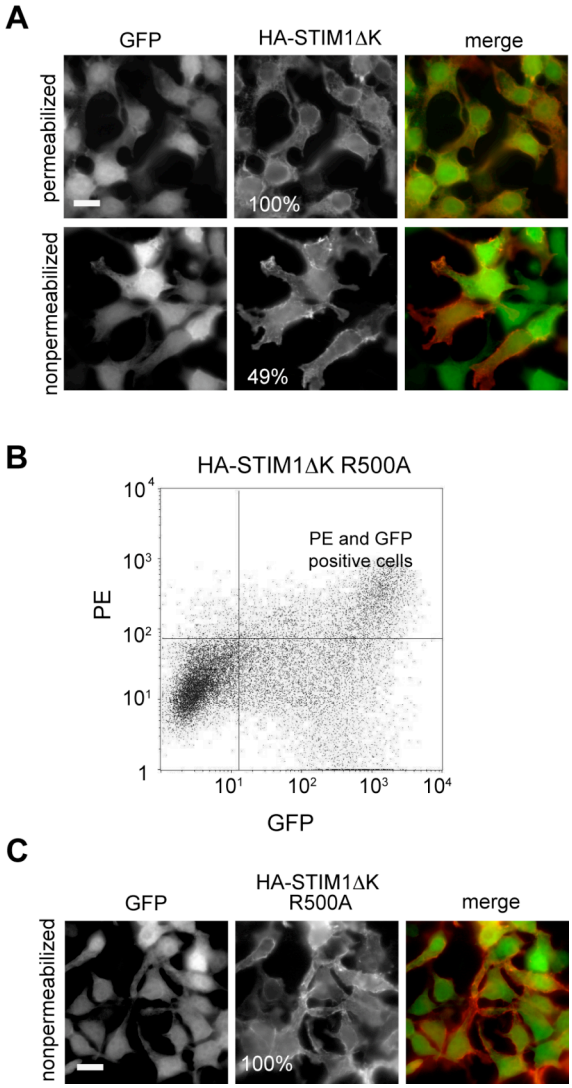

Figure 3.25 Deletion of K-rich region targets STIM1 to the cell surface.

(A) Immunofluorescence of HEK293T cells co-expressing GFP (green) and HA-STIM1ΔK (red) under permeabilized and nonpermeabilized conditions. The numbers indicate the percentage of cells with GFP and HA signals. **(B)** FACS profile of the cells co-expressing GFP and HA-STIM1ΔK R500A. **(C)** Immunofluorescence of HEK293T cells co-expressing GFP (green) and HA-STIM1ΔK R500A (red) under nonpermeabilized condition.

Next, in order to test whether the K-rich domain functions as Ca^{2+} sensor, a binding assay with a GFP-tagged C-terminal domain of STIM1 and CaM-coated beads was established. Binding of GFP-STIM1C to CaM-beads required Ca^{2+} and addition of EGTA abolished the interaction between STIM1 and CaM. On the other hand, the deletion of the K-rich domain reduced the

level of binding but fail to abolish it completely. This suggests the presence of additional Ca^{2+}/CaM-binding sites (Figure 3.26C).

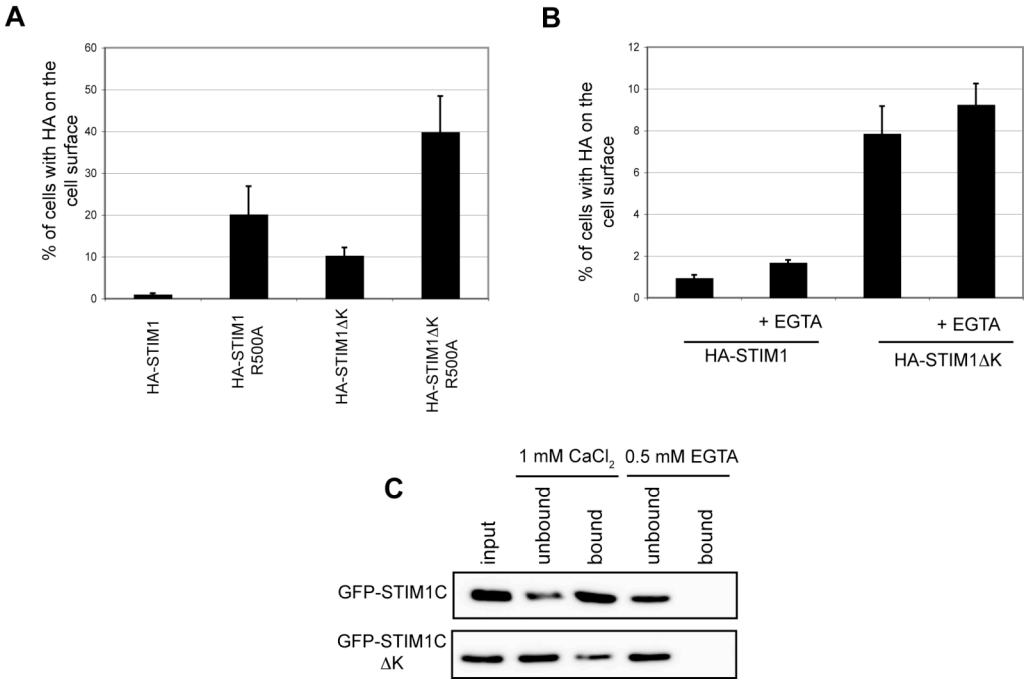

Figure 3.26 K-rich, which is regulated by Ca^{2+}/CaM binding, retains STIM1 in the ER.

(A) Quantification of the number of HEK293T cells (in %) with HA on the cell surface after detection by flow cytometry in cells expressing HA-STIM1, HA-STIM1 R500A, HA-STIM1ΔK and HA-STIM1ΔK R500A. **(B)** In cells with HA-STIM1 or HA-STIM1ΔK after adding 2 mM EGTA for 1 h. **(C)** Binding of GFP-STIM1C and GFP-STIM1C ΔK to CaM beads in the presence of 1 mM $CaCl_2$ or 0.5 mM EGTA. Unless stated otherwise this and all following CaM binding experiments were performed in 0.1% NP-40 and 150 mM NaCl buffer. The bound fraction corresponds to five times the amount of input and unbound fractions.

Due to the observation of a high cell-to-cell variation between cells with STIM1 on the surface and cells with intracellular STIM1, the cytosolic Ca^{2+} levels of individual cells were monitored. A GFP-tagged version of the nuclear factor of activated T cells (NFAT) was used as a cell-based Ca^{2+} indicator. GFP-NFAT shuttles between the cytosol and the nucleus. It accumulates in the cytosol at low and in the nucleus at high concentrations of cytosolic Ca^{2+} (154). Under our experimental conditions, 42% of the transfected cells showed nuclear accumulation of GFP-NFAT in medium (Figure 3.27A). A high cell-to-cell variation of GFP-NFAT distribution between the cytosol and the nucleus was observed in these cells. This cell-to-cell variation of the cytosolic Ca^{2+} may cause the observed differences in HA-STIM1 localization between individual cells. Control experiments showed that a decrease in cytosolic Ca^{2+} levels by addition of EGTA reduced the number of cells with GFP-NFAT in the nucleus to 20%, whereas an increase in cytosolic Ca^{2+} levels led to nuclear accumulation in 85% of Tg-treated cells (Figure 3.27B and C).

Taken together, these data suggest a regulated ER-retention mechanism, which is based on two types of signals: di-arginine retention signals and the Ca^{2+}/CaM-binding K-rich domain. The latter senses the cytosolic Ca^{2+} levels and triggers the release of STIM1 from the ER.

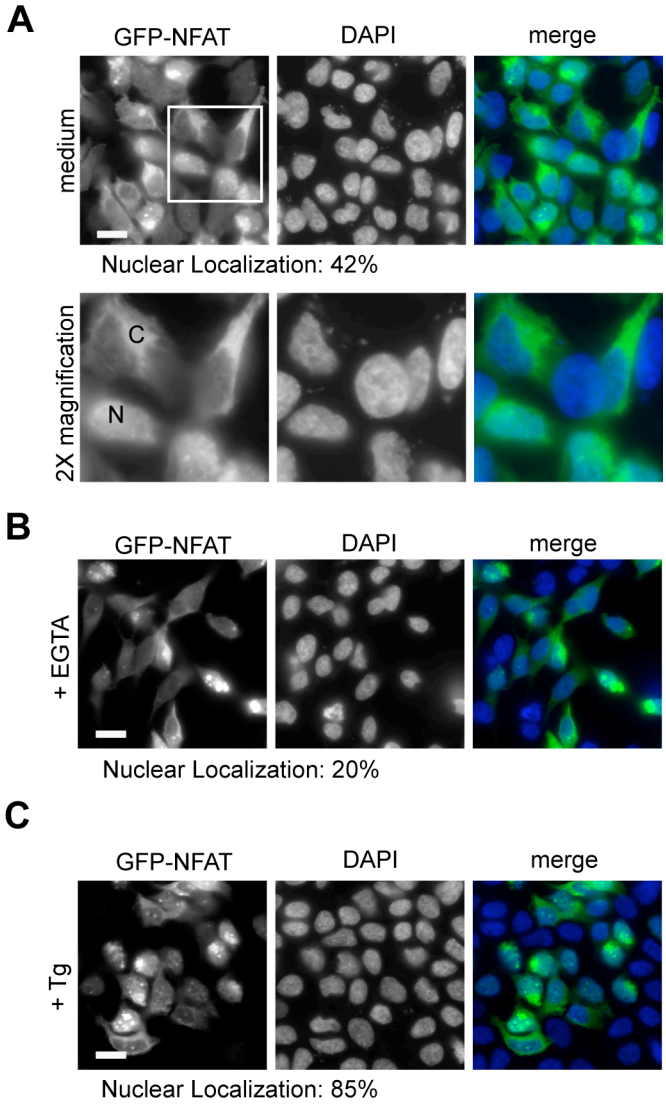

Figure 3.27 Cell-to-cell variation of cytosolic Ca^{2+} concentration.

(A) HEK293T cells expressing GFP-NFAT (green) in normal medium conditions (DMEM/F12, 10% FBS, 2 mM glutamine). The nuclei are stained with DAPI (blue). The bottom panels show a two-fold magnification of the indicated area and examples with nuclear (N) or cytosolic (C) GFP-NFAT staining are indicated. Hundred cells with GFP-NFAT accumulated in the nucleus or in the cytosol were counted and the percentage of cells with predominant nuclear signal is indicated. **(B)** Distribution of GFP-NFAT (green) in HEK293T cells after adding 2 mM EGTA for 30 min to the media. **(C)** Distribution of GFP-NFAT after addition of 0,5 μM Tg for 30 min to the media. The nuclei are stained with DAPI (blue).

3.3.4 Store-operated Ca^{2+}-entry interferes with STIM1 trafficking to the cell surface

Based on increased STIM1 trafficking to the cell surface at low concentrations of cytosolic Ca^{2+} levels, I hypothesized that SOCE and subsequent increase in cytosolic Ca^{2+} reduces the trafficking of STIM1 to the cell surface (Figure 3.28A). The increase of cytosolic Ca^{2+} can be achieved by addition of Tg, thereby blocking the Ca^{2+} uptake into the ER. An additional increase

in cytosolic Ca^{2+} can be achieved by co-expression of Orai1 and promoting uptake of extracellular Ca^{2+} into the cell (Figure 3.28A). In order to test this, cells were treated for 1 h with Tg prior to the measurement of surface localized HA-STIM1 by flow cytometry. Tg treatment of cells expressing HA-STIM1 resulted in a two-fold reduction of the number of cells with HA-STIM1 on the surface (Figure 3.28B). This Ca^{2+}-dependent regulation of STIM1 distribution depends on the K-rich region. Tg had no effect on the cell surface localization of cells expressing HA-STIM1ΔK (Figure 3.28B). Next, HA-STIM1 and HA-STIM1ΔK were cotransfected with Orai1. The addition of Tg induced contact site formation between the STIM1 variants and Orai1 resulted in Ca^{2+} influx, leading to a reduction of the number of cells with HA-STIM1 and HA-STIM1ΔK on the surface (Figure 3.28C).

Taken together, these data suggest that high cytosolic Ca^{2+} levels and direct interaction of STIM1 with Orai1 results in intracellular retention of STIM1, independent of its K-rich domain.

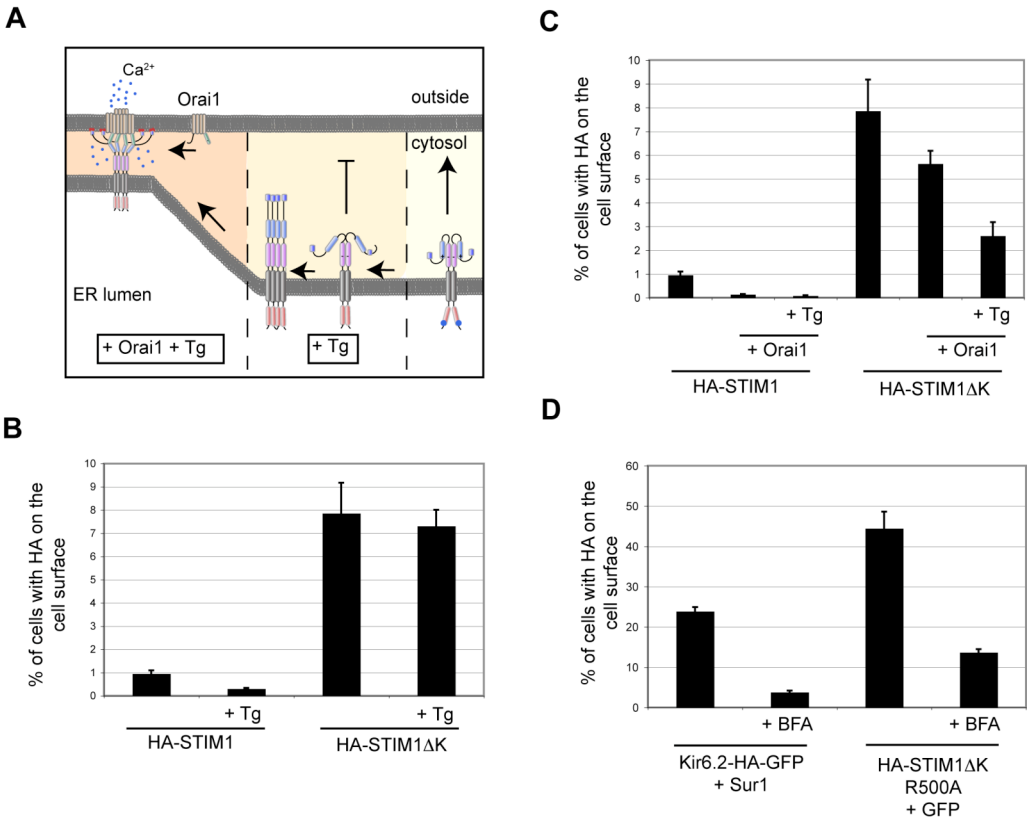

Figure 3.28 Trafficking of STIM1 is regulated by cytosolic Ca^{2+} levels.

(A) Cartoon describing the effect of an increase in cytosolic Ca^{2+} levels. In resting conditions, STIM1 can travel to the cell surface. Following addition of Tg and/or co-expression with Orai1, STIM1 is retained in the ER. The increasing gradient of yellow colour demonstrates the increase in cytosolic Ca^{2+} levels. Quantification of the number of HEK293T cells (in %) with HA on the cell surface after detection by flow cytometry in cells expressing: **(B)** HA-STIM1 and HA-STIM1ΔK without and with treatment with 1 μM Tg for 1 h. **(C)** HA-STIM1 and HA-STIM1ΔK as control, HA-STIM1 or HA-STIM1ΔK together with Orai1 without and with treatment with 1 μM Tg for 1 h. **(D)** In cells co-expressing Kir6.2-HA-GFP and Sur1 or HA-STIM1ΔK R500A and GFP. The cells were treated with 1 μg/ml BFA for 6 h before analysis by flow cytometry.

Next, I analyzed whether the trafficking of STIM1 to the cell surface is through Golgi. In order to investigate how STIM1 travels from the ER to the PM, the surface localization of HA-STIM1ΔK 500AQA in BFA-treated cells was analyzed. BFA-treatment reduced the number of cells with HA-STIM1ΔK 500AQA on their surface three to four fold (Figure 3.28D). A control experiment with Kir6.2-HA-GFP and Sur1 showed a similar result, suggesting that STIM1 travels via the classical secretory pathway to the cell surface.

3.3.5 Multiple Ca^{2+}/CaM binding sites regulate the function of STIM1

Since deletion of the K-rich domain did not completely abolish binding of STIM1 to Ca^{2+}/CaM, the STIM1-Ca^{2+}/CaM interaction was investigated in more detail. CaM can bind proteins through electrostatic and hydrophobic interactions (129). In order to test in which way CaM binds to STIM1, I performed two different binding conditions. In order to test the role of hydrophobic interactions, I performed the binding experiments in changing amounts of detergent (NP-40). The other condition was prepared to test the effect of electrostatic interactions and therefore I performed the binding experiments in different salt (NaCl) concentrations. Binding of GFP-STIM1C and GFP-STIM1C ΔK to Ca^{2+}/CaM was resistant to increasing amounts of detergent but sensitive to increased NaCl concentration (Figure 3.29A and B). This data indicated that Ca^{2+}/CaM binds STIM1 via electrostatic interactions.

Moreover, the contribution of electrostatic interaction was more pronounced in full-length GFP-STIM1C than in GFP-STIM1C ΔK, supporting an important contribution of basic residues in the K-rich domain to binding of Ca^{2+}/CaM.

Although the importance of K-rich domain in binding to Ca^{2+}/CaM was shown by decreased binding of GFP-STIM1C ΔK, the K-rich domain of STIM1 alone (last 25 amino acid residues) was not sufficient for binding (Figure 3.29C). On the other hand, the K-rich domain of STIM2 alone was sufficient for binding to Ca^{2+}/CaM (Figure 3.29C). In line with the lipid binding of STIM1 and STIM2, where STIM1 but not STIM2 requires its coiled-coil domains for binding to $PI(4,5)P_2$, it is plausible that mutimerization of STIM1 is required for binding to Ca^{2+}/CaM.

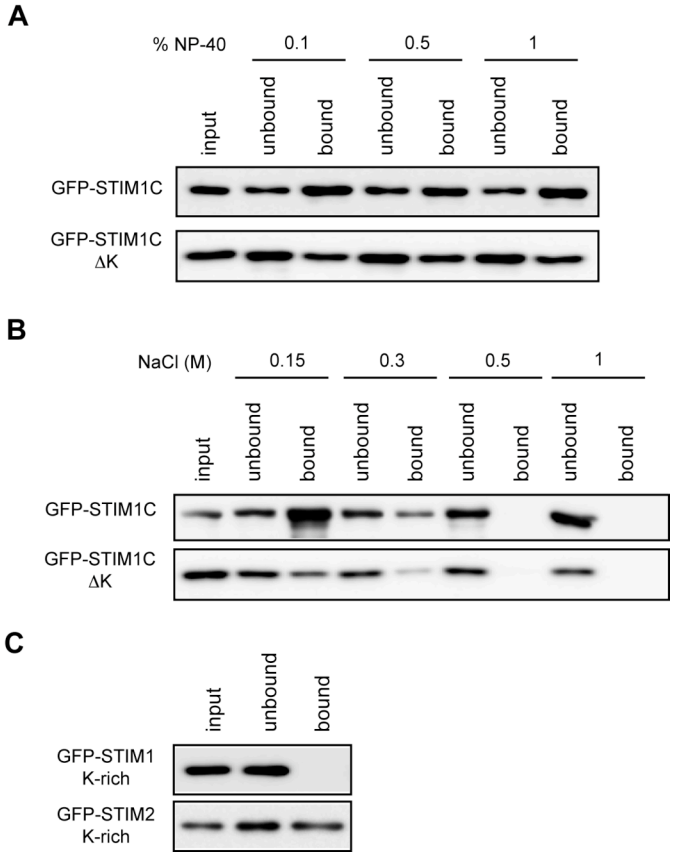

Figure 3.29 Binding of GFP-STIM1C and GFP-STIM1CDK to CaM beads in the presence different amounts of detergent and high salt.

(A) Binding of GFP-STIM1C and GFP-STIM1C ΔK to CaM beads in a buffer (25 mM Tris/HCl pH 7.5, 150 mM NaCl and 1 mM $CaCl_2$) with increasing NP-40 concentration. **(B)** Binding of GFP-STIM1C and GFP-STIM1C ΔK to CaM beads in a buffer (25 mM Tris/HCl pH 7.5, 0.1 % NP-40 and 1 mM $CaCl_2$) with increasing NaCl concentration. **(C)** Binding of GFP-STIM1 K-rich domain and GFP-STIM2 K-rich domain to CaM beads in CaM buffer.

In silico analysis of the STIM1 sequence by the calmodulin target database (130) revealed two putative CaM-binding sites (CaM-I and CaM-II) located in the evolutionary conserved CAD (Figure 3.30A). The polybasic region in CaM-I has been identified as a regulatory switch. It either binds Orai1 or interacts with an autoinhibitory domain in coiled-coil domain 1 of STIM1 (131, 132). The latter interaction arrests STIM1 in a closed conformation under resting conditions (132). Multimerization of the coiled-coil domains upon a decrease in the levels ER Ca^{2+} extends the STIM1 structure allowing binding of the polybasic region to the acidic domain at the C-terminus of Orai1 (131, 132). It has been suggested that this conformational change opens the CRAC channel (132).

As CaM recognizes a hydrophobic face of an α-helix with basic residues (129), I investigated whether CaM-I and CaM-II are required for binding to CaM beads. For this purpose the indicated hydrophobic residues or the lysine residues were mutated to alanine (Figure 3.30A). Both the hydrophobic residues ($H1_{AA}$, $H2_{AA}$, and combination of $H1_{AA}H2_{AA}$) and central polybasic residues (K3A) in CaM-I contributed to binding of GFP-STIM1C ΔK to CaM beads.

Mutation of the polybasic residues (reduction of binding by 84%, Figure 3.30C) had a stronger effect as compared to mutation of hydrophobic residues (reduction of binding by 50 to 68%, Figure 3.30B). This suggests the possibility that Ca^{2+}/CaM binding to the polybasic sequence controls conformational changes in STIM1. Deletion of the entire CaM-I domain reduced binding by 85%, similar to mutation of the polybasic residues, but did not abolish binding to Ca^{2+}/CaM completely (Figure 3.30D). This is consistent with the presence of a second CaM-binding site in STIM1ΔK.

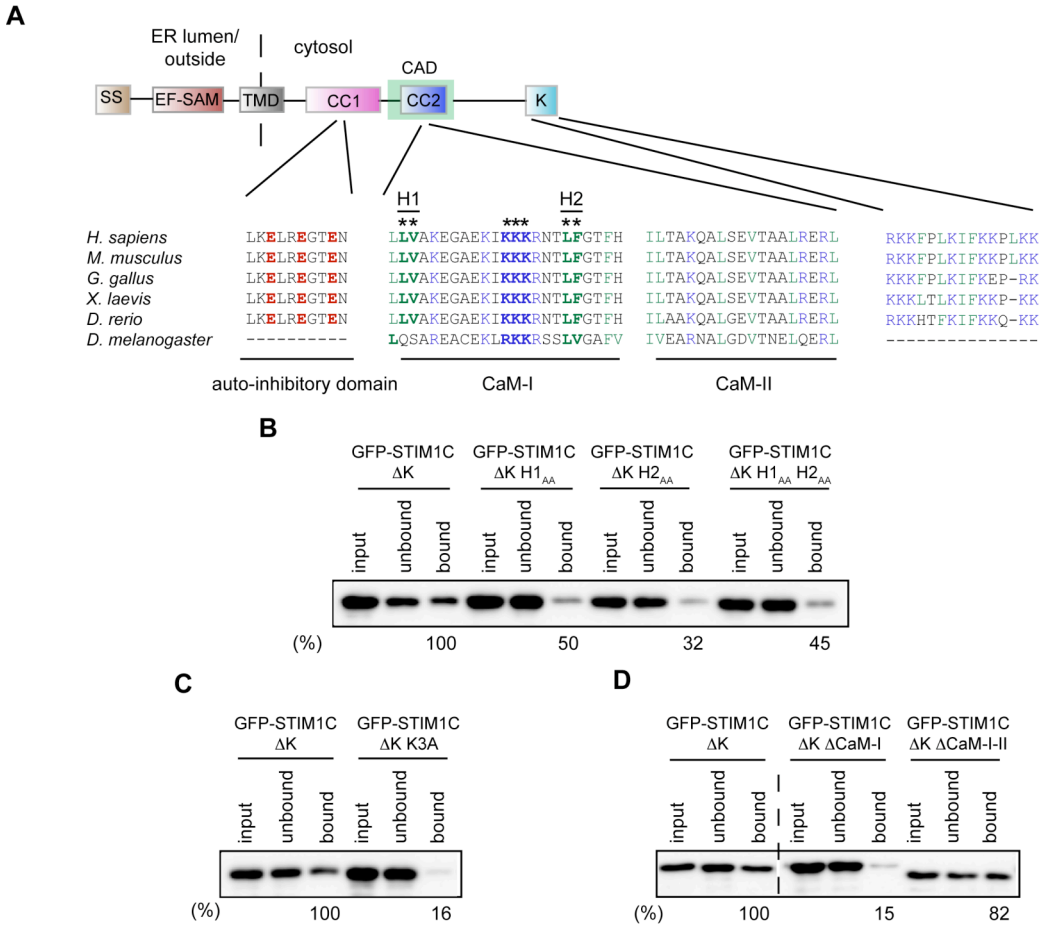

Figure 3.30 STIM1 has at least two Ca^{2+}/CaM binding sites.

(A) Cartoon of STIM1 with acidic auto-inhibitory domain located in the first coiled-coil domain, two predicted CaM-binding sites (CaM-I, residues 373-395 in human STIM1) and (CaM-II, residues 409-427) in the second coiled-coil domain overlapping with CAD, and the K-rich domain. The amino acid sequences of CaM-I, CaM-II and K-rich domains of different vertebrates and drosophila are shown and conserved acidic residues of the auto-inhibitory domain are indicated in red, conserved hydrophobic residues (H1 and H2) of CaM-I in green, and conserved basic residues of CaM-I in blue. Introduced mutations of either hydrophobic or K residues to A in CaM-I are marked with stars. **(B)** Binding of GFP-STIM1C ΔK and GFP-STIM1C ΔK with mutations of hydrophobic residues ($H1_{AA}$, $H2_{AA}$ and $H1_{AA}H2_{AA}$) in CaM-I to CaM beads. The bound fraction corresponds to five times the amount of input and unbound fractions. The bound fractions were quantified and the amount of bound GFP-STIM1C ΔK was set to 100. **(C)** Binding of GFP-STIM1C ΔK and GFP-STIM1C ΔK with mutations of basic residues (K3A) in CaM-I to CaM beads. **(D)** Binding of GFP-STIM1C ΔK with deletion of CaM-I (372-394) and deletion of the region covering both CaM-I and CaM-II domains (372-427) to CaM beads.

However, the deletion of a larger region covering CaM-I, CaM-II, and connecting residues stimulated binding to CaM beads to a level above binding of GFP-STIM1C ΔK (Figure 3.30D). This suggests that deletion of the regulatory switch domain may change the conformation of STIM1, which results in the exposure of additional CaM-binding sites.

Taken together, this data indicates that multiple Ca^{2+}/CaM molecules bind to STIM1 and may regulate its function.

3.3.6 The cell surface pool of STIM1 activates Orai1

Since STIM1 travels in a cytosolic Ca^{2+}-regulated manner to the cell surface, it was of interest to investigate whether STIM1 fulfils an additional function at the PM. At resting conditions, in the absence of Tg, HA-STIM1ΔK R500A localized in both reticular ER-like structures and in the PM (Figure 3.31A). This indicates that SOCE did not occur under these experimental conditions. Moreover, HA-STIM1ΔK R500A was not retained in the ER by co-expression of Orai1 (Figure 3.31B) as HA-STIM1 R500A was, suggesting that disruption of retention signals in STIM1 weaken the interaction with Orai1 at puncta.

In order to test the function of HA-STIM1ΔK R500A in SOCE, Ca^{2+} imaging experiments were performed. I found that the increase in cytosolic Ca^{2+} levels, upon 2-APB treatment, was weaker in cells co-expressing Orai1 and HA-STIM1ΔK or HA-STIM1ΔK R500A as compared to cells co-expressing Orai1 and wild type HA-STIM1 (Figure 3.32A). Only half of the Tg-induced Ca^{2+}-influx was sensitive towards the SOCE inhibitor 2-APB, whereas in cells co-expressing wild type STIM1 and Orai1, Ca^{2+}-influx was completely abolished by 2-APB (Figure 3.32A). These data suggest that surface-located HA-STIM1ΔK and HA-STIM1ΔK R500A function in an alternative Ca^{2+} influx process. Moreover, this SOCE-independent Ca^{2+} influx requires co-expression of Orai1. Co-expression of HA-STIM1ΔK R500A with TRPC1 or TRPC4 Ca^{2+} channels did not generate Ca^{2+} influx (data not shown). Since Orai2 showed the same response to 2-APB, either with HA-STIM1ΔK R500A or HA-STIM1 (data not shown) and Orai3 was activated by 2-APB (data not shown and (152)), it was not feasible to investigate whether surface STIM1ΔK R500A controls Orai2 and Orai3 in a SOCE-independent manner.

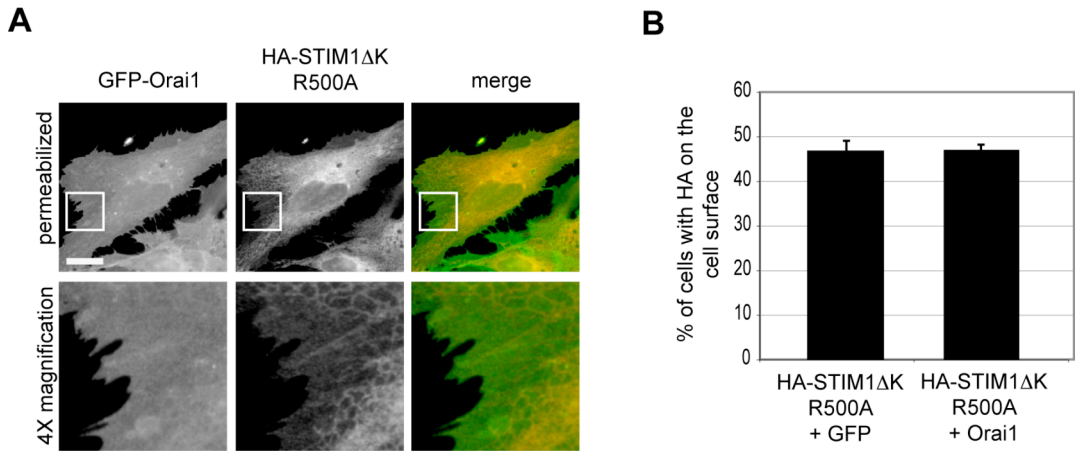

Figure 3.31 HA-STIM1ΔK R500A localizes to reticular ER and to the cell surface.

(A) RPE-1 cells were cotransfected with HA-STIM1ΔK R500A (red) and GFP-Orai1 (green). Upper panel shows the distribution of both proteins in permeabilized cells. Lower panel shows four times magnification of the indicated region. **(B)** Quantification of cell surface expression of HA-STIM1ΔK R500A on the surface after co-expression with GFP or Orai1.

Based on the observed 2-APB-insensitive Ca^{2+} influx (Figure 3.32A), I hypothesized that surface located pools of HA-STIM1ΔK and HA-STIM1ΔK R500A recruit and open Orai1. A control experiment in RPE-1 cells showed that depletion of Ca^{2+} from the ER lumen by Tg resulted in accumulation of HA-STIM1ΔK R500A and GFP-Orai1 in puncta, as seen in permeabilized cells (Figure 3.32B). However, the surface pool of HA-STIM1ΔK R500A did not co-localize with GFP-Orai1 puncta (Figure 3.32B).

This suggests the existence of two independent STIM1-Orai1 complexes: one between ER-located STIM1 and Orai1 and the other one between cell surface-located STIM1 and Orai1.

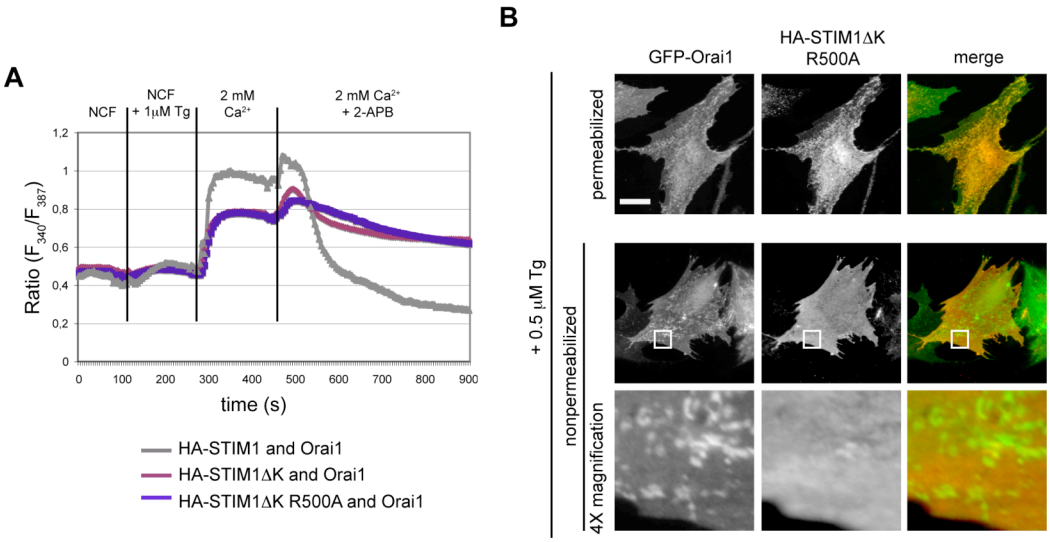

Figure 3.32 The surface pool of STIM1 is not involved in SOCE and co-localizes with Orai1.

(A) Ca^{2+} imaging of FURA2-AM loaded HEK293T cells expressing HA-STIM1, HA-STIM1ΔK or HA-STIM1ΔK R500A together with Orai1. Cells were kept in NCF Ringer solution for 5 min before imaging. Cells were treated with 1 µM Tg in order to induce SOCE. 2 mM Ca^{2+} containing Ringer solution was applied to observe Ca^{2+} influx. The SOCE was inhibited by adding of 50 µM 2-APB. The HA-STIM1 and Orai1 curve was normalised to the curve of HA-STIM1ΔK and Orai1 for a better comparison. **(B)** Localization of HA-STIM1ΔK R500A (red) and GFP-Orai1 (green) in RPE-1 cells after treatment with 0.5 µM Tg for 10 min. The upper panels show the co-localization at punctuate structures in a permeabilized cell, the middle panels show co-localization in a nonpermeabilized cell and the bottom panels show a four-fold magnification of the indicated area.

Focusing on the surface pool of HA-STIM1ΔK R500A in nonpermeabilized cells revealed two phenotypes: even distribution of HA-STIM1ΔK R500A and GFP-Orai1 over the entire PM or co-localization of the two proteins in ill-defined domains of the PM (Figure 3.33). Co-localization of HA-STIM1K R500A and Orai1 under nonpermeabilized conditions suggests that surface located STIM1 and Orai1 can interact and mediate SOCE-independent Ca^{2+} influx.

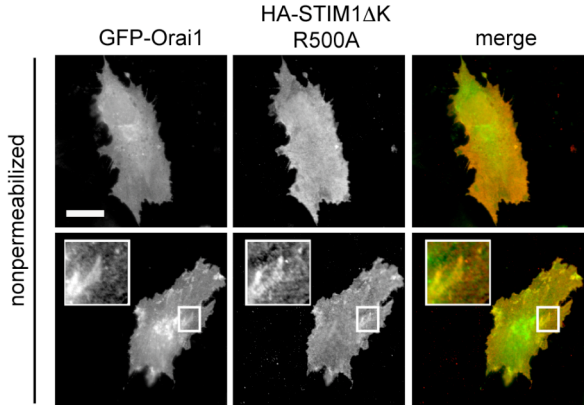

Figure 3.33 Different phenotypes of HA-STIM1ΔK R500A and GFP-Orai1 co-localizations.

Localization of HA-STIM1ΔK R500A (red) and GFP-Orai1 (green) in nonpermeabilized RPE-1 cells. The lower panels and the magnified inserts show a cell where GFP-Orai1 and the HA-STIM1ΔK R500A co-localize to yet unknown domains of PM.

4 Discussion

In this study, I contributed to the understanding of the mechanistic features of the ER-PM contact site formation in mammalian cells and analyzed the ER retention mechanisms of STIM1 in detail. First of all, I showed that the expression of transmembrane proteins with PM-lipid binding domains led to the formation of ER-PM contact sites. This principal is conserved in both yeast and mammalian cells. It was previously shown that Ist2 protein, which localizes to the cortical ER of yeast, makes contacts with the PM-lipids. The attachment of the lipid-binding domain of Ist2 (CSS^{Ist2}) to integral membrane proteins and their expression in mammalian cells resulted in the formation of ER-PM contact sites. The CSS^{Ist2} can be replaced by phospholipase C-δ1 PH domain, which binds $PI(4,5)P_2$ at the PM. Any ER membrane protein, used in this study, including CD4, MHC Class I heavy chain, Tap1 and Kir6.2, carrying a cytosolically exposed PM lipid-binding signal was capable of forming ER-PM contacts.

The phenomenon of ER-PM contact site formation is observed in mammalian STIM proteins, which function in store-operated Ca^{2+} entry (SOCE). Mammalian cells express two STIM proteins, STIM1 and STIM2. These proteins are activated upon depletion of ER Ca^{2+} and form ER-PM contact sites, where they interact with and activate PM Ca^{2+} channels. In addition to their interaction with the channel protein, I demonstrated that both proteins are capable of binding PM lipids via their K-rich domains.

Further analysis of the differences between STIM1 and STIM2 revealed that the localization of STIM2, which has the di-lysine ER retention signal, is restricted to the ER. On the other hand, STIM1 lacks this di-lysine signal and therefore can travel to the cell surface. However, in order to function in SOCE, STIM1 must be retained in the ER. To solve this puzzling phenomenon, I investigated STIM1 localization in detail and found two types of ER-retention mechanisms. In a search for additional ER-retention signals, I found multiple di-arginine signals that contribute to the retention of STIM1 in the ER. Moreover, I identified a role of the K-rich region in retention of STIM1. The K-rich region is capable of binding Ca^{2+}/CaM and the levels of cytosolic Ca^{2+} regulated the ER-retention of STIM1. Trafficking of STIM1 to the cell surface required inactivation of the K-rich domain.

4.1 Features required for ER-PM contact site formation

In mammalian cells, the ER is capable of interacting with the PM. This interaction requires localization of an ER domain in close proximity to PM, which is around 6-25 nm (61, 62). These contact sites are dynamic and transient. They are formed and dissociated frequently. For instance in epithelial Vero cells, the rate of the ER movement towards or away from the PM is 4.3–4.6 μm/second (155). By the help of artificial dimerizers, such as FKBP and FKBP-

rapamycin binding (FRB) protein these contact zones can be stabilized (62). Besides formation of ER-PM contact sites by using these artificial dimerizers, the formation of ER-PM contact sites is observed under physiological conditions. During SOCE, STIM proteins, which reside in the ER membrane, associate with the PM-localized Orai1 Ca^{2+} channel, thereby forming ER-PM contact sites (61, 124). Interestingly, activated and/or overexpressed STIM1 is capable of forming ER-PM contact sites in the absence of Orai1 and this contact site formation is independent of its function in SOCE (62). This is consistent with the formation of ER-PM contact sites by overexpression of CSS^{Ist2}-tagged membrane proteins (94).

The formation of ER-PM contact site in the absence of the PM localized Orai1, depends on the K-rich domain of STIMs (94). The formation of ER-PM contact sites was abolished in cells expressing YFP-$STIM1_{EF}\Delta K$ or YFP-$STIM2_{EF}\Delta K$. Moreover, in this study, liposome-binding experiments clearly showed that C-terminal domains of STIM1 and STIM2 bind to PM-lipids. STIM2 C-terminus showed better binding to PM-lipids than STIM1 C-terminus. Moreover, the deletion of the K-rich domains demolished this interaction (94). These data suggest that the K-rich domains of STIMs function as PM-lipid binding domains, as K-rich domain of CSS^{Ist2} does (91, 94).

The FRAP and FLIP experiments revealed that the ER-PM contact sites that are formed by expression of CSS^{Ist2}-tagged GFP-Kir6.2, are stable structures (94). This may be explained by the strong interaction of CSS^{Ist2} with the PM-lipids.

A PM-lipid binding signal should have two features, as it was previously demonstrated for the CSS^{Ist2}: a multimerization domain and a domain with multiple basic residues (K-rich) that interact with the PM-lipids. The multimerization domain of CSS^{Ist2} is the N-terminal region of the signal and is composed of threonine, histidine and serine stretches (T/H/S-cluster). The function of this T/H/S-cluster can be replaced by another multimerization domain such as a leucine zipper (90). This suggests that multimerization and a certain distance between ER and PM are required for the function. The C-terminal part of the CSS^{Ist2} consists of basic residues and an amphipathic α-helix. In a mutational analysis, it was shown that the basic residues upstream of the α-helix and the hydrophobic residues in the α-helix are crucial for the function of CSS^{Ist2} (85). Interestingly, *in vitro* liposome-binding experiments showed that STIM2 K-rich domain alone is capable of binding to PM-lipids, whereas STIM1 K-rich domain is not. STIM1 but not STIM2 needs its coiled-coil multimerization domain to interact with PM-lipids. With respect to the requirement of an extra multimerization domain, CSS^{Is2} and STIM1 are different than STIM2. The putative amphipathic α-helix of STIM2 may insert its hydrophobic patch to the lipid bilayer much more efficiently than the helices of CSS^{Ist2} or STIM1. Moreover, the hydrophobic patch of STIM2 by itself may drive multimerization, which promotes the binding to lipids. On the other hand the reason of the inability of STIM1 K-rich domain to bind to PM-lipids may be due to the presence of proline residues. The very C-terminal proline residue may result in kinking or

breaking the α-helix and therefore abolish the formation of a functional α-helix (156). STIM1 therefore might severely need its multimerization domain, which consists of two coiled-coil domains after the TMD (Figure 4.1), or other unknown factors in cells for interaction with PM-lipids.

Moreover, the concentration of a protein with the PM-lipid binding domain is of significant importance for the formation of ER-PM contact sites. The overexpressions of the STIM2C- or CSS^{Ist2}-tagged proteins led to the formation of ER-PM contact sites (94). This may be due to overexpression, which can promote the multimerization state of these proteins. The necessity of a multimerization domain for lipid binding might be explained by the avidity effect. The avidity of proteins can be described as the combined strength of multiple bond interactions. The affinity of a protein to another protein or to lipid is explained by the strength of a single bond, whereas in avidity, the combined synergistic bond strength is required (157). For instance, without multimerization and formation of multiple bonds, the protein with a PM-lipid binding signal can still interact with the PM-lipid but this interaction is not stable (158). Thus, via multimerization, many binding interactions are formed and thus transient unbinding of a single site does not allow the protein to diffuse away (157). At the same time, the phosphoinositides of the PM ($PI(4,5)P_2$ and $PI(3,4,5)P_3$) may be clustered by the interactions with these proteins, which in turn increases the strength of the binding as observed in other proteins carrying a membrane deforming BAR domain (159).

The exact mechanism of the ER-PM contact site formation remains elusive. However, there are several plausible scenarios. One is based on the dynamic feature of the ER. As ER makes transient contacts with the PM, the proteins that localize at the contact sites may stabilize the ER-PM connection through their PM-lipid binding domains. Supporting this idea, it was shown that under resting conditions, STIM1 can appear in the ER-PM contact sites without being activated, and leading to the opening of the Orai1 channel (62). Moreover, according to the study of Wu et al., which was based on the TIRF and electron microscopy (EM) experiments in Jurkat T cells, two thirds of the ER-PM contact sites were shown to exist before store depletion, whereas only one third of the ER-PM contact sites were found to be newly formed upon store depletion (61). Furthermore, upon STIM1 overexpression both pre-existing and newly formed ER-PM contact sites are elongated in length, suggesting that STIM1 functions as a stabilizer of these specific domains (61, 62). Moreover, by EM, overexpressed STIM1 was shown to localize pre-cortical ER domains (160). These domains differ from the rest of the ER, since they are localized close to the PM but do not form contacts with the PM. Upon activation of STIM1, these ER domains make contacts with the PM, creating the cortical ER (160).

STIM1 stabilizes the pre-existing ER-PM contact sites upon activation and multimerization. However, the mechanism of the formation of new ER-PM contact sites by recruitment of a deeper ER domain to the PM is still unclear. One possibility to create a newly formed ER-PM

contact site may occur by the contribution of COPI. COPI has been identified to function in retrograde transport from the Golgi to ER (57, 58). Besides its role in retrograde transport, COPI promotes vesicle budding from the ER membrane *in vitro* (161) and localizes to certain ER subdomains in mammalian cells (162). Consistently, Lavieu et al. showed that the di-lysine signal of Ist2 binds to COPI and knockdown of α or β-COP by siRNA destroys the formation of ER-PM contact sites (95). The interaction of Ist2 di-lysine signal with COPI may contribute to the localization of CSS^{Ist2}-tagged proteins to the specific domains of ER, which can be readily recruited to the PM.

CSS^{Ist2}-tagged proteins and STIM1 are shown to localize to specific ER domains, but how are these domains recruited to the PM? A possible answer to this question may be the contribution of microtubules to peripheral transport of the ER. STIM1 was shown to interact with the microtubule (+)-end-binding protein, EB1. Through this interaction and growing of the microtubules, the STIM1 molecules, which are localized in the deeper ER, may reach to the PM. However, in the same study, it was shown that in Hela cells, microtubule growth-dependent localization of STIM1 is not necessary for activation of SOCE upon depletion of ER Ca^{2+} stores (25). On the other hand, silencing of EB1 by shRNA destroyed the CSS^{Ist2}-dependent formation of ER-PM contact sites, but a direct interaction of Ist2 with EB1 was not shown (95). Interestingly, β-COP, which is a component of COPI complex, was initially identified as a microtubule binding protein at the Golgi (163). Therefore, binding of microtubules to the COPI, which interacts with the CSS^{Ist2}, may promote the recruitment of specialized ER domains to the PM. Moreover, as di-lysine signals, the di-arginine signals were previously shown to bind β-COP (164). A similar interaction may occur between STIM1 and β-COP. This may in turn result in binding to microtubules, which may drag the ER to the PM. This interaction between STIM1 and β-COP, which may further the understanding of ER-PM contact site formation, remains to be elucidated.

4.2 Regulation of ER-PM contact site formation

In order to interact with Orai1 and the PM-lipids, STIMs initially has to undergo conformational changes, which start with the multimerization of the N-termini. This multimerization extends to the C-terminal coiled-coil domains and continues with possible exposure of the channel binding (CAD) and the lipid-binding (K-rich) domain (103, 114, 115, 120). Under resting conditions, although STIM1 appears in the ER-PM contact sites, it remains inactive (62). This suggests that without a conformational change upon ER Ca^{2+} store depletion, only the presence of STIM1 in close proximity to PM is not sufficient to induce Ca^{2+} influx. Consistent with an inactive STIM1 molecule at resting state, it was shown that STIM1 exists as a dimer *in vitro* and the multimer formation is required for the activation of the Orai1 channel (115, 165). The Ca^{2+} uptake into the cell is strictly regulated, since very high cytosolic Ca^{2+} levels can result in apoptosis (166). Therefore, the activation and inactivation of STIM1 should be under tight control. In this section,

I discuss the regulation of STIM1 activation, which in turn regulates the formation of ER-PM contact site formation.

It has been shown that a polybasic stretch in CAD, which interacts and activates the Orai1 at the ER-PM contact sites, interacts with a negatively charged amino acid stretch in the first coiled-coil domain of STIM1. This domain is named auto-inhibitory domain and the interaction of this domain with CAD, keeps STIM1 inactive, probably in a conformation where CAD is shielded (123, 132). I found that this polybasic stretch binds to Ca^{2+}/CaM. This may suggest that Ca^{2+}/CaM binding regulates the transition of STIM1 from inactive (bound to auto-inhibitory domain) to the active state (bound to Orai1). Moreover, in Ca^{2+}/CaM binding experiments, I found that the deletion of both K-rich domain and the polybasic stretch in CAD did not abolish the binding of Ca^{2+}/CaM. This may suggest existence of other CaM-binding domains, which could become accessible upon a conformational change. During initiation of the SOCE and multimerization of STIM1, the auto-inhibitory domain is released from the CAD and the C-terminal domain goes into an extended conformation (132, 167). This conformational change might promote binding of Ca^{2+}/CaM to CAD and to yet undefined sites in STIM1. Moreover, these interactions of STIM1 with Ca^{2+}/CaM may in turn keep the protein in an extended conformation to allow binding of STIM1 K-rich domain to PM lipids and CAD to Orai1.

Moreover, by using isotermal calorimetry and nuclear magnetic resonance approaches Bauer et al. showed that synthetic peptides of STIM1 and STIM2 K-rich domains bind Ca^{2+}/CaM (127). In this study, I used purified GFP-tagged STIM1 C-terminal fragments and investigated their interactions with CaM-coated beads. This binding of STIM1 C-terminal fragments to CaM-beads required Ca^{2+}. I observed that the binding of GFP-STIM1CΔK to CaM-beads is reduced, suggesting a role of K-rich domain in binding Ca^{2+}/CaM. However, STIM1 K-rich domain alone (GFP-STIM1 K-rich) was not able to bind Ca^{2+}/CaM, whereas STIM2 K-rich domain alone (GFP-STIM2 K-rich) showed binding. Similar as for binding to PM-lipids, STIM1 may need its multimerization domain to bind Ca^{2+}/CaM, whereas STIM2 does not. Thus, in physiological conditions, the oligomerization of STIM1 may control binding to Ca^{2+}/CaM or to PM-lipids. There are two alternative explanations for the interplay between Ca^{2+}/CaM and PM-lipids in binding to K-rich domains of STIMs. First, Ca^{2+}/CaM may bind to the K-rich domain during activation of STIM1 in SOCE. This binding of Ca^{2+}/CaM may promote formation of an amphipathic α-helix (130), which in turn promotes binding of STIM1 K-rich domain to PM-lipids. Second, contrarily, the binding of Ca^{2+}/CaM may abolish the binding of STIM1 K-rich domain to PM-lipids. This may promote dissociation of ER-PM contact sites, thus termination of SOCE. In addition, Orai1 was shown to be inactivated by binding of Ca^{2+}/CaM to its N-terminus (133). Interestingly, this Ca^{2+}/CaM binding domain of Orai1 overlaps with a putative $PI(4,5)P_2$ binding domain (unpublished data). This suggests that Ca^{2+}/CaM and PM-lipids regulate the functions of both STIM1 and Orai1. This striking feature needs to be clarified by further experiments. Moreover, since the higher-order states of STIM1 either in resting state or in activated state during SOCE

is not fully described (108), it remains to be answered under which state of STIM1 the binding of Ca^{2+}/CaM takes place.

Based on these results I suggest the following model for the initiation of SOCE: the Ca^{2+}/CaM molecules bind STIM1 to keep it in an extended conformation. The binding of Ca^{2+}/CaM to CAD will abolish the inhibitory effect of the autoinhibitory domain and prepare the CAD for the interaction with the Orai1 C-terminus. On the other hand the binding of Ca^{2+}/CaM to the K-rich domain may promote formation of an α-helix, thus binding to PM-lipids. Taken together, at the ER-PM contact sites, negatively charged phosphoinositides can replace Ca^{2+}/CaM at the K-rich domain and the C-terminal acidic region in Orai1 substitutes Ca^{2+}/CaM at the CAD (Figure 4.1).

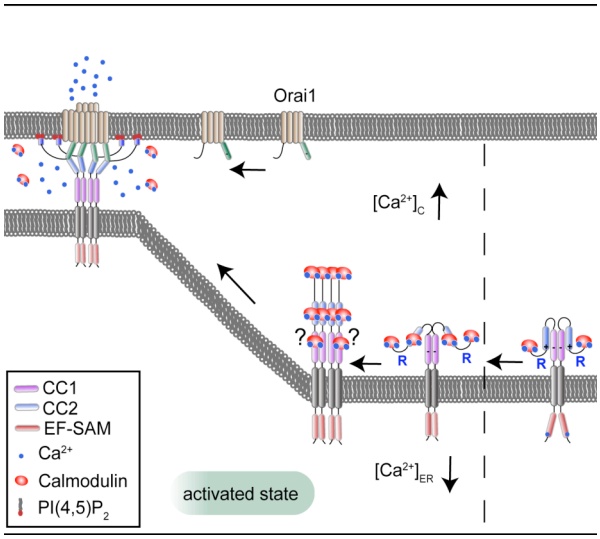

Figure 4.1 Proposed role of Ca^{2+}/CaM during activation of STIM1 in SOCE.

The Ca^{2+}/CaM molecules may bind STIM1 in its resting state (dimeric STIM1 is depicted but the oligomerization state of STIM1 under resting condition is not yet defined). This binding keeps STIM1 in a conformation, where the di-arginine signal at position 500RQR is exposed and functional. By depletion of ER Ca^{2+}, STIM1 forms higher-order oligomers. This conformational change promotes binding of additional Ca^{2+}/CaM to CAD and yet undefined regions. STIM1 molecules then travel to the ER-PM contact sites and recruit Orai1. Orai1 forms tetrameric channel and this channel is activated by interaction of STIM1 CAD with C-terminal domain of Orai1. At ER-PM contact sites Ca^{2+}/CaM is released from CAD and K-rich domain, enabling STIM1 interaction with Orai1 and PM-lipids ($PI(4,5)P_2$).

Furthermore, the mechanism of Orai1 recruitment to the ER-PM contact sites is also crucial for the activation of SOCE. It was shown that the channel is activated after the formation of ER-PM contact sites (62). This may suggest that STIM1 initially interacts with the PM-lipids and then with newly recruited Orai1. But how is Orai1 recruited to the ER-PM contact sites? One possible answer may be an association of Orai1 with lipid microdomains in the PM. Orai1 cytosolic N-terminus has a putative overlapping $PI(4,5)P_2$ and cholesterol binding domain (unpublished data). This feature of Orai1 might determine its specific lipid environment in the PM. It was also shown that Orai1 and STIM1 cluster in the detergent resistant domains of the PM, so called rafts (168, 169). Rafts contain cholesterol and sphingolipids and as well phospholipids such as

$PI(4,5)P_2$ (170). A proposed scenario therefore may be that sequestration of $PI(4,5)P_2$ by STIM1 results in recruitment of surrounding $PI(4,5)P_2$, which contain Orai1 via lateral diffusion (171).

4.3 Importance of ER-retention signals in STIM proteins

A prerequisite for the function of SOCE is that STIM proteins must be retained in the ER. In this study, I identified di-arginine (RXR) ER-retention signals in STIM1. The identity of the residue X modulates the efficiency of the signal, where negatively charged residues or small, non-polar side chains inactivates the signal (59). STIM1 has four arginine signals at positions 311RSR, 424RER, 500RQR and 530RQR. In addition, STIM2 has three potential di-arginine signals at positions, 303RLR, 428RER and 514RSR. The RER signal has been previously shown not to function as ER-retention signal. Moreover the N- and C-terminal residues around the signal affect the strength of the retention (59). In addition to the di-arginine signals, STIM2 has a di-lysine retention signal, whereas STIM1 lacks this di-lysine signal. Differences in the retention mechanisms of STIM1 and STIM2 may contribute to their physiological roles. A phylogenetic analysis showed that the STIM genes duplicated in fishes during chordate evolution (172). Further sequence alignment analysis suggested, that the di-lysine signal emerges in STIM2-like molecules after duplication, whereas all STIM1-like molecules lack this signal (R. Bhardwaj, unpublished data).

I focused on the retention of STIM1, since it was previously shown that this protein travels to the cell surface (101, 102). This suggests that STIM1 can escape from the retention under certain circumstances. In surface expression studies, I found that the 500RQR functions as the most active di-arginine ER retention signal compared to the others. The other signals had minor effects on the retention and this may be a consequence of their positions within the STIM1 C-terminal domain. The 311RSR resides in the coiled-coil domain and may be not accessible to the COPI machinery, which is responsible for retention. The 530RQR on the other hand is not in the coiled-coil domain but the surrounding amino acids are either acidic or non-polar in nature, which may affect the efficiency of the signal. I did not investigate the 424RER signal, which resides in CAD, as this kind of signal was previously shown to be inactive (59). The most active signal, 500RQR, is located downstream of the coiled-coil domains. Therefore, multimerization through the coiled-coil domains might not mask this signal. The existence of more than one di-arginine signals may suggest an alternative function. One possible function may be the interaction with COPI. COPI may bind to 311RSR and 530RQR at the ER and promote the formation of STIM1 specific ER domains, which are readily recruited to the PM, as in the case of Ist2 (95, 162).

The function of STIM2, which has a di-lysine signal and potential di-arginine signals, is restricted to the ER. Brandman et al., has shown that the STIM2 EF-hand domain is more

sensitive to drop of Ca^{2+} in the ER lumen than that of STIM1 (113). In addition to its more sensitive EF-hand domain, I showed that STIM2 has higher affinity to PM-lipids than STIM1 by *in vitro* liposome-binding experiments. Moreover, STIM2 can interact both with $PI(4,5)P_2$ and $PI(3,4,5)P_3$, whereas STIM1 only interacts with $PI(4,5)P_2$ (94). Since STIM2 is activated faster than STIM1 upon Ca^{2+} decreases in the ER lumen and since it has higher affinity to PM-lipids than STIM1, the function of STIM2 has to be restricted to the ER. The activation of STIM2 but not STIM1 upon subtle decrease of ER Ca^{2+} levels suggests that STIM2 refills cytosolic and ER Ca^{2+} upon small changes rather than amplifying signals as STIM1 does (113).

4.4 Regulated trafficking of STIM1 to the cell surface

In addition to di-arginine signals, I found that the K-rich domain of STIM1 contributes to its retention in the ER. The deletion of the K-rich domain promotes the trafficking of STIM1 to the cell surface. How could the K-rich domain without a di-lysine signal contribute to the retention of STIM1? There are two likely answers to this question. First, the interaction with the lipids might favour the retention in the ER. However, the lipid binding would occur after depletion of ER-stores and this can only explain why STIM1 does not travel to the cell surface upon depletion of the ER Ca^{2+} stores. Second, during resting conditions, a cytosolic trigger might affect the K-rich domain, which in turn keeps the protein in a conformation where the di-arginine signals are exposed and functional. The idea of having a cytosolic trigger arose from the finding that not all cells express STIM1 on their cell surface. Cell surface expression was not dependent on the concentration of the protein but indeed required a triggering factor. I observed differences in cytosolic Ca^{2+} levels between cells by using NFAT localization as reporter for cytosolic Ca^{2+} concentration. The observed cell-to-cell variation of NFAT localization suggested that the cytosolic Ca^{2+} levels regulate the distribution of STIM1. This was also supported by additional experiments where the depletion of cytosolic Ca^{2+} by addition of EGTA increased the number of cells expressing STIM1 on the surface. Consistently, localization of STIM1, which was lacking its K-rich domain, was not affected by the depletion of cytosolic Ca^{2+}. This suggests that the K-rich domain may function as a sensor for cytosolic Ca^{2+}.

The next question emerged was: how does the K-rich domain sense the cytosolic Ca^{2+}? The K-rich domain in addition to binding PM-lipids is capable of binding Ca^{2+}/CaM (94, 127). This binding of Ca^{2+}/CaM might enable STIM1 to sense the cytosolic Ca^{2+} indirectly. At low cytosolic Ca^{2+} levels, the Ca^{2+} unbound CaM might be released from STIM1 and this may result in a conformational change where the di-arginine ER-retention signal is masked. This in turn promotes the trafficking of STIM1 to the cell surface. Moreover, Brefeldin A treatment, a drug, which blocks trafficking through Golgi (66), revealed that the trafficking of HA-STIM1ΔK R500A to the cell surface occurs through Golgi.

However, this trafficking of STIM1 to the cell surface should take place during subtle changes of cytosolic Ca^{2+} levels so that the ER stores are not affected. In other words, STIM1 N-terminus should be bound to the Ca^{2+} in the ER and the protein should not multimerize through its N-terminus. Since multimerization of the N-terminus promotes accumulation at the ER-PM contact sites. On the other hand, a multimerization that is restricted to the C-termini of STIM1 may mask the di-arginine signal and promote trafficking to the cell surface (Figure 4.2).

4.5 Possible function of STIM1 at the cell surface

In initial studies it was found that STIM1 localizes to the cell surface (101, 102). Latter studies however, focused on the function of STIM1 pool, which stays in the ER (61, 103, 104, 114, 115, 120). In this study, I was interested in the function of STIM1 pool, which localizes to the cell surface.

The Ca^{2+} imaging experiments with STIM1ΔK and STIM1ΔK R500A, which lacks all retention signals, showed that the expression of these mutants lead to 2-APB resistant Ca^{2+} influx. 2-APB is a drug, which blocks SOCE, by inactivating the IP_3 receptors in the ER (152). Under the same conditions Orai1-dependent Ca^{2+} influx, which was triggered by single STIM1 R500A mutant or wild type STIM1, was 2-APB sensitive. This suggests that either the K-rich domain is required for 2-APB mediated termination of SOCE or that the surface pool of mutant STIM1 interacts with Orai1 and thereby forms a 2-APB resistant Ca^{2+} channel. The latter is supported by partial co-localizations of surface STIM1 and Orai1 in structures that are different from the Tg-induced puncta, typically observed during SOCE. Since with biochemical methods, such as surface biotinylation, it is not possible to discriminate between surface- and ER-located STIM1 (61), it remains open whether surface-located STIM1ΔK and STIM1ΔK R500A can directly bind Orai1.

A surface function of STIM1 has been suggested for the store-independent arachidonate-controlled (ARC) heteromeric Orai1/Orai3 Ca^{2+} influx channel (139). This channel is activated by arachidonic acid, which is a polyunsaturated fatty acid derived from $PI(4,5)P_2$, however physiological function of the channel is yet undefined (140, 173). Antibodies targeting the extracellular N-terminal domain of STIM1 or mutation of a N-linked glycosylation site, which abolished cell surface expression of STIM1, abrogated ARC channel activity (140).

Until now, it was proposed that STIM2 functions in Ca^{2+} uptake both for refilling of the stores and for signal amplification, whereas STIM1 only functions in the latter mechanism. According to the results presented here, I suggest that STIM1 is also capable of functioning in stabilizing basal Ca^{2+} levels. This alternative function of STIM1 does not take place at the ER-PM contact sites as it does for STIM2 but rather occurs at the cell surface. If STIM2 is sufficient to fine-tune the basal Ca^{2+} levels, why STIM1 should have a similar function? Differential expression levels

of these proteins in different cell lines may provide an explanation. Although STIM1 and STIM2 are ubiquitously expressed, there are variations in their expression levels (174). For example naive $CD4^+$ T cells express much less STIM2 than STIM1 (110). Furthermore, the function of STIM1 in basal regulation of Ca^{2+} levels may be conserved during evolution. Ancestral STIM molecules, which exist before gene duplication and emerging of STIM2-like molecules, may use their surface function to uptake of Ca^{2+} into the cytosol. Moreover, this surface function in controlling Ca^{2+} homeostasis might be conserved until today as a redundant safety mechanism in cells where the function of STIM2 is reduced or lost.

Taken together, STIM1 senses changes in Ca^{2+} levels in the ER and cytosol, allowing this sensor to respond over a wide range of Ca^{2+} signals. Besides activation during SOCE by a dramatic decrease in Ca^{2+} in the ER lumen, subtle changes in cytosolic Ca^{2+} levels promote surface localisation of STIM1, thereby allowing it to perform additional functions, such as refilling the Ca^{2+} stores and/or as initially suggested, interacting with ligands or receptors of lymphocytes (101).

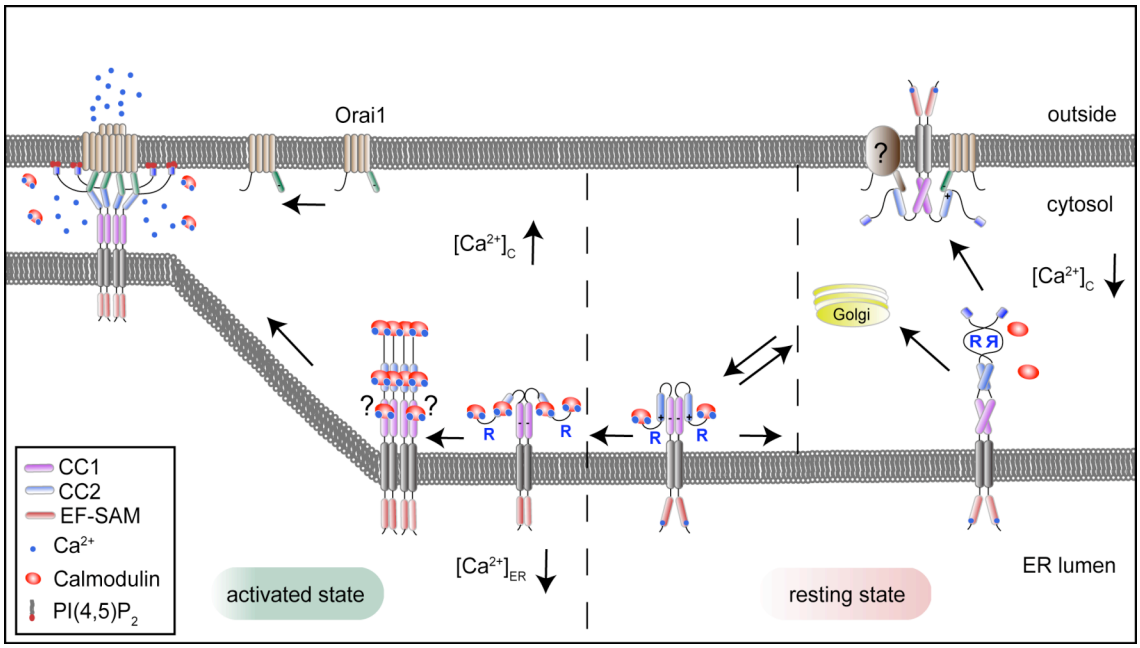

Figure 4.2 Proposed model for trafficking of STIM1 to the ER-PM contact sites or to the cell surface.

During resting state, where the STIM1 N-terminus is bound to Ca^{2+}, a decrease in cytosolic Ca^{2+} levels may release Ca^{2+} unbound CaM from the K-rich domain. This release of CaM, might promote a conformational change where the di-arginine signal at position 500RQR is shielded. STIM1 can then travel to the cell surface through Golgi and at the cell surface it may activate Ca^{2+} channels such as Orai1. The left part of the figure is described in Figure 4.1.

Although this study revealed many interesting findings, one limitation of the analysis of the localization of STIM1 and its mutants was the choice of cell type. In this study I used either HEK293T or RPE-1 cells due to the fact that they have good transfection efficiencies and are large enough to differentiate the intracellular structures by standard light microscopy. Additional functions of STIM1 in immune cells, in which STIM1 has a signal amplification function, remain to be identified. Moreover, in order to further analyze the function of STIM1 on the cell surface, and its interacting channels, electrophysiological approaches are required.

In summary, my PhD thesis reveals the mechanistic features of the ER-PM contact site formation in mammalian cells and expands our understanding of the additional functions of STIM1. I demonstrate here that the expression of transmembrane proteins with PM-lipid binding domains lead to the formation of ER-PM contact sites. STIM1, one of the PM-lipid binding proteins, remains in the ER by two types of mechanisms. One is retention by di-arginine signals; the other is retention by high cytosolic Ca^{2+}. STIM1 on the cell surface may interact with Orai1 or other yet unidentified channels in order to uptake Ca^{2+} into the cytosol. In addition to its known function as Ca^{2+} sensor of the ER lumen, I propose that by binding to Ca^{2+}/CaM, STIM1 senses cytosolic Ca^{2+} levels as well. Thus, STIM1 functions for the integration of Ca^{2+} signals in the cytosol and the ER.

5 Appendix

Standard Solutions and Buffers

10X PBS

For 1 l

80 g	NaCl
2.0 g	KCl
14.4 g	Na_2HPO_4
2.4 g	KH_2PO_4

1X PBS-T

For 1 l

100 ml	10X PBS
0.05%	Tween-20

10X TAE

For 1 l

48.4 g	Tris base
11.4 ml	glacial acetic acid
3.7 g	EDTA, disodium salt

2× SDS-Loading buffer

100 mM	Tris-HCl pH 6.8
20 %	Glycerol (v/v)
4 %	SDS (w/v)
100 mM	DTT
0.08 %	Bromphenolblue (w/v)

SDS-Running buffer

25 mM	Tris-HCl
192 mM	Glycine
0.1 %	SDS

Coomassie stain

0.2 %	Coomassie® Brilliant Blue R250
7 %	Acetic acid
50 %	Ethanol

Destain solution

7 %	Acetic acid
50 %	Methanol

10x Blotting buffer

For 1l

30.3 g (= 0.25 M) Trizma base

144 g (= 1.92 M) Glycine

LB-medium:

For 1l

10 g	bacto-tryptone
5 g	yeast extract
5 g	NaCl

pH 7.5

Mowiol

6 g	glycerol
2.4 g	Mowiol
6 ml	dH_2O
12 ml	0.2M Tris pH 8.5

6 List of figures and tables

6.1 List of figures

Figure 1.1 Morphology of the ER. 1
Figure 1.2 Proposed role of ERMES in Ca^{2+} exchange. 5
Figure 1.3 Proposed role of ERMES in mitochondrial protein import. 5
Figure 1.4 Proposed role of ERMES in phospholipids exchange. 6
Figure 1.5 Lipid transport at ER-Golgi contact sites 7
Figure 1.6 Regulated trafficking of inward rectifying potassium channel 9
Figure 1.7 PI4P turnover at ER-PM contact sites 11
Figure 1.8 Proposed function of Junctophilin-2 in cardiac myocytes. 12
Figure 1.9 Domain structure of yeast Ist2. 13
Figure 1.10 Signaling pathway that connects SOCE with NFAT-dependent gene transcription in T cells. 16
Figure 1.11 Domain structure of STIM proteins 17
Figure 3.1 The HA tag in GFP-Ist2-HA^{7-8} faces the ER lumen and/or extracellular space. 44
Figure 3.2 Ist2 localizes to intracellular structures in different cell types. 45
Figure 3.3 Yeast Ist2 localizes to patch-like ER structures in U2OS cells. 46
Figure 3.4 The CSS^{Ist2} traps CD4 at intracellular structures. 47
Figure 3.5 CSS^{Ist2} drags CD4 into patch-like ER structures. 48
Figure 3.6 Mutations in CSS^{Ist2} abolish the binding to PM lipids. 50
Figure 3.7 CD4-GFP-CSS^{Ist2} localizes at PM-associated ER patches. 51
Figure 3.8 The CSS^{Ist2} sorts different membrane proteins into peripheral ER patches. 53
Figure 3.9 CSS^{Ist2} functions as a strong signal. 54
Figure 3.10 CSS^{Ist2}-dependent ER-PM contact site formation does not alter the trafficking from ER to Golgi 56
Figure 3.11 PM-associated ER domains are stable structures. 57
Figure 3.12 CSS^{Ist2}-driven peripheral patches are in continuity with the ER. 58
Figure 3.13 The CSS^{Ist2} interacts with $PI(4,5)P_2$ at the PM. 59
Figure 3.14 The domain structure of STIMs and comparisons of their K-rich domains with the K-rich region of CSS^{Ist2}. 61
Figure 3.15 STIM2C targets Kir6.2-GFP to similar peripheral structures as CSS^{Ist2} with dot- or patch-like appearance. 62
Figure 3.16 STIM2C and the CSS^{Ist2} interact with similar domains at the PM. 63
Figure 3.17 Binding of the C-terminal domain of STIM1 and STIM2 to liposomes. 64
Figure 3.18 Contribution of different domains STIM1 and STIM2 to the lipid binding. 66
Figure 3.19 Effect of mutations in the K-rich domain of STIM2 on lipid binding and localization at ER–PM contacts. 68

Figure 3.20 HA-STIM1 can reach the surface of HEK293T cells. 71
Figure 3.21 STIM2 K-rich region prevents the surface expression of HA-STIM1. 72
Figure 3.22 Di-arginine signals retain STIM1 in the ER. 73
Figure 3.23 R500A mutation does not interfere with the function of STIM1 74
Figure 3.24 Deletion of extreme N-terminus of STIM1 abolishes its surface localization. 75
Figure 3.25 Deletion of K-rich region targets STIM1 to the cell surface. 76
Figure 3.26 K-rich, which is regulated by Ca^{2+}/CaM binding, retains STIM1 in the ER. 77
Figure 3.27 Cell-to-cell variation of cytosolic Ca^{2+} concentration. 78
Figure 3.28 Trafficking of STIM1 is regulated by cytosolic Ca^{2+} levels. 79
Figure 3.29 Binding of GFP-STIM1C and GFP-STIM1CΔK to CaM beads in the presence different amounts of detergent and high salt. 81
Figure 3.30 STIM1 has at least two Ca^{2+}/CaM binding sites. 82
Figure 3.31 HA-STIM1ΔK R500A localizes to reticular ER and to the cell surface. 84
Figure 3.32 The surface pool of STIM1 is not involved in SOCE and co-localizes with Orai1. 85
Figure 3.33 Different phenotypes of HA-STIM1ΔK R500A and GFP-Orai1 co-localizations. 85
Figure 4.1 Proposed role of Ca^{2+}/CaM during activation of STIM1 in SOCE. 91
Figure 4.2 Proposed model for trafficking of STIM1 to the ER-PM contact sites or to the cell surface. 95

6.2 List of Tables

Table 2.1 Standard PCR reaction mixture 21
Table 2.2 Standard PCR conditions 22
Table 2.3 PCR reaction mixture for site-directed mutagenesis 22
Table 2.4 PCR conditions for site-directed mutagenesis 22
Table 2.5 Ligation Reaction mixture 24
Table 2.6 Plasmids used in this study 24
Table 2.7 Cell lines used in this study 27
Table 2.8 Culturing conditions of cell lines used in this study 27
Table 2.9 Transfection conditions for different cell lines used in this study 28
Table 2.10 Transfection reaction mixture 29
Table 2.11 Antibodies used in immunofluorescence experiments 30
Table 2.12 Lipids used for preparation of liposomes 36
Table 2.13 PM-PI(4,5)P_2 -like liposome preparation (1 ml of lipid mixture) 37
Table 2.14 Solution mixture for polyacrylamide gel preparation 39
Table 2.15 Antibodies used in immunoblotting experiments 40
Table 2.16 Antibodies used in flow cytometry experiments 41
Table 3.1 Accumulation of the indicated ER proteins at peripheral patches induced by expression of CD4-GFP-CSS^{Ist2}, MHCI-GFP-CSS^{Ist2} and TAP1-GFP-CSS^{Ist2} in U2OS cells. 55

7 References

1. English AR, Zurek N, & Voeltz GK (2009) Peripheral ER structure and function. *Curr Opin Cell Biol* 21(4):596-602.

2. Tzur YB, Wilson KL, & Gruenbaum Y (2006) SUN-domain proteins: 'Velcro' that links the nucleoskeleton to the cytoskeleton. *Nat Rev Mol Cell Biol* 7(10):782-788.

3. Terasaki M & Jaffe LA (1991) Organization of the sea urchin egg endoplasmic reticulum and its reorganization at fertilization. *J Cell Biol* 114(5):929-940.

4. Baumann O & Walz B (2001) Endoplasmic reticulum of animal cells and its organization into structural and functional domains. *Int Rev Cytol* 205:149-214.

5. Amar-Costesec A, Dublet B, & Beaufay H (1989) Translocation and proteolytic processing of nascent secretory polypeptide chains: two functions associated with the ribosomal domain of the endoplasmic reticulum. *Biol Cell* 65(2):99-108.

6. Kreibich G, Ulrich BL, & Sabatini DD (1978) Proteins of rough microsomal membranes related to ribosome binding. I. Identification of ribophorins I and II, membrane proteins characteristics of rough microsomes. *J Cell Biol* 77(2):464-487.

7. Hobman TC, Zhao B, Chan H, & Farquhar MG (1998) Immunoisolation and characterization of a subdomain of the endoplasmic reticulum that concentrates proteins involved in COPII vesicle biogenesis. *Mol Biol Cell* 9(6):1265-1278.

8. Shibata Y, Voeltz GK, & Rapoport TA (2006) Rough sheets and smooth tubules. *Cell* 126(3):435-439.

9. Voeltz GK, Rolls MM, & Rapoport TA (2002) Structural organization of the endoplasmic reticulum. *EMBO Rep* 3(10):944-950.

10. Voeltz GK & Prinz WA (2007) Sheets, ribbons and tubules - how organelles get their shape. *Nat Rev Mol Cell Biol* 8(3):258-264.

11. Zimmerberg J & Kozlov MM (2006) How proteins produce cellular membrane curvature. *Nat Rev Mol Cell Biol* 7(1):9-19.

12. Pucadyil TJ & Schmid SL (2009) Conserved functions of membrane active GTPases in coated vesicle formation. *Science* 325(5945):1217-1220.

13. Voeltz GK, Prinz WA, Shibata Y, Rist JM, & Rapoport TA (2006) A class of membrane proteins shaping the tubular endoplasmic reticulum. *Cell* 124(3):573-586.

14. De Craene JO*, et al.* (2006) Rtn1p is involved in structuring the cortical endoplasmic reticulum. *Mol Biol Cell* 17(7):3009-3020.

15. Tolley N*, et al.* (2008) Overexpression of a plant reticulon remodels the lumen of the cortical endoplasmic reticulum but does not perturb protein transport. *Traffic* 9(1):94-102.

16. Zurek N, Sparks L, & Voeltz G (2011) Reticulon short hairpin transmembrane domains are used to shape ER tubules. *Traffic* 12(1):28-41.

17. Anderson DJ & Hetzer MW (2008) Reshaping of the endoplasmic reticulum limits the rate for nuclear envelope formation. *J Cell Biol* 182(5):911-924.

18. Puhka M, Vihinen H, Joensuu M, & Jokitalo E (2007) Endoplasmic reticulum remains continuous and undergoes sheet-to-tubule transformation during cell division in mammalian cells. *J Cell Biol* 179(5):895-909.

19. Benyamini P, Webster P, & Meyer DI (2009) Knockdown of p180 eliminates the terminal differentiation of a secretory cell line. *Mol Biol Cell* 20(2):732-744.

20. Shibata Y*, et al.* (Mechanisms determining the morphology of the peripheral ER. *Cell* 143(5):774-788.

21. Terasaki M, Chen LB, & Fujiwara K (1986) Microtubules and the endoplasmic reticulum are highly interdependent structures. *J Cell Biol* 103(4):1557-1568.

22. Lee C & Chen LB (1988) Dynamic behavior of endoplasmic reticulum in living cells. *Cell* 54(1):37-46.

23. Waterman-Storer CM & Salmon ED (1998) Endoplasmic reticulum membrane tubules are distributed by microtubules in living cells using three distinct mechanisms. *Curr Biol* 8(14):798-806.

24. Dreier L & Rapoport TA (2000) In vitro formation of the endoplasmic reticulum occurs independently of microtubules by a controlled fusion reaction. *J Cell Biol* 148(5):883-898.

25. Grigoriev I*, et al.* (2008) STIM1 is a MT-plus-end-tracking protein involved in remodeling of the ER. *Curr Biol* 18(3):177-182.

26. Kumar J, Yu H, & Sheetz MP (1995) Kinectin, an essential anchor for kinesin-driven vesicle motility. *Science* 267(5205):1834-1837.

27. Zhang X*, et al.* (2010) Kinectin-mediated endoplasmic reticulum dynamics supports focal adhesion growth in the cellular lamella. *J Cell Sci* 123(Pt 22):3901-3912.

28. Ong LL, Lim AP, Er CP, Kuznetsov SA, & Yu H (2000) Kinectin-kinesin binding domains and their effects on organelle motility. *J Biol Chem* 275(42):32854-32860.

29. Pizzo P & Pozzan T (2007) Mitochondria-endoplasmic reticulum choreography: structure and signaling dynamics. *Trends Cell Biol* 17(10):511-517.

30. Kornmann B & Walter P (2010) ERMES-mediated ER-mitochondria contacts: molecular hubs for the regulation of mitochondrial biology. *J Cell Sci* 123(Pt 9):1389-1393.

31. de Brito OM & Scorrano L (2008) Mitofusin 2 tethers endoplasmic reticulum to mitochondria. *Nature* 456(7222):605-610.

32. Csordas G*, et al.* (2006) Structural and functional features and significance of the physical linkage between ER and mitochondria. *J Cell Biol* 174(7):915-921.

33. Merkwirth C & Langer T (2008) Mitofusin 2 builds a bridge between ER and mitochondria. *Cell* 135(7):1165-1167.

34. Meisinger C*, et al.* (2007) The morphology proteins Mdm12/Mmm1 function in the major beta-barrel assembly pathway of mitochondria. *Embo J* 26(9):2229-2239.

35. Osman C*, et al.* (2009) The genetic interactome of prohibitins: coordinated control of cardiolipin and phosphatidylethanolamine by conserved regulators in mitochondria. *J Cell Biol* 184(4):583-596.

36. Wang X & Schwarz TL (2009) The mechanism of Ca2+ -dependent regulation of kinesin-mediated mitochondrial motility. *Cell* 136(1):163-174.

37. D'Angelo G, Vicinanza M, & De Matteis MA (2008) Lipid-transfer proteins in biosynthetic pathways. *Curr Opin Cell Biol* 20(4):360-370.

38. Kawano M, Kumagai K, Nishijima M, & Hanada K (2006) Efficient trafficking of ceramide from the endoplasmic reticulum to the Golgi apparatus requires a VAMP-associated protein-interacting FFAT motif of CERT. *J Biol Chem* 281(40):30279-30288.

39. Peretti D, Dahan N, Shimoni E, Hirschberg K, & Lev S (2008) Coordinated lipid transfer between the endoplasmic reticulum and the Golgi complex requires the VAP proteins and is essential for Golgi-mediated transport. *Mol Biol Cell* 19(9):3871-3884.

40. Breslow DK & Weissman JS (2010) Membranes in balance: mechanisms of sphingolipid homeostasis. *Mol Cell* 40(2):267-279.

41. Rapoport TA (2007) Protein translocation across the eukaryotic endoplasmic reticulum and bacterial plasma membranes. *Nature* 450(7170):663-669.

42. Swanton E & Bulleid NJ (2003) Protein folding and translocation across the endoplasmic reticulum membrane. *Mol Membr Biol* 20(2):99-104.

43. Ellgaard L & Helenius A (2003) Quality control in the endoplasmic reticulum. *Nat Rev Mol Cell Biol* 4(3):181-191.

44. Fewell SW, Travers KJ, Weissman JS, & Brodsky JL (2001) The action of molecular chaperones in the early secretory pathway. *Annu Rev Genet* 35:149-191.

45. Hendershot LM (2000) Giving protein traffic the green light. *Nat Cell Biol* 2(6):E105-106.

46. Meunier L, Usherwood YK, Chung KT, & Hendershot LM (2002) A subset of chaperones and folding enzymes form multiprotein complexes in endoplasmic reticulum to bind nascent proteins. *Mol Biol Cell* 13(12):4456-4469.

47. Letourneur F, Hennecke S, Demolliere C, & Cosson P (1995) Steric masking of a dilysine endoplasmic reticulum retention motif during assembly of the human high affinity receptor for immunoglobulin E. *J Cell Biol* 129(4):971-978.

48. Teasdale RD & Jackson MR (1996) Signal-mediated sorting of membrane proteins between the endoplasmic reticulum and the golgi apparatus. *Annu Rev Cell Dev Biol* 12:27-54.

49. Jackson MR, Nilsson T, & Peterson PA (1993) Retrieval of transmembrane proteins to the endoplasmic reticulum. *J Cell Biol* 121(2):317-333.

50. Michelsen K, Yuan H, & Schwappach B (2005) Hide and run. Arginine-based endoplasmic-reticulum-sorting motifs in the assembly of heteromultimeric membrane proteins. *EMBO Rep* 6(8):717-722.

51. Zerangue N, Schwappach B, Jan YN, & Jan LY (1999) A new ER trafficking signal regulates the subunit stoichiometry of plasma membrane K(ATP) channels. *Neuron* 22(3):537-548.

52. Wieland FT, Gleason ML, Serafini TA, & Rothman JE (1987) The rate of bulk flow from the endoplasmic reticulum to the cell surface. *Cell* 50(2):289-300.

53. Barlowe C (2003) Signals for COPII-dependent export from the ER: what's the ticket out? *Trends Cell Biol* 13(6):295-300.

54. Spang A (2009) On vesicle formation and tethering in the ER-Golgi shuttle. *Curr Opin Cell Biol* 21(4):531-536.

55. Barlowe C*, et al.* (1994) COPII: a membrane coat formed by Sec proteins that drive vesicle budding from the endoplasmic reticulum. *Cell* 77(6):895-907.

56. Pelham HR (1989) Control of protein exit from the endoplasmic reticulum. *Annu Rev Cell Biol* 5:1-23.

57. Lewis MJ & Pelham HR (1992) Ligand-induced redistribution of a human KDEL receptor from the Golgi complex to the endoplasmic reticulum. *Cell* 68(2):353-364.

58. Eugster A, Frigerio G, Dale M, & Duden R (2004) The alpha- and beta'-COP WD40 domains mediate cargo-selective interactions with distinct di-lysine motifs. *Mol Biol Cell* 15(3):1011-1023.

59. Zerangue N*, et al.* (2001) Analysis of endoplasmic reticulum trafficking signals by combinatorial screening in mammalian cells. *Proc Natl Acad Sci U S A* 98(5):2431-2436.

60. Pichler H*, et al.* (2001) A subfraction of the yeast endoplasmic reticulum associates with the plasma membrane and has a high capacity to synthesize lipids. *Eur J Biochem* 268(8):2351-2361.

61. Wu MM, Buchanan J, Luik RM, & Lewis RS (2006) Ca2+ store depletion causes STIM1 to accumulate in ER regions closely associated with the plasma membrane. *J Cell Biol* 174(6):803-813.

62. Varnai P, Toth B, Toth DJ, Hunyady L, & Balla T (2007) Visualization and manipulation of plasma membrane-endoplasmic reticulum contact sites indicates the presence of additional molecular components within the STIM1-Orai1 Complex. *J Biol Chem* 282(40):29678-29690.

63. Lange Y & Steck TL (1997) Quantitation of the pool of cholesterol associated with acyl-CoA:cholesterol acyltransferase in human fibroblasts. *J Biol Chem* 272(20):13103-13108.

64. van Meer G, Voelker DR, & Feigenson GW (2008) Membrane lipids: where they are and how they behave. *Nat Rev Mol Cell Biol* 9(2):112-124.

65. Urbani L & Simoni RD (1990) Cholesterol and vesicular stomatitis virus G protein take separate routes from the endoplasmic reticulum to the plasma membrane. *J Biol Chem* 265(4):1919-1923.

66. Donaldson JG, Finazzi D, & Klausner RD (1992) Brefeldin A inhibits Golgi membrane-catalysed exchange of guanine nucleotide onto ARF protein. *Nature* 360(6402):350-352.

67. Olkkonen VM & Lehto M (2004) Oxysterols and oxysterol binding proteins: role in lipid metabolism and atherosclerosis. *Ann Med* 36(8):562-572.

68. Kandutsch AA, Taylor FR, & Shown EP (1984) Different forms of the oxysterol-binding protein. Binding kinetics and stability. *J Biol Chem* 259(20):12388-12397.

69. Levine TP & Munro S (2002) Targeting of Golgi-specific pleckstrin homology domains involves both PtdIns 4-kinase-dependent and -independent components. *Curr Biol* 12(9):695-704.

70. Schulz TA & Prinz WA (2007) Sterol transport in yeast and the oxysterol binding protein homologue (OSH) family. *Biochim Biophys Acta* 1771(6):769-780.

71. Canagarajah BJ, Hummer G, Prinz WA, & Hurley JH (2008) Dynamics of cholesterol exchange in the oxysterol binding protein family. *J Mol Biol* 378(3):737-748.

72. Sullivan DP, Ohvo-Rekila H, Baumann NA, Beh CT, & Menon AK (2006) Sterol trafficking between the endoplasmic reticulum and plasma membrane in yeast. *Biochem Soc Trans* 34(Pt 3):356-358.

73. Stefan CJ*, et al.* (2011) Osh proteins regulate phosphoinositide metabolism at ER-plasma membrane contact sites. *Cell* 144(3):389-401.

74. Kaiser SE*, et al.* (2005) Structural basis of FFAT motif-mediated ER targeting. *Structure* 13(7):1035-1045.

75. Takeshima H, Komazaki S, Nishi M, Iino M, & Kangawa K (2000) Junctophilins: a novel family of junctional membrane complex proteins. *Mol Cell* 6(1):11-22.

76. van Oort RJ*, et al.* (2011) Disrupted junctional membrane complexes and hyperactive ryanodine receptors after acute junctophilin knockdown in mice. *Circulation* 123(9):979-988.

77. Bers DM (2004) Macromolecular complexes regulating cardiac ryanodine receptor function. *J Mol Cell Cardiol* 37(2):417-429.

78. Graves TK & Hinkle PM (2003) Ca(2+)-induced Ca(2+) release in the pancreatic beta-cell: direct evidence of endoplasmic reticulum Ca(2+) release. *Endocrinology* 144(8):3565-3574.

79. Rose CR & Konnerth A (2001) Stores not just for storage. intracellular calcium release and synaptic plasticity. *Neuron* 31(4):519-522.

80. Nishi M, Mizushima A, Nakagawara K, & Takeshima H (2000) Characterization of human junctophilin subtype genes. *Biochem Biophys Res Commun* 273(3):920-927.

81. Im YJ*, et al.* (2007) The N-terminal membrane occupation and recognition nexus domain of Arabidopsis phosphatidylinositol phosphate kinase 1 regulates enzyme activity. *J Biol Chem* 282(8):5443-5452.

82. Ito K*, et al.* (2001) Deficiency of triad junction and contraction in mutant skeletal muscle lacking junctophilin type 1. *J Cell Biol* 154(5):1059-1067.

83. Komazaki S & Nakamura H (2004) Functional analysis of mammalian genes using amphibian embryonic cells. *J Electron Microsc (Tokyo)* 53(1):87-92.

84. Garbino A & Wehrens XH (2010) Emerging role of junctophilin-2 as a regulator of calcium handling in the heart. *Acta Pharmacol Sin* 31(9):1019-1021.

85. Maass K*, et al.* (2009) A signal comprising a basic cluster and an amphipathic alpha-helix interacts with lipids and is required for the transport of Ist2 to the yeast cortical ER. *J Cell Sci* 122(Pt 5):625-635.

86. Juschke C, Ferring D, Jansen RP, & Seedorf M (2004) A novel transport pathway for a yeast plasma membrane protein encoded by a localized mRNA. *Curr Biol* 14(5):406-411.

87. Juschke C, Wachter A, Schwappach B, & Seedorf M (2005) SEC18/NSF-independent, protein-sorting pathway from the yeast cortical ER to the plasma membrane. *J Cell Biol* 169(4):613-622.

88. Griffith J, Mari M, De Maziere A, & Reggiori F (2008) A cryosectioning procedure for the ultrastructural analysis and the immunogold labelling of yeast Saccharomyces cerevisiae. *Traffic* 9(7):1060-1072.

89. Perktold A, Zechmann B, Daum G, & Zellnig G (2007) Organelle association visualized by three-dimensional ultrastructural imaging of the yeast cell. *FEMS Yeast Res* 7(4):629-638.

90. Franz A, Maass K, & Seedorf M (2007) A complex peptide-sorting signal, but no mRNA signal, is required for the Sec-independent transport of Ist2 from the yeast ER to the plasma membrane. *FEBS Lett* 581(3):401-405.

91. Fischer MA, Temmerman K, Ercan E, Nickel W, & Seedorf M (2009) Binding of plasma membrane lipids recruits the yeast integral membrane protein Ist2 to the cortical ER. *Traffic* 10(8):1084-1097.

92. Olivier C*, et al.* (2005) Identification of a conserved RNA motif essential for She2p recognition and mRNA localization to the yeast bud. *Mol Cell Biol* 25(11):4752-4766.

93. Jambhekar A*, et al.* (2005) Unbiased selection of localization elements reveals cis-acting determinants of mRNA bud localization in Saccharomyces cerevisiae. *Proc Natl Acad Sci U S A* 102(50):18005-18010.

94. Ercan E*, et al.* (2009) A conserved, lipid-mediated sorting mechanism of yeast Ist2 and mammalian STIM proteins to the peripheral ER. *Traffic* 10(12):1802-1818.

95. Lavieu G*, et al.* (2010) Induction of cortical endoplasmic reticulum by dimerization of a coatomer-binding peptide anchored to endoplasmic reticulum membranes. *Proc Natl Acad Sci U S A* 107(15):6876-6881.

96. Galindo BE & Vacquier VD (2005) Phylogeny of the TMEM16 protein family: some members are overexpressed in cancer. *Int J Mol Med* 16(5):919-924.

97. Schroeder BC, Cheng T, Jan YN, & Jan LY (2008) Expression cloning of TMEM16A as a calcium-activated chloride channel subunit. *Cell* 134(6):1019-1029.

98. Yang YD*, et al.* (2008) TMEM16A confers receptor-activated calcium-dependent chloride conductance. *Nature* 455(7217):1210-1215.

99. Caputo A*, et al.* (2008) TMEM16A, a membrane protein associated with calcium-dependent chloride channel activity. *Science* 322(5901):590-594.

100. Suzuki J, Umeda M, Sims PJ, & Nagata S (2010) Calcium-dependent phospholipid scrambling by TMEM16F. *Nature* 468(7325):834-838.

101. Oritani K & Kincade PW (1996) Identification of stromal cell products that interact with pre-B cells. *J Cell Biol* 134(3):771-782.

102. Manji SS*, et al.* (2000) STIM1: a novel phosphoprotein located at the cell surface. *Biochim Biophys Acta* 1481(1):147-155.

103. Liou J*, et al.* (2005) STIM is a Ca2+ sensor essential for Ca2+-store-depletion-triggered Ca2+ influx. *Curr Biol* 15(13):1235-1241.

104. Luik RM, Wu MM, Buchanan J, & Lewis RS (2006) The elementary unit of store-operated Ca2+ entry: local activation of CRAC channels by STIM1 at ER-plasma membrane junctions. *J Cell Biol* 174(6):815-825.

105. Zhang SL*, et al.* (2005) STIM1 is a Ca2+ sensor that activates CRAC channels and migrates from the Ca2+ store to the plasma membrane. *Nature* 437(7060):902-905.

106. Putney JW, Jr. (2007) New molecular players in capacitative Ca2+ entry. *J Cell Sci* 120(Pt 12):1959-1965.

107. Cahalan MD (2009) STIMulating store-operated Ca(2+) entry. *Nat Cell Biol* 11(6):669-677.

108. Hogan PG, Lewis RS, & Rao A (2010) Molecular basis of calcium signaling in lymphocytes: STIM and ORAI. *Annu Rev Immunol* 28:491-533.

109. Berridge MJ, Lipp P, & Bootman MD (2000) Signal transduction. The calcium entry pas de deux. *Science* 287(5458):1604-1605.

110. Oh-hora M & Rao A (2008) Calcium signaling in lymphocytes. *Curr Opin Immunol* 20(3):250-258.

111. Stathopulos PB, Zheng L, Li GY, Plevin MJ, & Ikura M (2008) Structural and mechanistic insights into STIM1-mediated initiation of store-operated calcium entry. *Cell* 135(1):110-122.

112. Stathopulos PB, Li GY, Plevin MJ, Ames JB, & Ikura M (2006) Stored Ca2+ depletion-induced oligomerization of stromal interaction molecule 1 (STIM1) via the EF-SAM region: An initiation mechanism for capacitive Ca2+ entry. *J Biol Chem* 281(47):35855-35862.

113. Brandman O, Liou J, Park WS, & Meyer T (2007) STIM2 is a feedback regulator that stabilizes basal cytosolic and endoplasmic reticulum Ca2+ levels. *Cell* 131(7):1327-1339.

114. Park CY*, et al.* (2009) STIM1 clusters and activates CRAC channels via direct binding of a cytosolic domain to Orai1. *Cell* 136(5):876-890.

115. Yuan JP*, et al.* (2009) SOAR and the polybasic STIM1 domains gate and regulate Orai channels. *Nat Cell Biol* 11(3):337-343.

116. Honnappa S*, et al.* (2009) An EB1-binding motif acts as a microtubule tip localization signal. *Cell* 138(2):366-376.

117. Baba Y*, et al.* (2006) Coupling of STIM1 to store-operated Ca2+ entry through its constitutive and inducible movement in the endoplasmic reticulum. *Proc Natl Acad Sci U S A* 103(45):16704-16709.

118. Ji W*, et al.* (2008) Functional stoichiometry of the unitary calcium-release-activated calcium channel. *Proc Natl Acad Sci U S A* 105(36):13668-13673.

119. Penna A*, et al.* (2008) The CRAC channel consists of a tetramer formed by Stim-induced dimerization of Orai dimers. *Nature* 456(7218):116-120.

120. Muik M*, et al.* (2008) Dynamic coupling of the putative coiled-coil domain of ORAI1 with STIM1 mediates ORAI1 channel activation. *J Biol Chem* 283(12):8014-8022.

121. Li Z*, et al.* (2007) Mapping the interacting domains of STIM1 and Orai1 in Ca2+ release-activated Ca2+ channel activation. *J Biol Chem* 282(40):29448-29456.

122. Muik M*, et al.* (2009) A Cytosolic Homomerization and a Modulatory Domain within STIM1 C Terminus Determine Coupling to ORAI1 Channels. *J Biol Chem* 284(13):8421-8426.

123. Wang Y, Deng X, & Gill DL (2010) Calcium signaling by STIM and Orai: intimate coupling details revealed. *Sci Signal* 3(148):pe42.

124. Liou J, Fivaz M, Inoue T, & Meyer T (2007) Live-cell imaging reveals sequential oligomerization and local plasma membrane targeting of stromal interaction molecule 1 after Ca2+ store depletion. *Proc Natl Acad Sci U S A* 104(22):9301-9306.

125. Huang GN*, et al.* (2006) STIM1 carboxyl-terminus activates native SOC, I(crac) and TRPC1 channels. *Nat Cell Biol* 8(9):1003-1010.

126. Walsh CM*, et al.* (2010) Role of phosphoinositides in STIM1 dynamics and store-operated calcium entry. *Biochem J* 425(1):159-168.

127. Bauer MC, O'Connell D, Cahill DJ, & Linse S (2008) Calmodulin binding to the polybasic C-termini of STIM proteins involved in store-operated calcium entry. *Biochemistry* 47(23):6089-6091.

128. James P, Vorherr T, & Carafoli E (1995) Calmodulin-binding domains: just two faced or multi-faceted? *Trends Biochem Sci* 20(1):38-42.

129. Crivici A & Ikura M (1995) Molecular and structural basis of target recognition by calmodulin. *Annu Rev Biophys Biomol Struct* 24:85-116.

130. Yap KL*, et al.* (2000) Calmodulin target database. *J Struct Funct Genomics* 1(1):8-14.

131. Calloway N, Vig M, Kinet JP, Holowka D, & Baird B (2009) Molecular clustering of STIM1 with Orai1/CRACM1 at the plasma membrane depends dynamically on depletion of Ca2+ stores and on electrostatic interactions. *Mol Biol Cell* 20(1):389-399.

132. Korzeniowski MK, Manjarres IM, Varnai P, & Balla T (2010) Activation of STIM1-Orai1 involves an intramolecular switching mechanism. *Sci Signal* 3(148):ra82.

133. Mullins FM, Park CY, Dolmetsch RE, & Lewis RS (2009) STIM1 and calmodulin interact with Orai1 to induce Ca2+-dependent inactivation of CRAC channels. *Proc Natl Acad Sci U S A* 106(36):15495-15500.

134. Derler I*, et al.* (2009) A Ca2(+)release-activated Ca2(+) (CRAC) modulatory domain (CMD) within STIM1 mediates fast Ca2(+)-dependent inactivation of ORAI1 channels. *J Biol Chem* 284(37):24933-24938.

135. Srikanth S*, et al.* (A novel EF-hand protein, CRACR2A, is a cytosolic Ca2+ sensor that stabilizes CRAC channels in T cells. *Nat Cell Biol* 12(5):436-446.

136. Smyth JT, Dehaven WI, Bird GS, & Putney JW, Jr. (2008) Ca2+-store-dependent and -independent reversal of Stim1 localization and function. *J Cell Sci* 121(Pt 6):762-772.

137. Yuan JP, Zeng W, Huang GN, Worley PF, & Muallem S (2007) STIM1 heteromultimerizes TRPC channels to determine their function as store-operated channels. *Nat Cell Biol* 9(6):636-645.

138. Zeng W*, et al.* (2008) STIM1 gates TRPC channels, but not Orai1, by electrostatic interaction. *Mol Cell* 32(3):439-448.

139. Mignen O, Thompson JL, & Shuttleworth TJ (2007) STIM1 regulates Ca2+ entry via arachidonate-regulated Ca2+-selective (ARC) channels without store depletion or translocation to the plasma membrane. *J Physiol* 579(Pt 3):703-715.

140. Mignen O, Thompson JL, & Shuttleworth TJ (2009) The molecular architecture of the arachidonate-regulated Ca2+-selective ARC channel is a pentameric assembly of Orai1 and Orai3 subunits. *J Physiol* 587(Pt 17):4181-4197.

141. Hauser CT & Tsien RY (2007) A hexahistidine-Zn2+-dye label reveals STIM1 surface exposure. *Proc Natl Acad Sci U S A* 104(10):3693-3697.

142. Temmerman K & Nickel W (2009) A novel flow cytometric assay to quantify interactions between proteins and membrane lipids. *J Lipid Res* 50(6):1245-1254.

143. Sapay N, Guermeur Y, & Deleage G (2006) Prediction of amphipathic in-plane membrane anchors in monotopic proteins using a SVM classifier. *BMC Bioinformatics* 7:255.

144. Steyer JA & Almers W (2001) A real-time view of life within 100 nm of the plasma membrane. *Nat Rev Mol Cell Biol* 2(4):268-275.

145. Heemels MT & Ploegh H (1995) Generation, translocation, and presentation of MHC class I-restricted peptides. *Annu Rev Biochem* 64:463-491.

146. Momburg F & Hammerling GJ (1998) Generation and TAP-mediated transport of peptides for major histocompatibility complex class I molecules. *Adv Immunol* 68:191-256.

147. de la Salle H*, et al.* (1999) HLA class I deficiencies due to mutations in subunit 1 of the peptide transporter TAP1. *J Clin Invest* 103(5):R9-R13.

148. van Endert PM (1999) Role of nucleotides and peptide substrate for stability and functional state of the human ABC family transporters associated with antigen processing. *J Biol Chem* 274(21):14632-14638.

149. Ferreri-Jacobia M, Mak DO, & Foskett JK (2005) Translational mobility of the type 3 inositol 1,4,5-trisphosphate receptor Ca2+ release channel in endoplasmic reticulum membrane. *J Biol Chem* 280(5):3824-3831.

150. Heo WD*, et al.* (2006) PI(3,4,5)P3 and PI(4,5)P2 lipids target proteins with polybasic clusters to the plasma membrane. *Science* 314(5804):1458-1461.

151. Rogers TB, Inesi G, Wade R, & Lederer WJ (1995) Use of thapsigargin to study Ca2+ homeostasis in cardiac cells. *Biosci Rep* 15(5):341-349.

152. DeHaven WI, Smyth JT, Boyles RR, Bird GS, & Putney JW, Jr. (2008) Complex actions of 2-aminoethyldiphenyl borate on store-operated calcium entry. *J Biol Chem* 283(28):19265-19273.

153. Diver JM, Sage SO, & Rosado JA (2001) The inositol trisphosphate receptor antagonist 2-aminoethoxydiphenylborate (2-APB) blocks Ca2+ entry channels in human platelets: cautions for its use in studying Ca2+ influx. *Cell Calcium* 30(5):323-329.

154. Flanagan WM, Corthesy B, Bram RJ, & Crabtree GR (1991) Nuclear association of a T-cell transcription factor blocked by FK-506 and cyclosporin A. *Nature* 352(6338):803-807.

155. Wozniak MJ*, et al.* (2009) Role of kinesin-1 and cytoplasmic dynein in endoplasmic reticulum movement in VERO cells. *J Cell Sci* 122(Pt 12):1979-1989.

156. Barlow DJ & Thornton JM (1988) Helix geometry in proteins. *J Mol Biol* 201(3):601-619.

157. Lemmon MA & Ferguson KM (2000) Signal-dependent membrane targeting by pleckstrin homology (PH) domains. *Biochem J* 350 Pt 1:1-18.

158. Klein DE, Lee A, Frank DW, Marks MS, & Lemmon MA (1998) The pleckstrin homology domains of dynamin isoforms require oligomerization for high affinity phosphoinositide binding. *J Biol Chem* 273(42):27725-27733.

159. Saarikangas J*, et al.* (2009) Molecular mechanisms of membrane deformation by I-BAR domain proteins. *Curr Biol* 19(2):95-107.

160. Orci L*, et al.* (2009) From the Cover: STIM1-induced precortical and cortical subdomains of the endoplasmic reticulum. *Proc Natl Acad Sci U S A* 106(46):19358-19362.

161. Bednarek SY*, et al.* (1995) COPI- and COPII-coated vesicles bud directly from the endoplasmic reticulum in yeast. *Cell* 83(7):1183-1196.

162. Orci L*, et al.* (1994) Coatomer-rich endoplasmic reticulum. *Proc Natl Acad Sci U S A* 91(25):11924-11928.

163. Allan VJ & Kreis TE (1986) A microtubule-binding protein associated with membranes of the Golgi apparatus. *J Cell Biol* 103(6 Pt 1):2229-2239.

164. Michelsen K*, et al.* (2007) Novel cargo-binding site in the beta and delta subunits of coatomer. *J Cell Biol* 179(2):209-217.

165. Zhou Y*, et al.* (2009) STIM1 gates the store-operated calcium channel ORAI1 in vitro. *Nat Struct Mol Biol* 17(1):112-116.

166. Clapham DE (2007) Calcium signaling. *Cell* 131(6):1047-1058.

167. Muik M*, et al.* (2011) STIM1 couples to ORAI1 via an intramolecular transition into an extended conformation. *Embo J* 30(9):1678-1689.

168. Jardin I, Salido GM, & Rosado JA (2008) Role of lipid rafts in the interaction between hTRPC1, Orai1 and STIM1. (Translated from eng) *Channels (Austin)* 2(6):401-403.

169. Simons K & Toomre D (2000) Lipid rafts and signal transduction. (Translated from eng) *Nat Rev Mol Cell Biol* 1(1):31-39.

170. Pike LJ (2009) The challenge of lipid rafts. (Translated from eng) *J Lipid Res* 50 Suppl:S323-328.

171. Niemela PS*, et al.* (2010) Membrane proteins diffuse as dynamic complexes with lipids. (Translated from eng) *J Am Chem Soc* 132(22):7574-7575.

172. Cai X (2007) Molecular evolution and functional divergence of the Ca(2+) sensor protein in store-operated Ca(2+) entry: stromal interaction molecule. (Translated from eng) *PLoS One* 2(7):e609.

173. Roberts-Crowley ML & Rittenhouse AR (2009) Arachidonic acid inhibition of L-type calcium (CaV1.3b) channels varies with accessory CaVbeta subunits. (Translated from eng) *J Gen Physiol* 133(4):387-403.

174. Williams RT*, et al.* (2001) Identification and characterization of the STIM (stromal interaction molecule) gene family: coding for a novel class of transmembrane proteins. (Translated from eng) *Biochem J* 357(Pt 3):673-685.